USGS
science for a changing world

ECCOE Landsat Quarterly Calibration and Validation Report—Quarter 4, 2025

Open-File Report 2026–1014

U.S. Department of the Interior
U.S. Geological Survey

ECCOE Landsat Quarterly Calibration and Validation Report—Quarter 4, 2025

By Md Obaidul Haque, Md Nahid Hasan, Ashish Shrestha, Rajagopalan Rengarajan, Mark Lubke, Daniel Steinwand, Paul Bresnahan, Jerad L. Shaw, Kathryn Ruslander, Esad Micijevic, Michael J. Choate, Cody Anderson, Jeff Clauson, Kurt Thome, Amit Angal, Raviv Levy, Jeff Miller, and Cibele Teixeira Pinto

Open-File Report 2026–1014

U.S. Department of the Interior
U.S. Geological Survey

U.S. Geological Survey, Reston, Virginia: 2026

Suggested citation:
Haque, M.O., Hasan, M.N., Shrestha, A., Rengarajan, R., Lubke, M., Steinwand, D., Bresnahan, P., Shaw, J.L., Ruslander, K., Micijevic, E., Choate, M.J., Anderson, C., Clauson, J., Thome, K., Angal, A., Levy, R., Miller, J., and Teixeira Pinto, C., 2026, ECCOE Landsat quarterly calibration and validation report—Quarter 4, 2025: U.S. Geological Survey Open-File Report 2026–1014, 57 p., https://doi.org/10.3133/ofr20261014.

Associated data for this publication:
U.S. Geological Survey, 2021, EarthExplorer: U.S. Geological Survey database, https://earthexplorer.usgs.gov.

ISSN 2331-1258 (online)

Contents

Executive Summary....1
Plain Language Summary....1
Introduction....1
Background....2
Purpose and Scope....2
Processing Level Definitions....2
Level 0....2
Level 1....2
Level 2....2
Landsat Collection Definitions....3
Landsat Collection 1....3
Landsat Collection 2....3
Landsat 9 Radiometric Performance Summary....3
Landsat 9 Operational Land Imager Signal-to-Noise Ratio....3
Landsat 9 Thermal Infrared Sensor Noise Performance....3
Landsat 9 Radiometric Stability....10
Landsat 9 Relative Gains....16
Landsat 9 to Landsat 8 Operational Land Imager Radiometric Cross Comparison....16
Landsat 9 Geometric Performance Summary....21
Landsat 9 Band Registration Accuracy....21
Landsat 9 Operational Land Imager to Thermal Infrared Sensor Alignment....24
Landsat 9 Geometric Accuracy....24
Landsat 9 Geodetic Accuracy....24
Landsat 9 to Landsat 8 Operational Land Imager Geometric Coregistration....27
Landsat 8 Radiometric Performance Summary....28
Landsat 8 Operational Land Imager Signal-to-Noise Ratio....28
Landsat 8 Thermal Infrared Sensor Noise Performance....28
Landsat 8 Radiometric Stability....36
Landsat 8 Absolute Radiometric Calibration....36
Landsat 8 Relative Gains....44
Landsat 8 Geometric Performance Summary....48
Landsat 8 Band Registration Accuracy....48
Landsat 8 Operational Land Imager to Thermal Infrared Sensor Alignment....48
Landsat 8 Geometric Accuracy....48
Landsat 8 Geodetic Accuracy....53
Quarterly Level 2 Validation Results....53
Level 2 Surface Reflectance Pseudoinvariant Calibration Site Trending....53
Summary....56
References Cited....56

Figures

1. Graph showing Landsat 9 Operational Land Imager signal-to-noise ratio performance, December 2025 5
2. Graph showing Landsat 9 Operational Land Imager coastal/aerosol band lifetime signal-to-noise ratio stability 6
3. Graph showing Landsat 9 Operational Land Imager blue band lifetime signal-to-noise ratio stability 6
4. Graph showing Landsat 9 Operational Land Imager green band lifetime signal-to-noise ratio stability 7
5. Graph showing Landsat 9 Operational Land Imager red band lifetime signal-to-noise ratio stability 7
6. Graph showing Landsat 9 Operational Land Imager near infrared band lifetime signal-to-noise ratio stability 8
7. Graph showing Landsat 9 Operational Land Imager shortwave infrared 1 band lifetime signal-to-noise ratio stability 8
8. Graph showing Landsat 9 Operational Land Imager shortwave infrared 2 band lifetime signal-to-noise ratio stability 9
9. Graph showing Landsat 9 Operational Land Imager cirrus band lifetime signal-to-noise ratio stability 9
10. Graph showing Landsat 9 Operational Land Imager panchromatic band lifetime signal-to-noise ratio stability 10
11. Graph showing Landsat 9 Thermal Infrared Sensor band 10 lifetime noise performance 11
12. Graph showing Landsat 9 Thermal Infrared Sensor band 11 lifetime noise performance 11
13. Graph showing Landsat 9 Operational Land Imager coastal/aerosol band lifetime radiometric stability 12
14. Graph showing Landsat 9 Operational Land Imager blue band lifetime radiometric stability 12
15. Graph showing Landsat 9 Operational Land Imager green band lifetime radiometric stability 13
16. Graph showing Landsat 9 Operational Land Imager red band lifetime radiometric stability 13
17. Graph showing Landsat 9 Operational Land Imager near infrared band lifetime radiometric stability 14
18. Graph showing Landsat 9 Operational Land Imager shortwave infrared 1 band lifetime radiometric stability 14
19. Graph showing Landsat 9 Operational Land Imager shortwave infrared 2 band lifetime radiometric stability 15
20. Graph showing Landsat 9 Operational Land Imager panchromatic band lifetime radiometric stability 15
21. Graph showing Landsat 9 Operational Land Imager cirrus band lifetime radiometric stability 16
22. Graph showing Landsat 9 Thermal Infrared Sensor band 10 lifetime radiometric stability 17
23. Graph showing Landsat 9 Thermal Infrared Sensor band 11 lifetime radiometric stability 17

24. Graph showing Landsat 9 Operational Land Imager coastal/aerosol band per-detector change in relative gains between quarter 3 and quarter 4, 2025 18
25. Graph showing Landsat 9 Operational Land Imager shortwave infrared 1 band per-detector change in relative gains between quarter 3 and quarter 4, 2025 18
26. Graph showing Landsat 9 Operational Land Imager shortwave infrared 2 band per-detector change in relative gains between quarter 3 and quarter 4, 2025 19
27. Graph showing Landsat 9 Operational Land Imager panchromatic band per-detector change in relative gains between quarter 3 and quarter 4, 2025 19
28. Graph showing Landsat 9 Operational Land Imager shortwave infrared 1 lifetime jumps in detector responsivity 20
29. Graph showing Landsat 9 Operational Land Imager shortwave infrared 2 lifetime jumps in detector responsivity 20
30. Graph showing Landsat 9 to Landsat 8 Operational Land Imager Libya 4 pseudoinvariant calibration site top of atmosphere reflectance cross comparison 21
31. Graph showing Landsat 9 Operational Land Imager lifetime band (excluding cirrus) registration accuracy by quarter 22
32. Graph showing Landsat 9 Thermal Infrared Sensor lifetime band registration accuracy by quarter 23
33. Graph showing Landsat 9 Thermal Infrared Sensor to Operational Land Imager lifetime band registration accuracy by quarter 23
34. Graph showing Landsat 9 Thermal Infrared Sensor to Operational Land Imager lifetime pitch alignment 25
35. Graph showing Landsat 9 Thermal Infrared Sensor to Operational Land Imager lifetime roll alignment 25
36. Graph showing Landsat 9 Thermal Infrared Sensor to Operational Land Imager lifetime yaw alignment 26
37. Graph showing Landsat 9 lifetime geometric accuracy by quarter 26
38. Graph showing Landsat 9 lifetime geodetic accuracy by quarter 27
39. Graph showing coregistration error between Landsat 9 and Landsat 8 Level 1 terrain-corrected products, quarter 4, 2025 28
40. Graph showing Landsat 8 Operational Land Imager signal-to-noise ratio performance, December 2025 30
41. Graph showing Landsat 8 Operational Land Imager coastal/aerosol band lifetime signal-to-noise ratio stability 30
42. Graph showing Landsat 8 Operational Land Imager blue band lifetime signal-to-noise ratio stability 31
43. Graph showing Landsat 8 Operational Land Imager green band lifetime signal-to-noise ratio stability 31
44. Graph showing Landsat 8 Operational Land Imager red band lifetime signal-to-noise ratio stability 32
45. Graph showing Landsat 8 Operational Land Imager near infrared band lifetime signal-to-noise ratio stability 32
46. Graph showing Landsat 8 Operational Land Imager shortwave infrared 1 band lifetime signal-to-noise ratio stability 33
47. Graph showing Landsat 8 Operational Land Imager shortwave infrared 2 band lifetime signal-to-noise ratio stability 33
48. Graph showing Landsat 8 Operational Land Imager cirrus band lifetime signal-to-noise ratio stability 34

49. Graph showing Landsat 8 Operational Land Imager panchromatic band lifetime signal-to-noise ratio stability 34
50. Graph showing Landsat 8 Thermal Infrared Sensor band 10 lifetime noise performance 35
51. Graph showing Landsat 8 Thermal Infrared Sensor band 11 lifetime noise performance 35
52. Graph showing Landsat 8 Operational Land Imager coastal/aerosol band lifetime radiometric stability 37
53. Graph showing Landsat 8 Operational Land Imager blue band lifetime radiometric stability 37
54. Graph showing Landsat 8 Operational Land Imager green band lifetime radiometric stability 38
55. Graph showing Landsat 8 Operational Land Imager red band lifetime radiometric stability 38
56. Graph showing Landsat 8 Operational Land Imager near infrared band lifetime radiometric stability 39
57. Graph showing Landsat 8 Operational Land Imager shortwave infrared 1 band lifetime radiometric stability 39
58. Graph showing Landsat 8 Operational Land Imager shortwave infrared 2 band lifetime radiometric stability 40
59. Graph showing Landsat 8 Operational Land Imager panchromatic band lifetime radiometric stability 40
60. Graph showing Landsat 8 Operational Land Imager cirrus band lifetime radiometric stability 41
61. Graph showing Landsat 8 Thermal Infrared Sensor band 10 radiometric stability (side A) for the first approximately 700 days of the mission 41
62. Graph showing Landsat 8 Thermal Infrared Sensor band 11 radiometric stability (side A) for the first approximately 700 days of the mission 42
63. Graph showing Landsat 8 Thermal Infrared Sensor band 10 radiometric stability (side B) 42
64. Graph showing Landsat 8 Thermal Infrared Sensor band 11 radiometric stability (side B) 43
65. Graph showing Landsat 8 Operational Land Imager lifetime gain trends and calibration gain updates 43
66. Graph showing Landsat 8 Thermal Infrared Sensor gain degradation since the safehold event on November 1, 2020 44
67. Graph showing Landsat 8 Operational Land Imager coastal/aerosol band per-detector change in relative gains between quarter 3 and quarter 4, 2025 45
68. Graph showing Landsat 8 Operational Land Imager shortwave infrared 1 band per-detector change in relative gains between quarter 3 and quarter 4, 2025 45
69. Graph showing Landsat 8 Operational Land Imager shortwave infrared 2 band per-detector change in relative gains between quarter 3 and quarter 4, 2025 46
70. Graph showing Landsat 8 Operational Land Imager panchromatic band per-detector change in relative gains between quarter 3 and quarter 4, 2025 46
71. Graph showing Landsat 8 Operational Land Imager shortwave infrared 1 lifetime jumps in detector responsivity 47
72. Graph showing Landsat 8 Operational Land Imager shortwave infrared 2 lifetime jumps in detector responsivity 47

73. Graph showing Landsat 8 Operational Land Imager lifetime band registration accuracy by quarter....49
74. Graph showing Landsat 8 Thermal Infrared Sensor lifetime band registration accuracy by quarter....50
75. Graph showing Landsat 8 Thermal Infrared Sensor to Operational Land Imager lifetime band registration accuracy by quarter....50
76. Graph showing Landsat 8 Thermal Infrared Sensor to Operational Land Imager lifetime pitch alignment....51
77. Graph showing Landsat 8 Thermal Infrared Sensor to Operational Land Imager lifetime roll alignment....51
78. Graph showing Landsat 8 Thermal Infrared Sensor to Operational Land Imager lifetime yaw alignment....52
79. Graph showing Landsat 8 lifetime geometric accuracy by quarter....54
80. Graph showing Landsat 8 lifetime geodetic accuracy by quarter....54
81. Graph showing Libya 4 pseudoinvariant calibration site surface reflectance trending, Landsat 8 Operational Land Imager, Collection 2....55
82. Graph showing Libya 4 pseudoinvariant calibration site surface reflectance trending, Landsat 9 Operational Land Imager, Collection 2....55

Tables

1. Landsat 9 Operational Land Imager radiometric performance summary, quarter 4, 2025....4
2. Landsat 9 Thermal Infrared Sensor radiometric performance summary, quarter 4, 2025....4
3. Landsat 8 and Landsat 9 Operational Land Imager typical radiances for each spectral band....5
4. Landsat 9 geometric performance summary, quarter 4, 2025....22
5. Landsat 8 Operational Land Imager radiometric performance summary, quarter 4, 2025....29
6. Landsat 8 Thermal Infrared Sensor radiometric performance summary, quarter 4, 2025....29
7. Landsat 8 geometric performance summary, quarter 4, 2025....49

Conversion Factors

International System of Units to U.S. customary units

Multiply	By	To obtain
	Length	
nanometer (nm)	0.00000003937	inch (in.)
meter (m)	3.281	foot (ft)
meter (m)	1.094	yard (yd)

Temperature in Kelvin (K) may be converted to degrees Celsius (°C) as follows:

$$°C = K - 273.15.$$

Supplemental Information

Radiance is given in watts per square meter per steradian per micrometer (W/m^2 sr µm).

Within this report, quarter 1 is from January to March, quarter 2 is from April to June, quarter 3 is from July to September, and quarter 4 is from October to December. For example, quarter 4, 2025, was from October to December 2025. For consistent presentation of results for the ECCOE Landsat Quarterly Calibration and Validation Reports, parts of this report were written following a previously developed template.

Abbreviations

Please refer to https://www.usgs.gov/landsat-missions/landsat-glossary-and-acronyms for lists of Landsat glossary terms and other Landsat abbreviations.

~	approximately
ASTER	Advanced Spaceborne Thermal Emission and Reflection Radiometer
CA	coastal/aerosol
Cal/Val	Calibration and Validation
CE90	circular error with 90 percent confidence
CNES	Centre National D'Etudes Spatiales
CPF	calibration parameter file
DOQ	digital orthophoto quadrangle
ECCOE	EROS Cal/Val Center of Excellence
EO	Earth observation
EROS	Earth Resources Observation and Science
ETM+	Enhanced Thematic Mapper Plus
GCP	ground control point
K	Kelvin
L0Ra	Level 0 Reformatted Archive
L0Rp	Level 0 Reformatted Product
L1	Level 1
L1TP	L1 Terrain Precision Correction
$L_{typical}$	typical radiance
NEΔT	noise equivalent change in temperature
OLI	Operational Land Imager
PICS	pseudoinvariant calibration sites
SADA	Solar Array Drive Assembly
SNR	signal-to-noise ratio
SSM	Scene Select Mechanism
SWIR	shortwave infrared
TIRS	Thermal Infrared Sensor
TOA	top of atmosphere
USGS	U.S. Geological Survey

ECCOE Landsat Quarterly Calibration and Validation Report—Quarter 4, 2025

By Md Obaidul Haque,[1] Md Nahid Hasan,[1] Ashish Shrestha,[1] Rajagopalan Rengarajan,[1] Mark Lubke,[1] Daniel Steinwand,[1] Paul Bresnahan,[1] Jerad L. Shaw,[1] Kathryn Ruslander,[1] Esad Micijevic,[2] Michael J. Choate,[2] Cody Anderson,[2] Jeff Clauson,[2] Kurt Thome,[3] Amit Angal,[4] Raviv Levy,[4] Jeff Miller,[4] and Cibele Teixeira Pinto[4]

Executive Summary

The U.S. Geological Survey Earth Resources Observation and Science Calibration and Validation (Cal/Val) Center of Excellence (ECCOE) focuses on improving the accuracy, precision, calibration, and product quality of remote-sensing data, leveraging years of multiscale optical system geometric and radiometric calibration and characterization experience. The ECCOE Landsat Cal/Val Team continually monitors the geometric and radiometric performance of active Landsat missions and makes calibration adjustments, as needed, to maintain data quality at the highest level.

This report provides observed geometric and radiometric analysis results for Landsats 8 and 9 for quarter 4 (October–December) of 2025. All data used to compile the Cal/Val analysis results presented in this report are freely available from the U.S. Geological Survey EarthExplorer website: https://earthexplorer.usgs.gov.

One specific activity that the ECCOE Landsat Cal/Val Team closely monitored was a Landsat 9 safehold anomaly. On October 17, 2025, Landsat 9 experienced a Solar Array Drive Assembly potentiometer fault. The onboard fault response put both the Operational Land Imager sensor and the Thermal Infrared Sensor into safe mode. Additionally, the Thermal Infrared Sensor focal plane assembly was turned off, but the cryocooler remained on. On October 20, 2025, the Solar Array Drive Assembly recovery commanding was successfully performed to put the spacecraft into nadir viewing mode. The following day, Operational Land Imager activation and recovery started, including focal plane assembly warmup. After reaching nominal operational temperatures and achieving thermal stability, science imaging resumed on October 23, 2025.

Additional information about the Landsat 9 safehold anomaly is here: https://www.usgs.gov/landsat-missions/news/landsat-9-returns-normal-operations-following-brief-safehold.

Plain Language Summary

The U.S. Geological Survey Earth Resources Observation and Science Calibration and Validation Center of Excellence Team assesses and calibrates Landsat remote-sensing data to ensure that high-quality data products are publicly available. These data products are used to make informed decisions about natural resources and the environment. This report is part of a series of quarterly reports intended to provide updated observed geometric and radiometric analysis results for Landsats 8 and 9.

Introduction

The U.S. Geological Survey (USGS) Earth Resources Observation and Science (EROS) Calibration and Validation (Cal/Val) Center of Excellence (ECCOE) focuses on improving the accuracy, precision, and quality of remote-sensing data, leveraging years of multiscale optical and thermal system geometric and radiometric calibration and characterization experience (USGS, 2021b).

This report provides observed geometric and radiometric analysis results for Landsats 8 and 9 for quarter 4 (October–December) of 2025. All data used to compile the Cal/Val analysis results presented in this report are freely available from the USGS EarthExplorer website: https://earthexplorer.usgs.gov (USGS, 2021a). Reports presenting data from previous quarters use similar language (for example, Haque and others, 2024).

One specific activity that the ECCOE Landsat Cal/Val Team closely monitored was a Landsat 9 safehold anomaly. On October 17, 2025, Landsat 9 experienced a Solar Array Drive Assembly (SADA) potentiometer fault. The onboard fault response put both the Operational Land Imager (OLI)

[1]KBR, Inc.; work done under contract to the U.S. Geological Survey.

[2]U.S. Geological Survey.

[3]National Aeronautics and Space Administration.

[4]Science Systems and Applications, Inc.; work done under contract to the National Aeronautics and Space Administration.

sensor and the Thermal Infrared Sensor (TIRS) into safe mode. Additionally, the TIRS focal plane assembly was turned off, but the cryocooler remained on. On October 20, 2025, the SADA recovery commanding was successfully performed to put the spacecraft into nadir viewing mode. The following day, OLI activation and recovery started, including focal plane assembly warmup. After reaching nominal operational temperatures and achieving thermal stability, science imaging resumed on October 23, 2025. Additional information about the Landsat 9 safehold anomaly is here: https://www.usgs.gov/landsat-missions/news/landsat-9-returns-normal-operations-following-brief-safehold.

Background

The U.S. Department of the Interior is directed to ensure that U.S. land imaging needs are met in the future and to maintain U.S. leadership in civil land imaging and land science. Those directives come in the context of the Future of Land Imaging Interagency Working Group's report titled "A Plan for a U.S. National Land Imaging Program" (Executive Office of the President of the United States, 2007) and two recent Earth observation (EO) publications (Executive Office of the President of the United States, 2014, 2016). These reports identified Landsat and other key USGS EO assets as critical components in the national EO structure, where several assets were ranked in the top 10 of more than 300 assets. Among these assets, Landsat ranked third or higher.

Maintaining continuity with past data is essential for addressing future land imaging science needs. The USGS-operated Landsat program holds the longest continuous record of satellite-based Earth imaging. Landsat data quality is viewed by the remote-sensing user community as a gold standard (National Geospatial Advisory Committee, 2020).

To ensure the continued excellent quality of Landsat data, the USGS EROS Center has identified (1) maintaining a well-calibrated multidecade remote-sensing archive for science and (2) developing and understanding land remote-sensing requirements and land imaging solutions as key strategic pillars. Understanding the land imaging requirements of current and future users, along with an ability to assess the capabilities of current and future systems for meeting those requirements, is key to meeting future land imaging science needs. In the past, Cal/Val activities at the USGS EROS Center that addressed the previously mentioned pillars were spread across multiple groups. The USGS EROS Center strategically brought the groups together and formed a single team in a unified project called the ECCOE to enable the USGS to more efficiently address national and global land remote-sensing needs.

Purpose and Scope

The purpose of this report is to provide the latest geometric and radiometric performance results for all active Landsat missions. This report provides observed geometric and radiometric analysis results for Landsats 8 and 9 for quarter 4 (October–December, 2025). All data used to compile the results presented in this report are available from the USGS EarthExplorer website: https://earthexplorer.usgs.gov (USGS, 2021a).

Processing Level Definitions

This report frequently references Landsat processing levels. Descriptions of these processing levels are in the following subsections.

Level 0

The Level 0 Reformatted Archive (L0Ra) and Level 0 Reformatted Product (L0Rp) formats do not have sensor chip assembly or band alignment applied. L0Ra data are sensor data and spacecraft ancillary data that are reformatted for easier processing. Minor corrections to the ancillary data (such as frame number and time-code corrections) are applied, and ancillary raw data units are converted to engineering units. Image data are left in counts or digital numbers. L0Ra and L0Rp files are in the same format, but the content is different. L0Ra files contain an entire interval of imagery, whereas L0Rp files only contain a smaller part of the L0Ra data: a Worldwide Reference System-2 scene-based subset.

Level 1

The standard Level 1 (L1) image data are radiometrically and geometrically corrected. L1 Geometric Systematic Correction products are radiometrically calibrated with only systematic geometric corrections applied by using the spacecraft ephemeris data. L1 Systematic Terrain Correction products are radiometrically calibrated with systematic geometric corrections applied using the spacecraft ephemeris data and digital elevation model data to correct for relief displacement. L1 Terrain Precision Correction (L1TP) products are radiometrically calibrated, georegistered ground control points (GCPs), and orthorectified using digital elevation model data to correct for relief displacement.

Level 2

The Level 2 (L2) science products are generated from L1 inputs that meet the less than 76-degree solar zenith angle constraint and include the required auxiliary data inputs to generate a scientifically viable product. L2 science products represent surface reflectance and surface temperature. Surface

reflectance is the fraction of incoming solar radiation that is reflected from the Earth's surface. Surface reflectance product generation accounts for the temporally, spatially, and spectrally varying scattering and absorbing effects of atmospheric gases, aerosols, and water vapor, which are necessary to reliably characterize the Earth's land surface.

Surface temperature is the measurement of the temperature of the surface of the Earth in Kelvin (K). Provisional surface temperature is generated from the Landsat Collection 2 L1 thermal infrared bands, top of atmosphere (TOA) reflectance, Advanced Spaceborne Thermal Emission and Reflection Radiometer (ASTER) Global Emissivity Database data, ASTER Normalized Difference Vegetation Index data, and atmospheric profiles of geopotential height, specific humidity, and air temperature extracted from reanalysis data.

Landsat Collection Definitions

This report frequently references Landsat collections. In 2016, the USGS reorganized the Landsat archive into a tiered-collection management structure. This structure ensures that all Landsat L1 products provide a consistent archive of known data quality while controlling continuous improvement of the archive and access to all data as they are acquired. The implementation of collections represents a substantial change in the management of the Landsat archive by ensuring consistent quality over time and across all instruments.

Landsat Collection 1

Landsat Collection 1 was released in 2016 and introduced collection tiers for L1 data products based on data quality and the level of processing. The tier definition purpose was to support easier identification of suitable scenes for time-series pixel-level analysis. In addition to tiered products, several changes were first introduced with the release of Collection 1 processing. Collection 1 data processing and distribution ended on December 30, 2022, 2 years after the release of Landsat Collection 2 in December 2020. Additional information about the Collection 1 products is available at https://www.usgs.gov/landsat-missions/landsat-collection-1.

Landsat Collection 2

Landsat Collection 2 was released in December 2020 and marked the second major reprocessing effort on the Landsat archive (USGS, 2020a, b). Collection 2 represented several data product improvements that harnessed recent advancements in data processing, algorithm development, and data access and distribution capabilities. Additional information about the Collection 2 products is available at https://www.usgs.gov/landsat-missions/landsat-collection-2.

Landsat 9 Radiometric Performance Summary

The Landsat 9 on-orbit radiometric performance for this reporting quarter (quarter 4, 2025) meets all requirements as outlined in USGS (2022). The quarterly OLI and TIRS radiometric performance summaries are provided in tables 1 and 2, respectively.

Landsat 9 Operational Land Imager Signal-to-Noise Ratio

The signal-to-noise ratio (SNR) for each of the OLI spectral bands is characterized at a prescribed band-specific typical radiance ($L_{typical}$) level, as described in table 3. The SNR of a detector at a given radiance level is defined as the mean of the measured pixel radiances acquired over a homogenous target divided by their standard deviation. A curve is fit to the SNR at the measured radiance levels and is evaluated at the prescribed $L_{typical}$ level. Before launch, the SNR was characterized at multiple stages of the instrument build, culminating in the testing of the fully integrated instrument.

The Landsat 9 OLI SNR is evaluated on orbit each month using onboard calibrator data and is slightly better than the Landsat 8 OLI SNR (between 3.49 and 8.72 percent band-dependent improvement at the $L_{typical}$ level). It is consistently two to three times better than requirements and about eight times better than the Landsat 7 Enhanced Thematic Mapper Plus (ETM+) SNR. The per-band OLI median SNR at the $L_{typical}$ level (yellow bars) for December 2025, which for all bands, easily exceeds the OLI SNR requirements (blue bars) by more than 50 percent, is shown in figure 1. Lifetime SNR stability at $L_{typical}$ for each OLI band is represented in figures 2, 3, 4, 5, 6, 7, 8, 9, and 10; monthly SNR values (for the detectors that have median SNRs for all bands) are denoted by the diamonds, and the uncertainties in the monthly SNR model are denoted by the error bars. The SNR for each band has remained stable over time (within the uncertainty of the models and much greater than the required levels). From Haque and others (2024), radiometric updates implemented during the Landsat 9 data archive reprocessing effort resulted in slight per-band improvement in the Landsat 9 OLI SNR (between 0.03 and 3.84 percent).

Landsat 9 Thermal Infrared Sensor Noise Performance

Noise can be defined as variation in detected signal over time when observing a stable source of radiation. For thermal sensors, noise is usually expressed in terms of a change in brightness temperature (that is, the noise equivalent change in temperature [NEΔT]). NEΔT is estimated as the standard

Table 1. Landsat 9 Operational Land Imager radiometric performance summary, quarter 4 (October–December), 2025.

[The previous quarter is quarter 3 (July–September), 2025. OLI, Operational Land Imager; <, less than; SNR, signal-to-noise ratio; $L_{typical}$, typical radiance; -, not applicable; L_{high}, high radiance; RMS, root mean square; stdev, standard deviation; ≤, less than or equal to; W/m² sr µm, watt per square meter per steradian per micrometer; σ, sigma; spec, specification]

Requirement	Measured value from this quarter	Measured value from previous quarter[1]	Required value	Unit
OLI ghosting	Meets	Meets	Varies	Percent
OLI absolute radiance uncertainty	1.9	1.9	<5	Percent
OLI absolute reflectance uncertainty	2.3	2.3	<3	Percent
OLI median SNR $L_{typical}$	Meets	Meets	Varies	-
OLI median SNR L_{high}	Meets	Meets	Varies	-
OLI uniformity full field of view	0.30	0.30	<0.5	Percent
OLI uniformity banding RMS	0.10	0.10	<1	Percent
OLI uniformity banding stdev	0.10	0.10	<0.25	Percent
OLI uniformity streaking	0.2	0.2	≤0.5, 1	Percent
OLI coherent noise	Meets	Meets	Less than coherent noise threshold curve	-
OLI saturation radiances	Meets	Meets	Varies	W/m² sr µm
OLI 16-day radiometric stability	0.05	0.05	<1	Percent (2σ)
OLI 60-second radiometric stability	0.2	0.2	<0.5	Percent (2σ)
OLI inoperable detectors	0	0	<0.1	Percent
OLI out-of-spec detectors	<0.25	<0.25	<0.25	Percent

[1]From Haque and others (2026).

Table 2. Landsat 9 Thermal Infrared Sensor radiometric performance summary, quarter 4 (October–December), 2025.

[The previous quarter is quarter 3 (July–September), 2025. TIRS, Thermal Infrared Sensor; ~, approximately; <, less than; NEΔT, noise equivalent change in temperature; K, Kelvin; RMS, root mean square; stdev, standard deviation; -, not applicable; >, greater than; W/m² sr µm, watt per square meter per steradian per micrometer; σ, sigma; spec, specification]

Requirement	Measured value from this quarter	Measured value from previous quarter[1]	Required value	Unit
TIRS absolute radiance uncertainty	~1	~1	<2	Percent
TIRS NEΔT (at 300 K)	0.07	0.07	<0.4	K
TIRS uniformity full field of view	0.06	0.06	<0.5	Percent
TIRS uniformity banding RMS	0.12	0.12	<0.5	Percent
TIRS uniformity banding stdev	0.06	0.06	<0.5	Percent
TIRS uniformity streaking	0.15	0.15	<0.5	Percent
TIRS coherent noise	Meets	Meets	Less than coherent noise threshold curve	-
TIRS saturation radiances	~25.0, ~23.0	~25.0, ~23.0	>20.5, >17.8	W/m² sr µm
TIRS 40-minute radiometric stability	<0.3	<0.3	<0.7	Percent (1σ)
TIRS inoperable detectors	0	0	<0.1	Percent
TIRS out-of-spec detectors	0	0	<0.25	Percent

[1]From Haque and others (2026).

Table 3. Landsat 8 and Landsat 9 Operational Land Imager typical radiances for each spectral band (from Haque and others, 2024).

[OLI, Operational Land Imager; nm, nanometer; $L_{typical}$, typical radiance; W/m² sr µm, watt per square meter per steradian per micrometer]

OLI band number	Spectral band	Center wavelength (nm)	$L_{typical}$ (W/m² sr µm)
1	Coastal/aerosol	443	40
2	Blue	482	40
3	Green	561	30
4	Red	655	22
5	Near infrared	865	14
6	Shortwave infrared 1	1,609	4.0
7	Shortwave infrared 2	2,201	1.7
8	Panchromatic	590	23
9	Cirrus	1,373	6.0

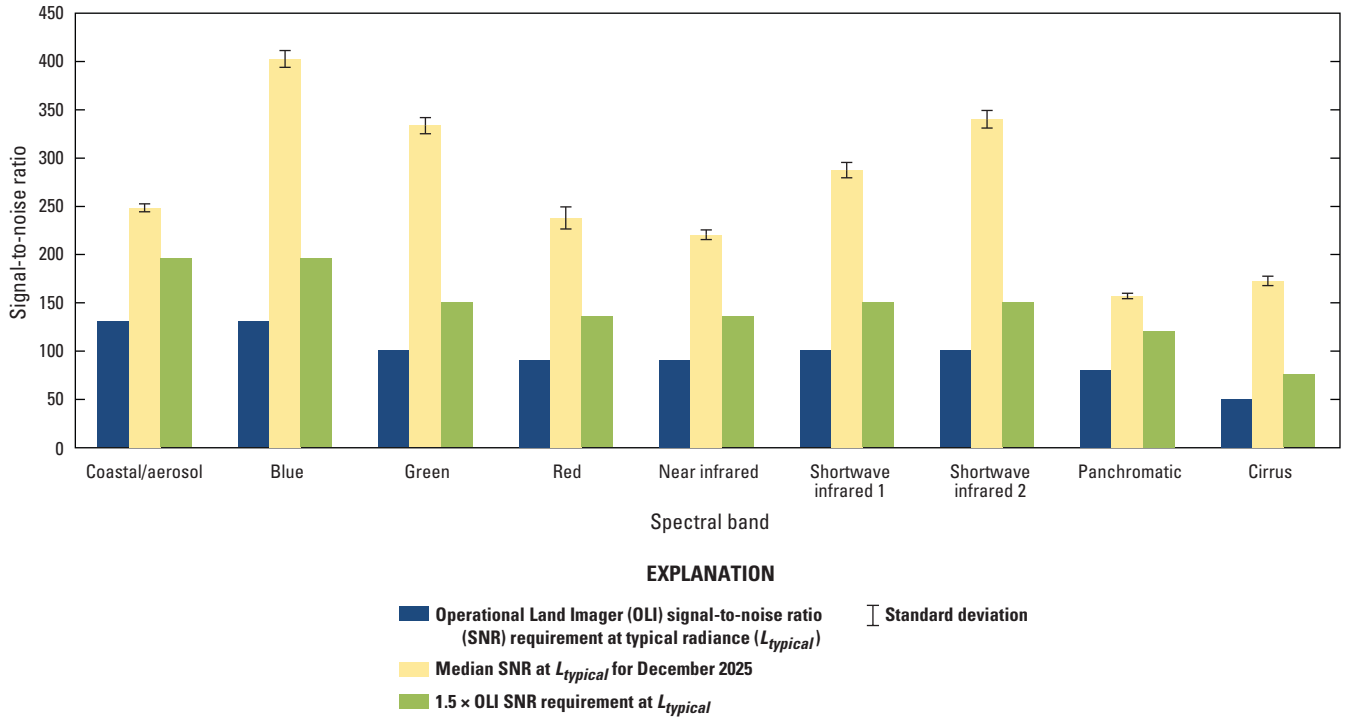

Figure 1. Graph showing Landsat 9 Operational Land Imager signal-to-noise ratio performance, December 2025.

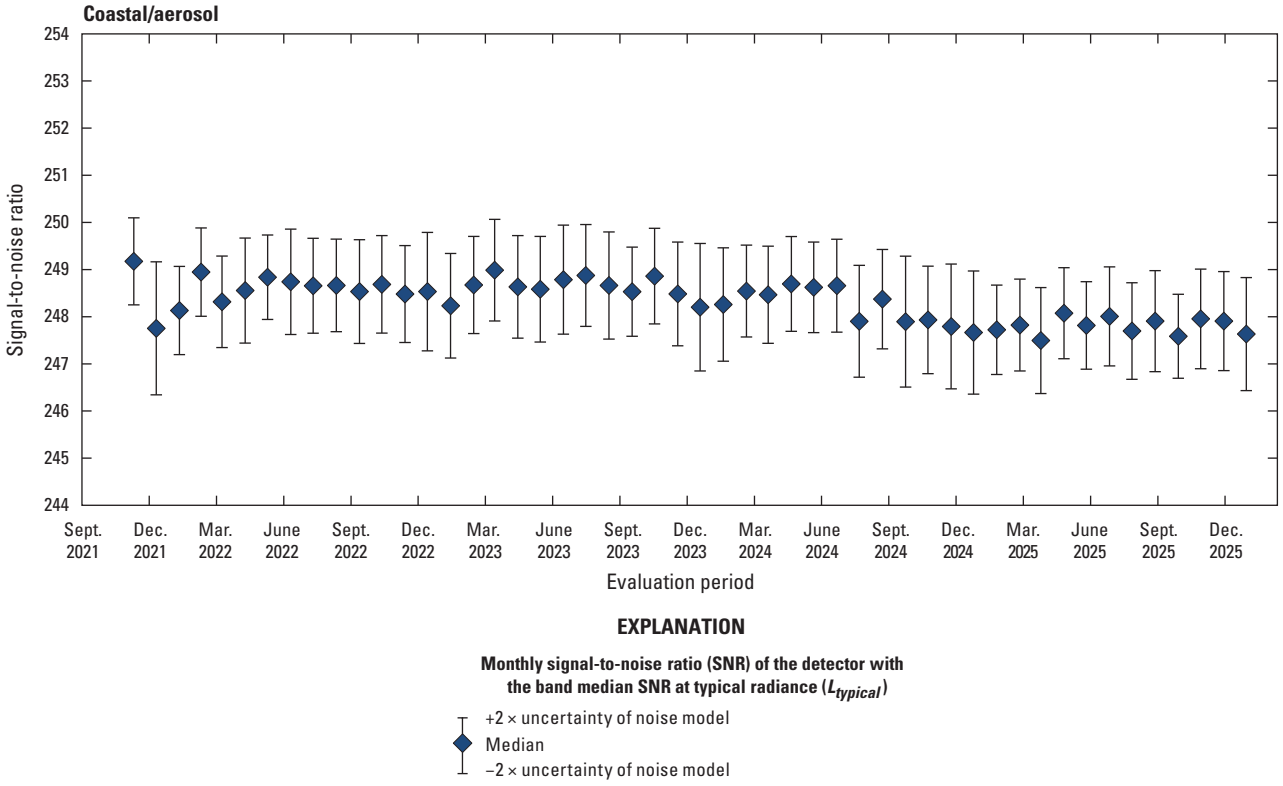

Figure 2. Graph showing Landsat 9 Operational Land Imager coastal/aerosol band lifetime signal-to-noise ratio stability.

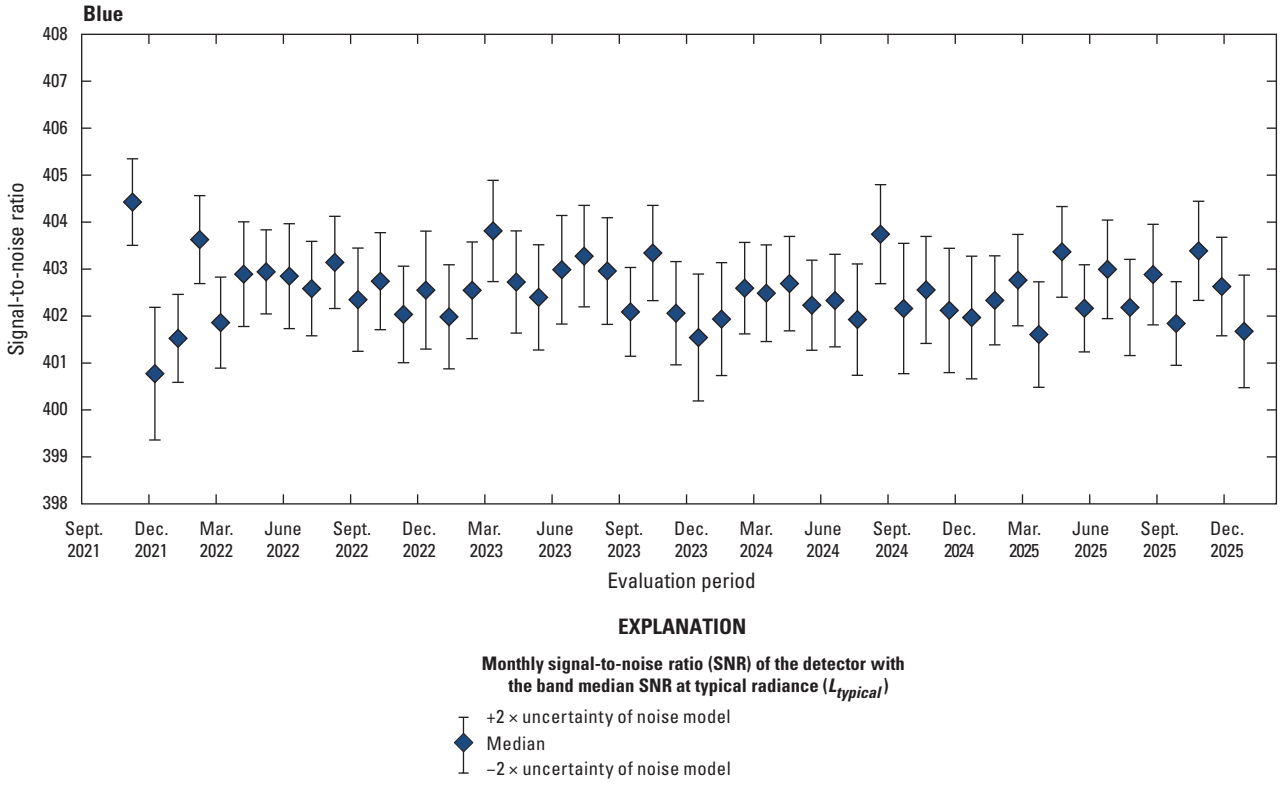

Figure 3. Graph showing Landsat 9 Operational Land Imager blue band lifetime signal-to-noise ratio stability.

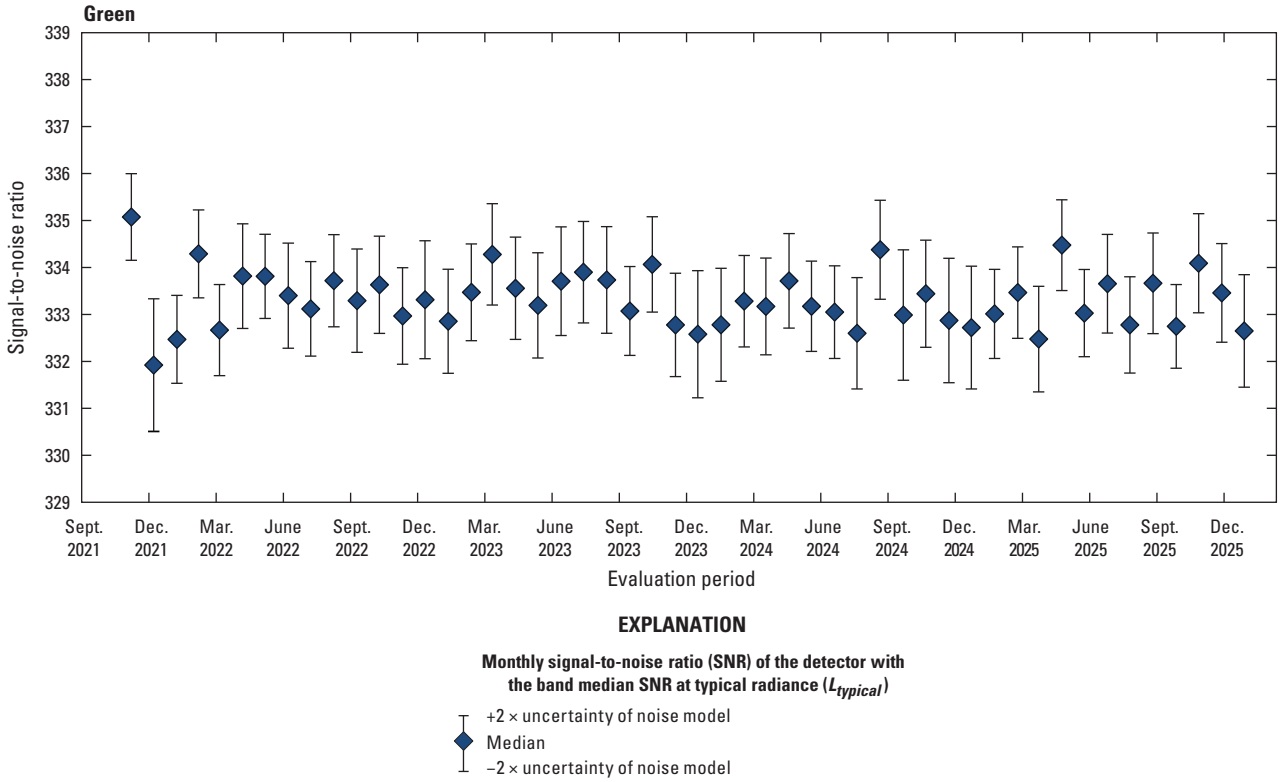

Figure 4. Graph showing Landsat 9 Operational Land Imager green band lifetime signal-to-noise ratio stability.

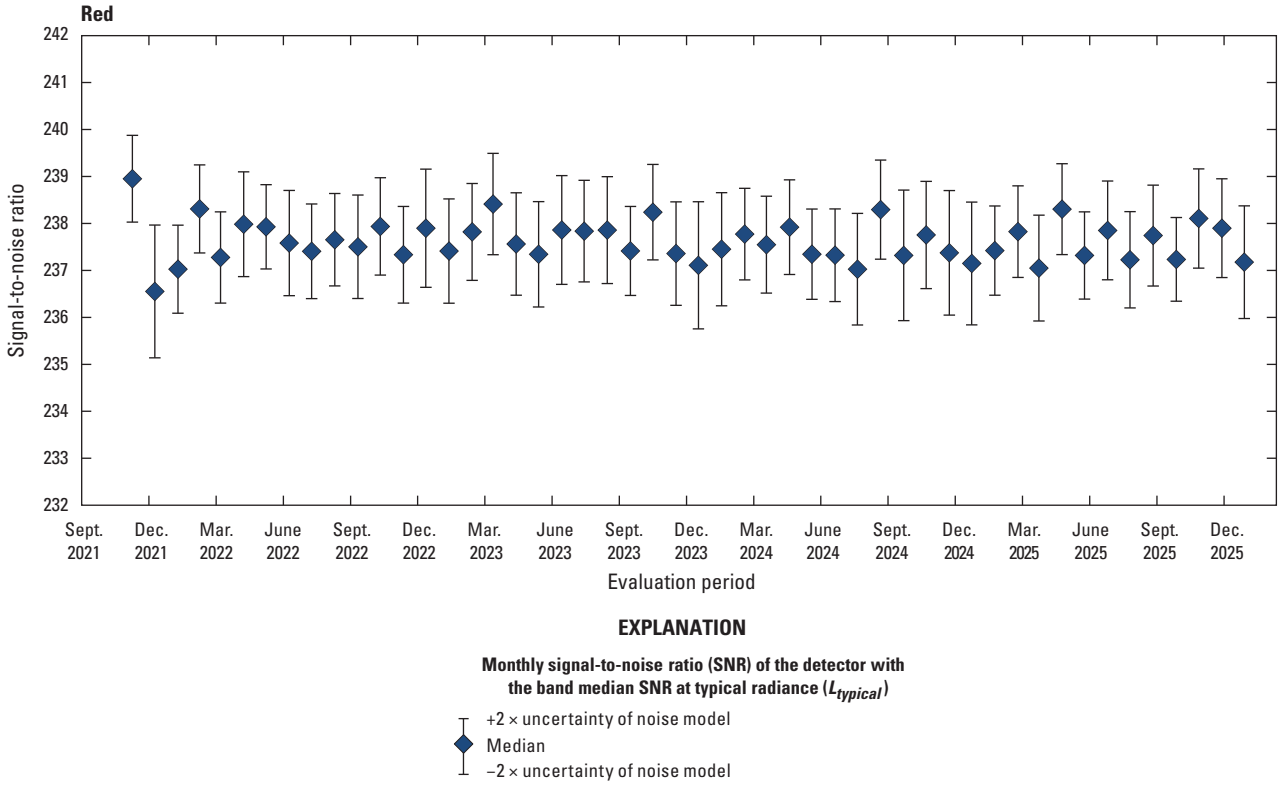

Figure 5. Graph showing Landsat 9 Operational Land Imager red band lifetime signal-to-noise ratio stability.

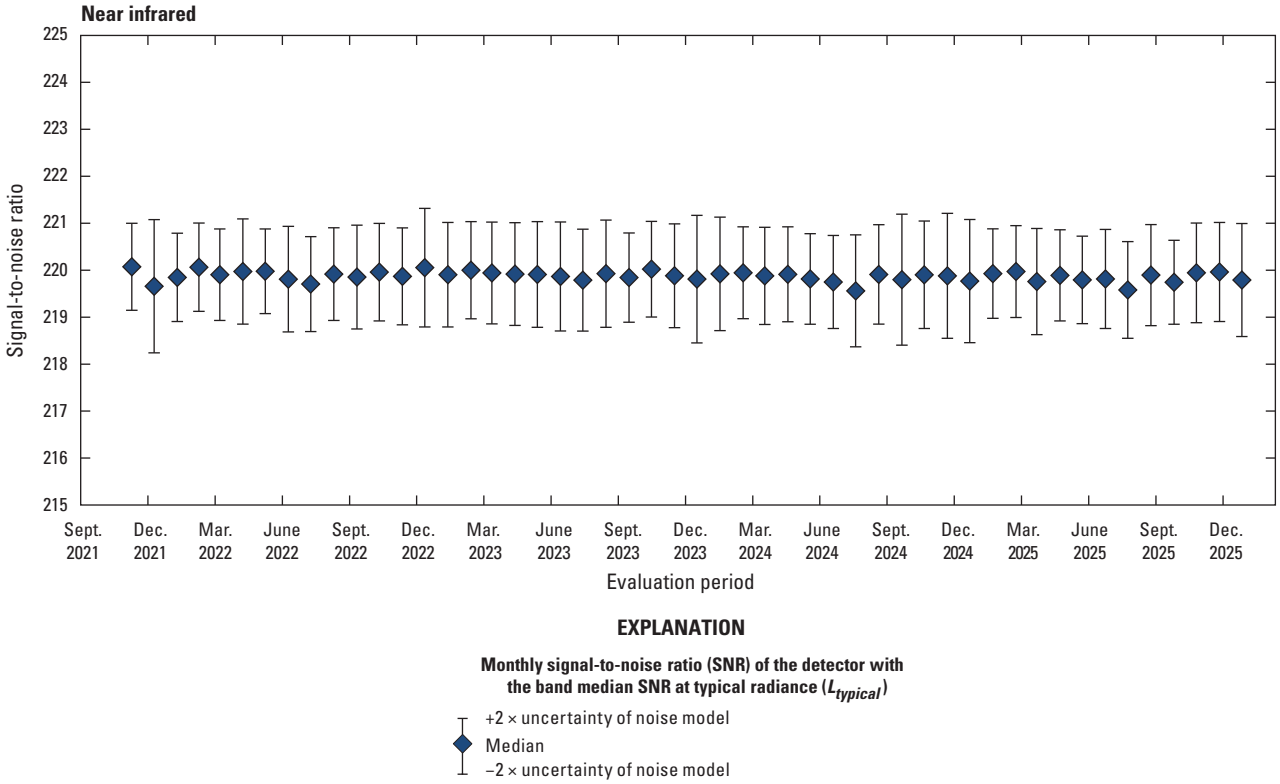

Figure 6. Graph showing Landsat 9 Operational Land Imager near infrared band lifetime signal-to-noise ratio stability.

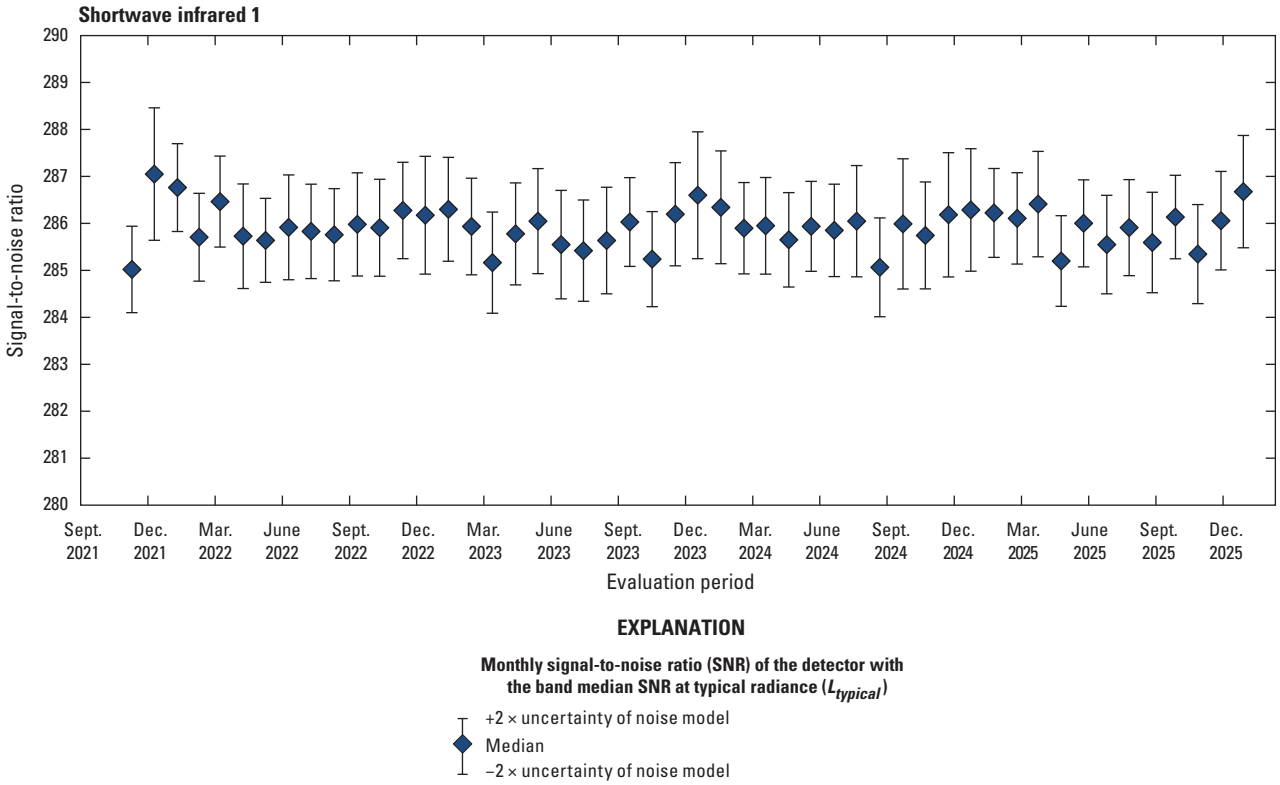

Figure 7. Graph showing Landsat 9 Operational Land Imager shortwave infrared 1 band lifetime signal-to-noise ratio stability.

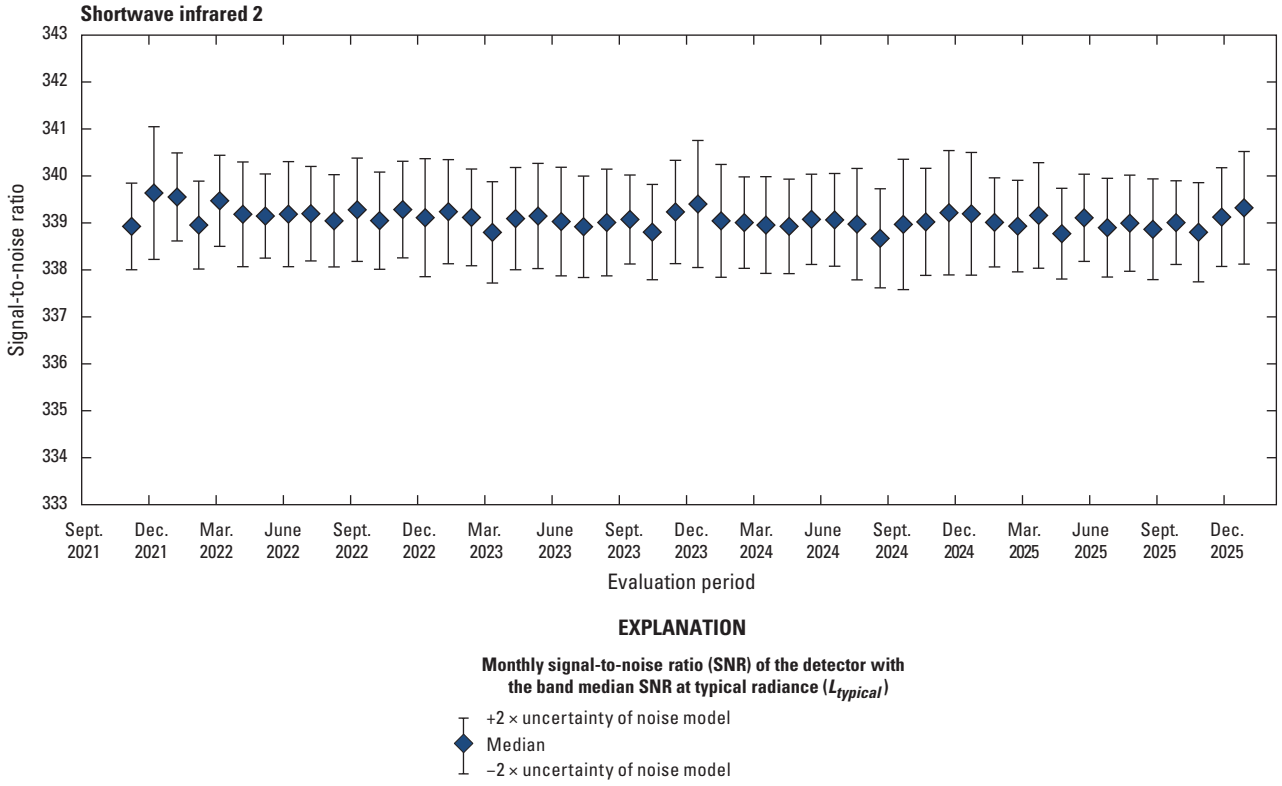

Figure 8. Graph showing Landsat 9 Operational Land Imager shortwave infrared 2 band lifetime signal-to-noise ratio stability.

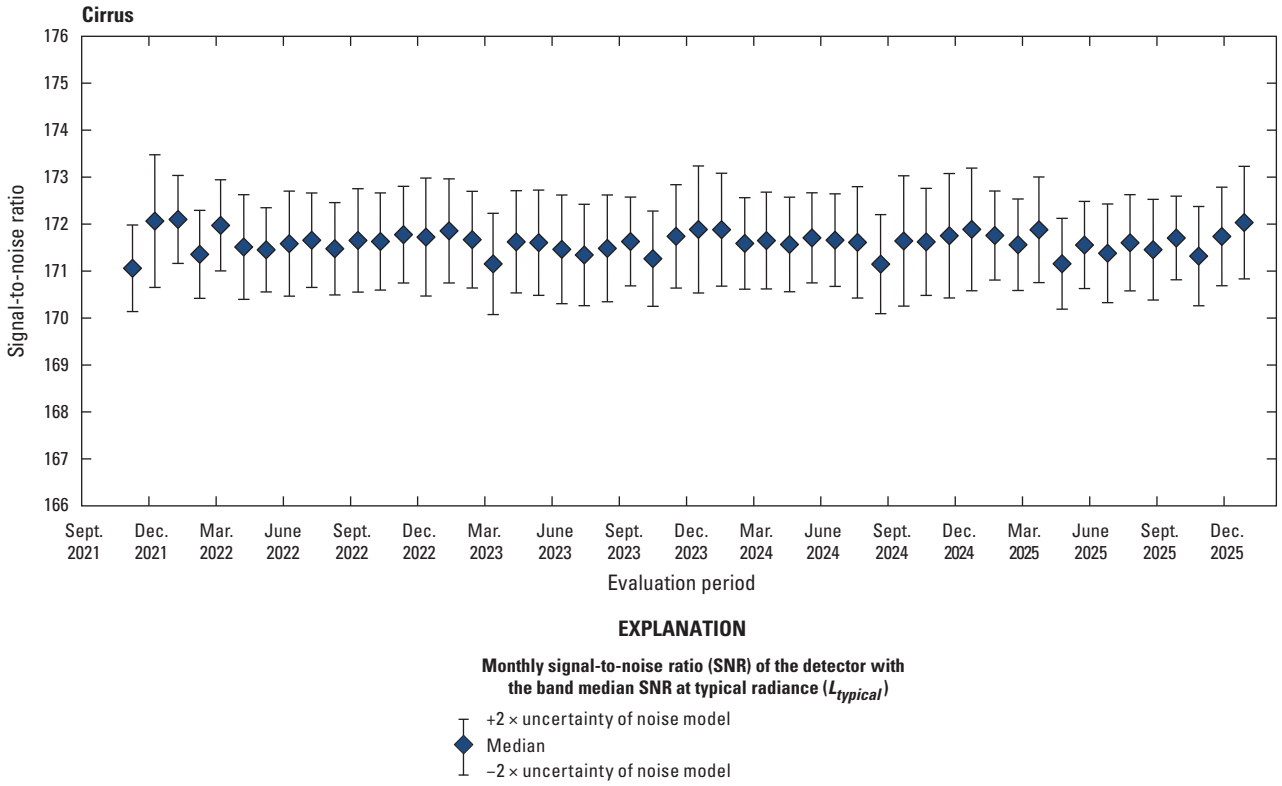

Figure 9. Graph showing Landsat 9 Operational Land Imager cirrus band lifetime signal-to-noise ratio stability.

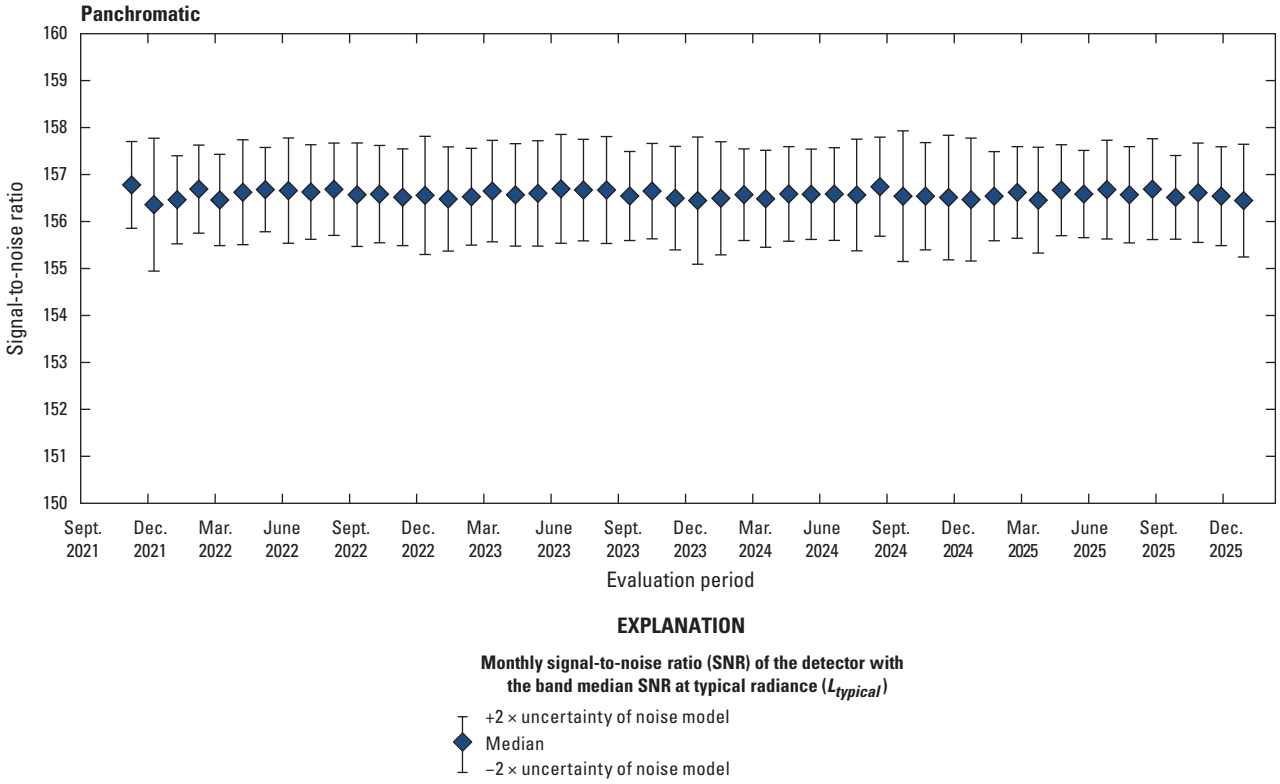

Figure 10. Graph showing Landsat 9 Operational Land Imager panchromatic band lifetime signal-to-noise ratio stability.

deviation of detector data acquired over a uniform radiance source and then converted to temperature. Noise performance is completed on blackbody and deep space TIRS data (Barsi and others, 2022).

All Landsat 9 TIRS detectors have similar NEΔT. At 300 K, band-average noise performance for both thermal bands is about six times better than the requirement (less than 0.4 K) and about three times better than the NEΔT of the Landsat 7 ETM+ thermal band at that same temperature. Lifetime averages of NEΔT at 300 K for TIRS band 10 are shown in figure 11, and the same averages for TIRS band 11 are shown in figure 12. In both figures, colored diamonds are used to indicate the observed NEΔT values as measured over time.

Landsat 9 Radiometric Stability

Radiometric stability of an instrument is fundamental to low uncertainty in the radiometric calibration of data products generated from its measurements. The radiometric response stability is characterized for all OLI and TIRS bands using the instruments' responses to signals from the onboard calibration devices collected over time (USGS, 2021c). The bias and gain stability of an instrument are contributing factors to variability within a radiometrically calibrated product.

The per-band Landsat 9 OLI radiometric stability over the lifetime of the instrument is shown in figures 13, 14, 15, 16, 17, 18, 19, 20, and 21. Within each figure, the x-axis represents years since launch (September 27, 2021), and the y-axis represents the response relative to the normalized first 3 months of image data acquisitions. Except for the coastal/aerosol (CA) band, which was corrected for the first time in the quarter 3 (July–September), 2024, calibration parameter file (CPF), and regularly corrected thereafter, all onboard calibrators demonstrate stable responses over time at a level less than approximately (~) 0.3 percent with no significant trends. This response indicates no change in responsivity and indicates high radiometric stability of the instrument over its lifetime. As a result of the October 2025 Landsat 9 SADA anomaly, an out-of-cycle CPF was released with updated OLI and TIRS relative gains. Additional gain corrections are planned for all OLI bands in the quarter 1, 2026, CPF. Note that, because of the stable responses, the scale for these figures has been reduced when compared with the equivalent Landsat 8 figures to show additional detail.

Early mission TIRS responsivity remained stable to within 0.05 percent in bands 10 and 11. On March 12, 2022, the TIRS cryocooler electronics reset suddenly, leading to instrument power down and loss of thermal control. Once thermal control was recovered, the internal responsivity metric indicated that the response had changed by about 0.35 and

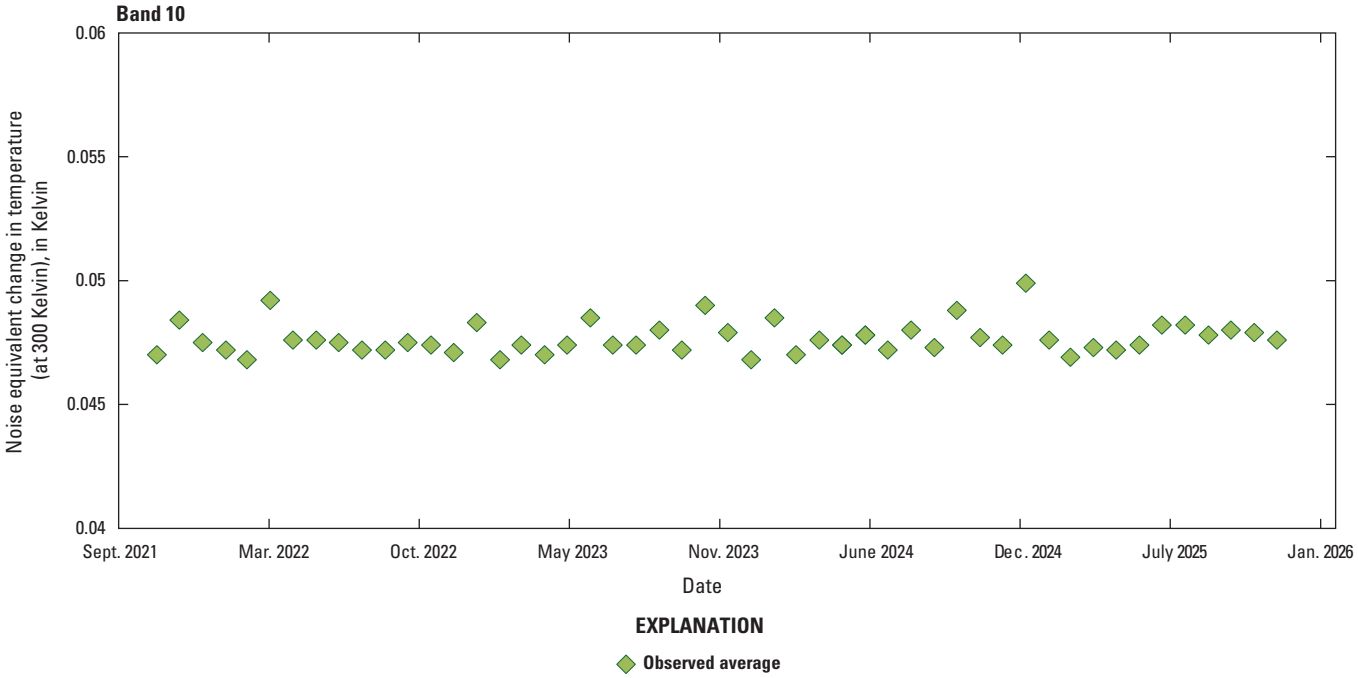

Figure 11. Graph showing Landsat 9 Thermal Infrared Sensor band 10 lifetime noise performance.

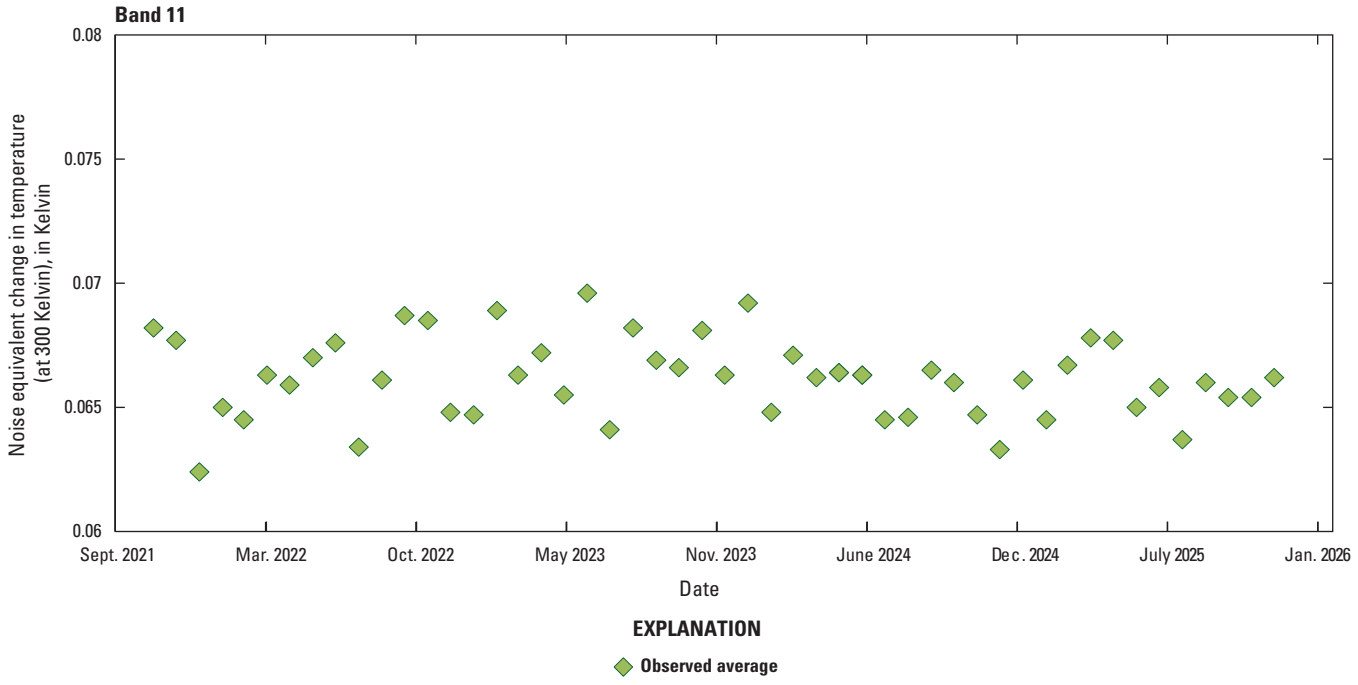

Figure 12. Graph showing Landsat 9 Thermal Infrared Sensor band 11 lifetime noise performance.

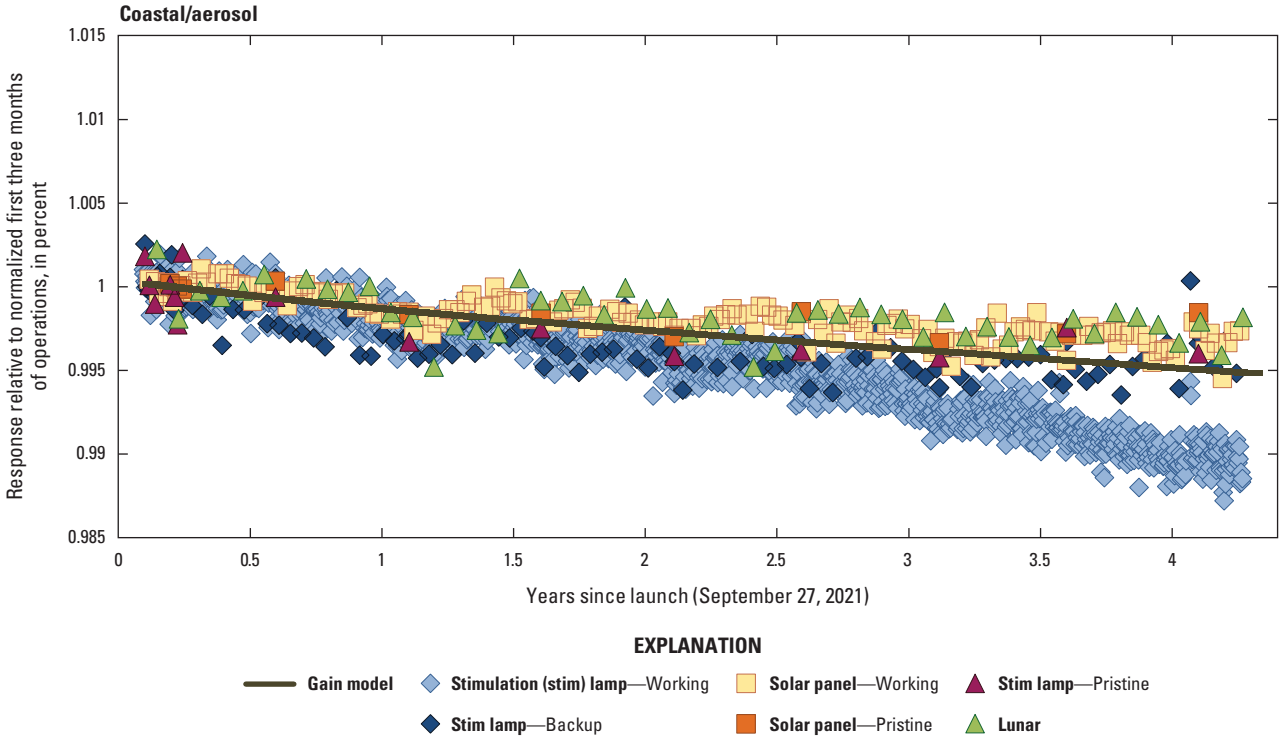

Figure 13. Graph showing Landsat 9 Operational Land Imager coastal/aerosol band lifetime radiometric stability.

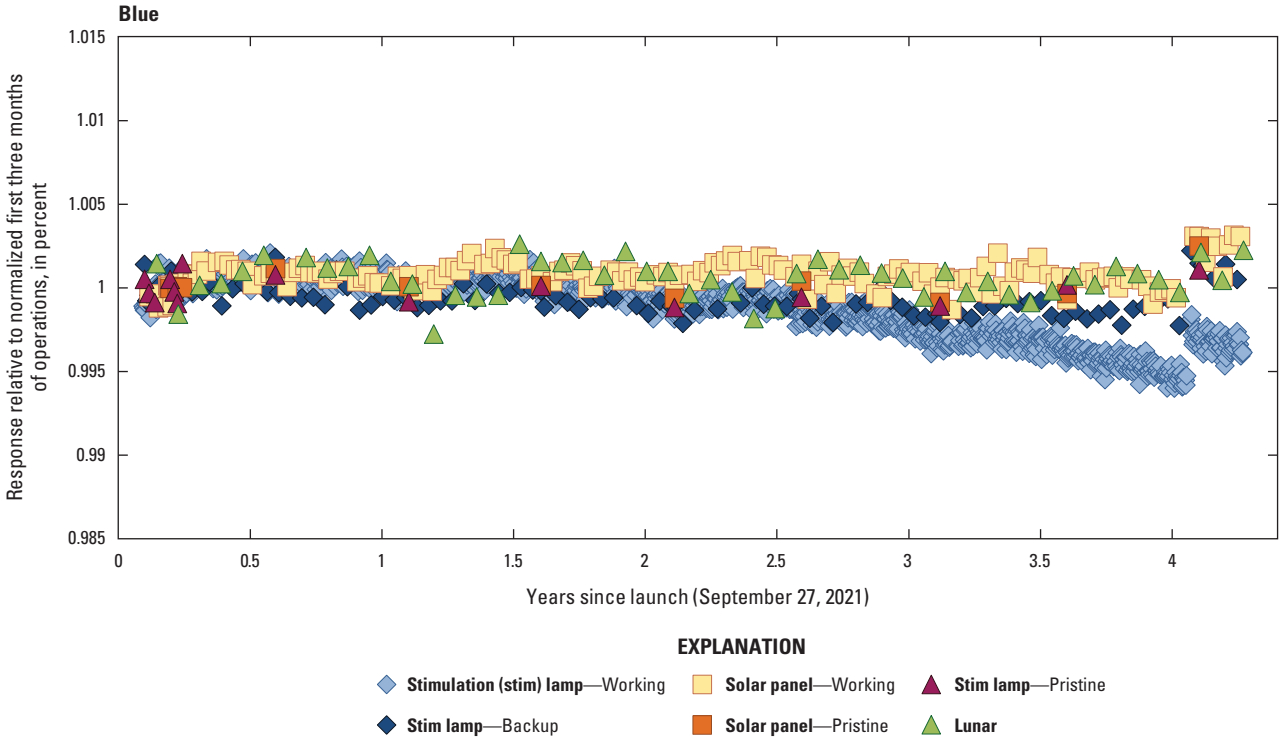

Figure 14. Graph showing Landsat 9 Operational Land Imager blue band lifetime radiometric stability.

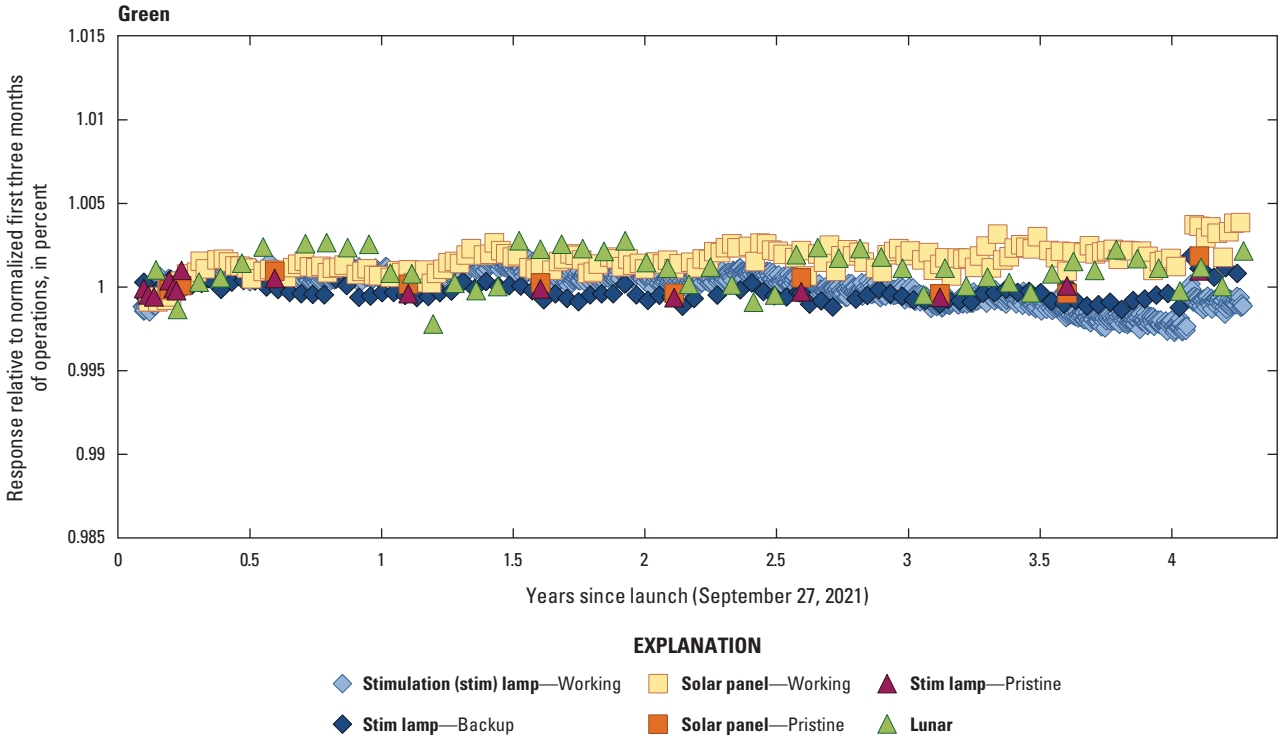

Figure 15. Graph showing Landsat 9 Operational Land Imager green band lifetime radiometric stability.

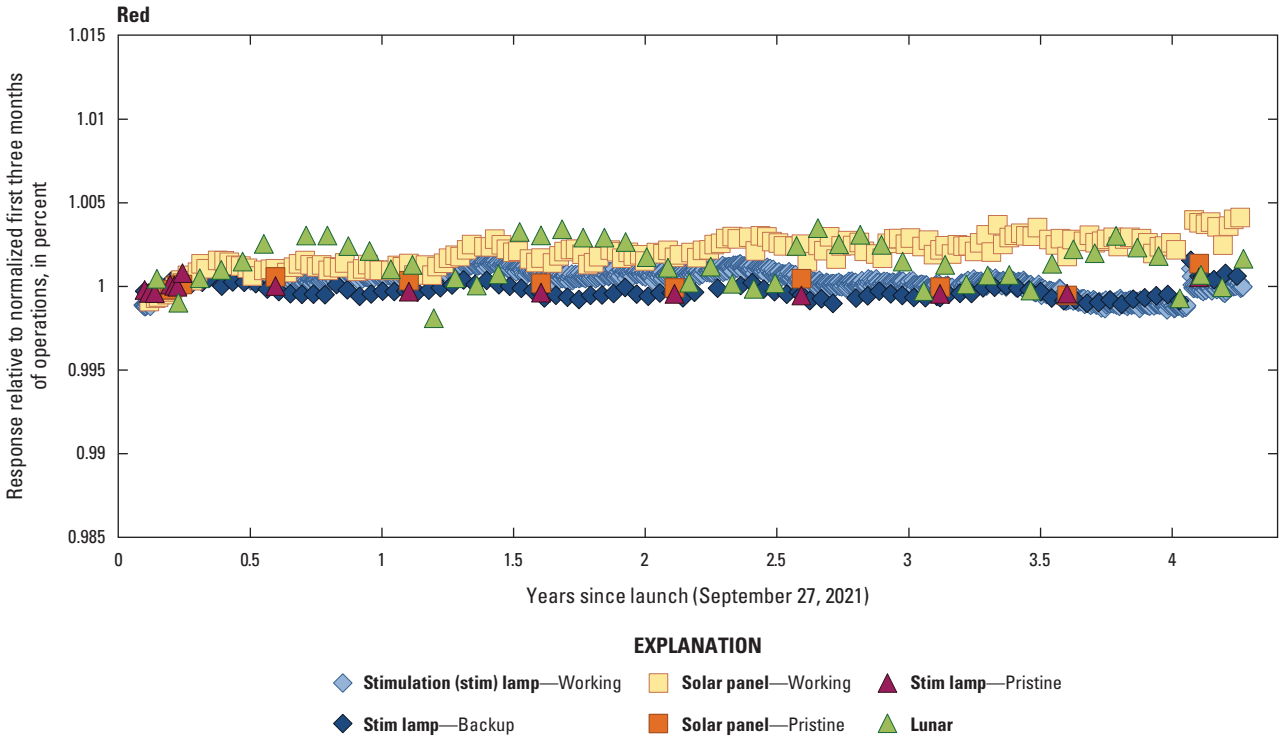

Figure 16. Graph showing Landsat 9 Operational Land Imager red band lifetime radiometric stability.

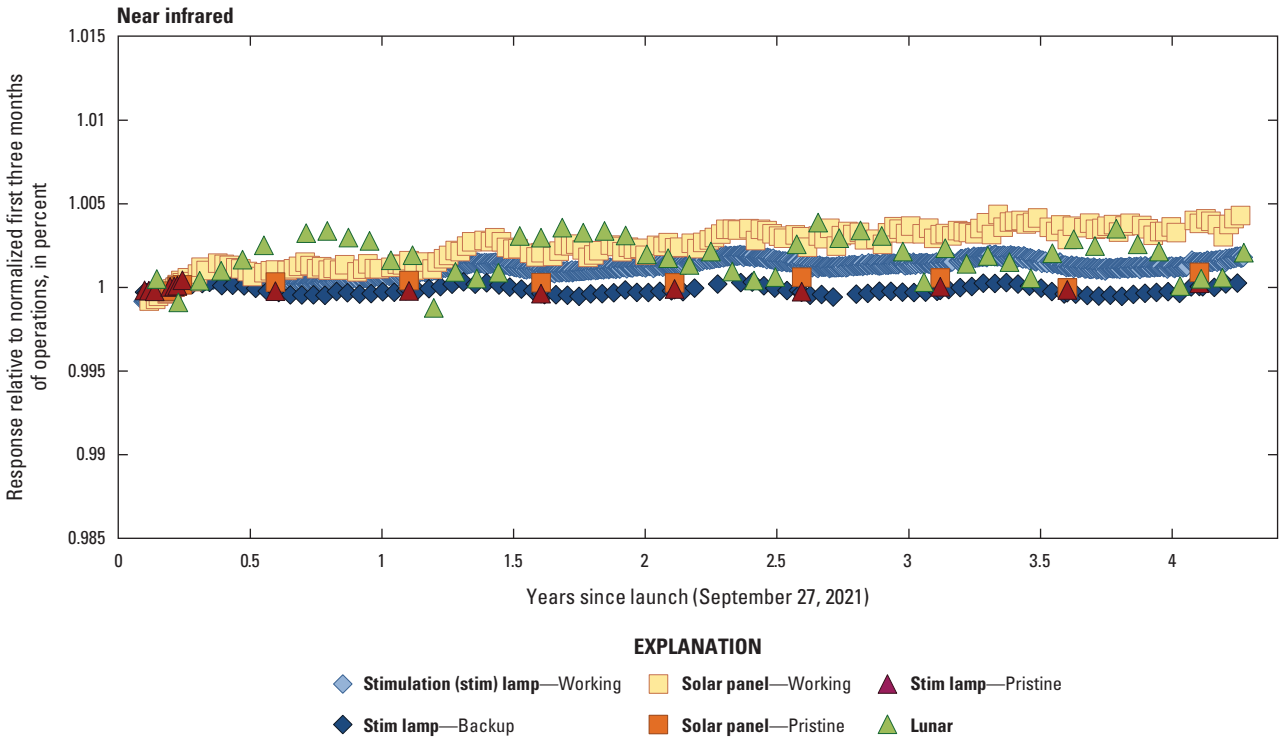

Figure 17. Graph showing Landsat 9 Operational Land Imager near infrared band lifetime radiometric stability.

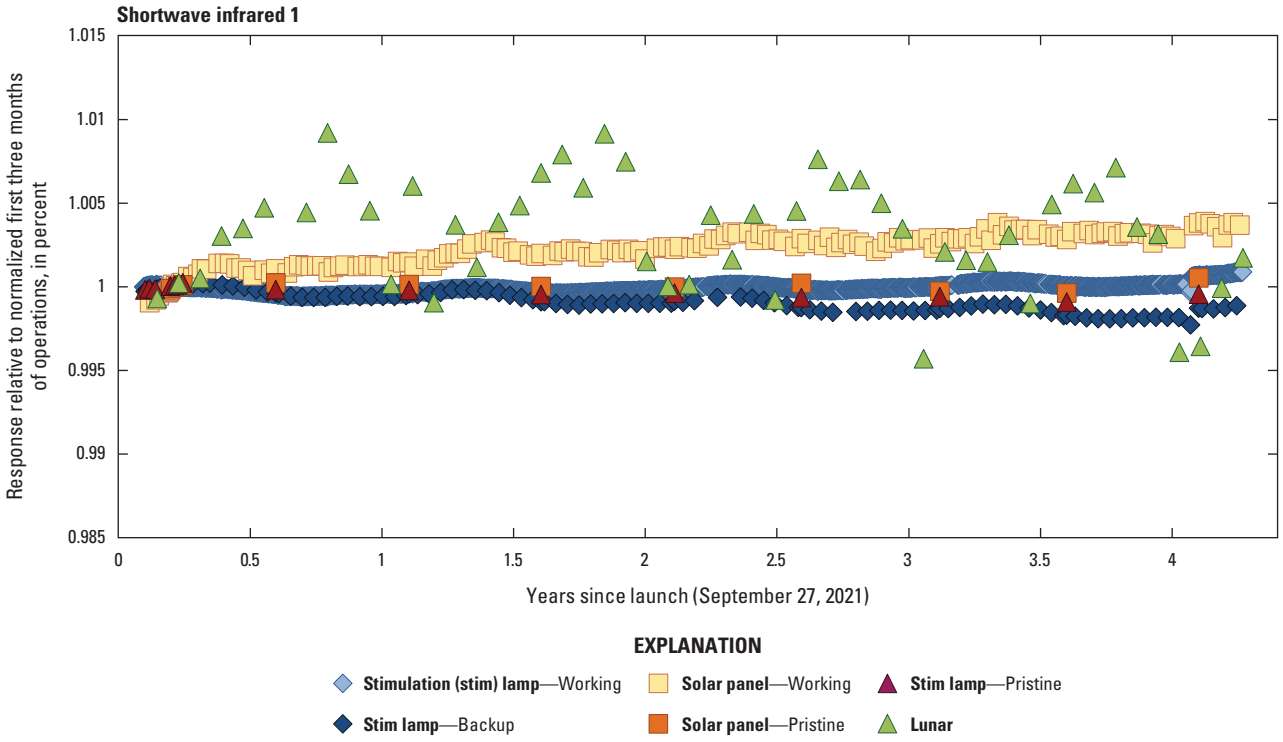

Figure 18. Graph showing Landsat 9 Operational Land Imager shortwave infrared 1 band lifetime radiometric stability.

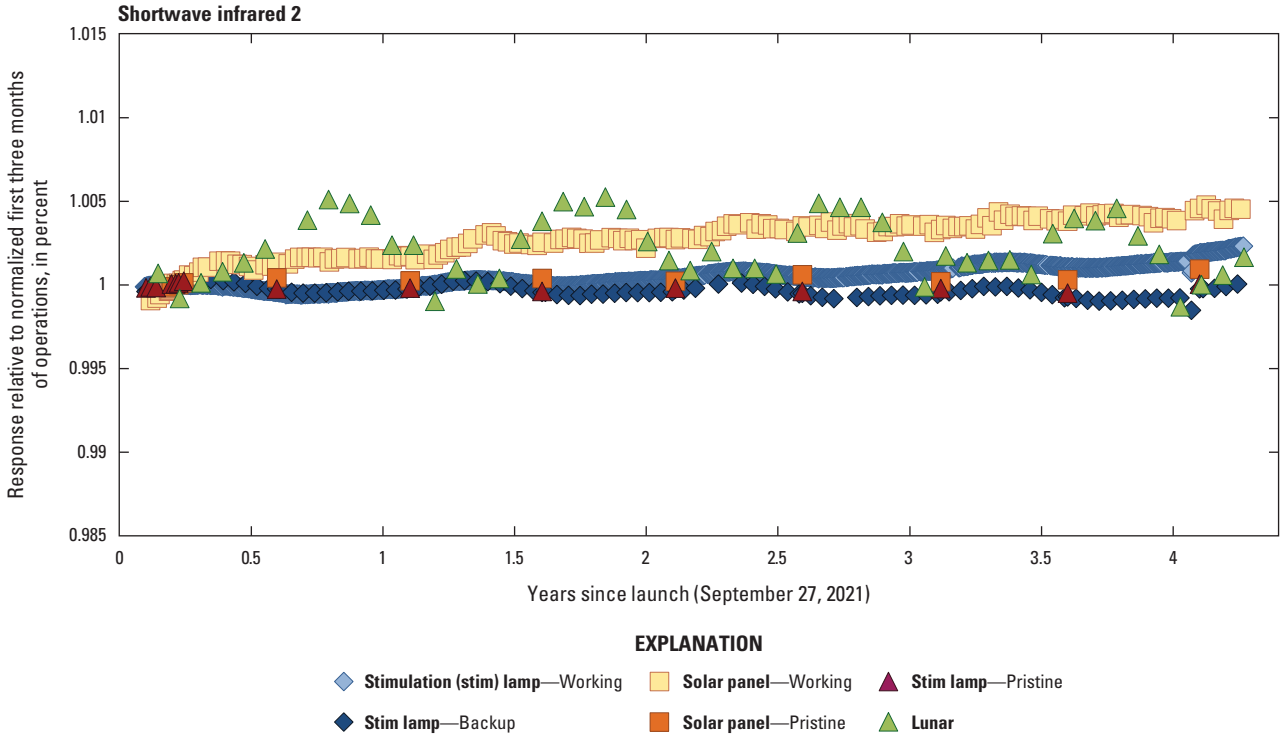

Figure 19. Graph showing Landsat 9 Operational Land Imager shortwave infrared 2 band lifetime radiometric stability.

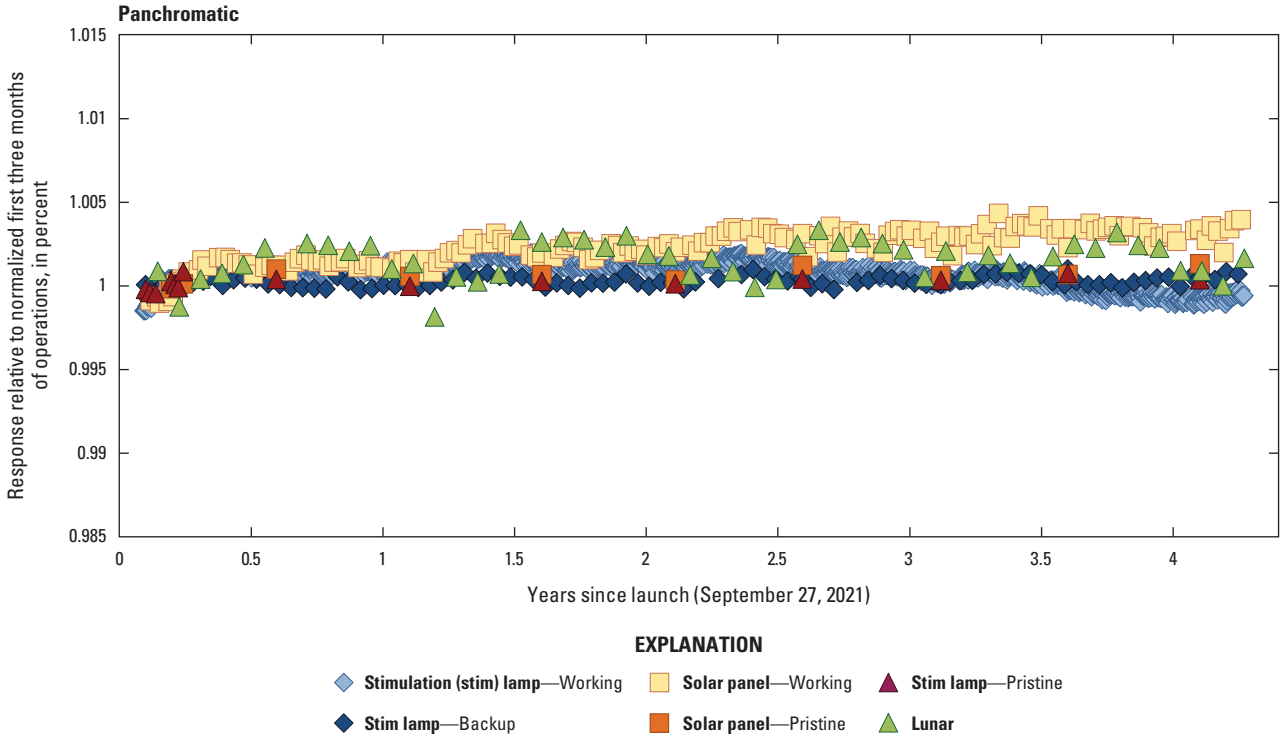

Figure 20. Graph showing Landsat 9 Operational Land Imager panchromatic band lifetime radiometric stability.

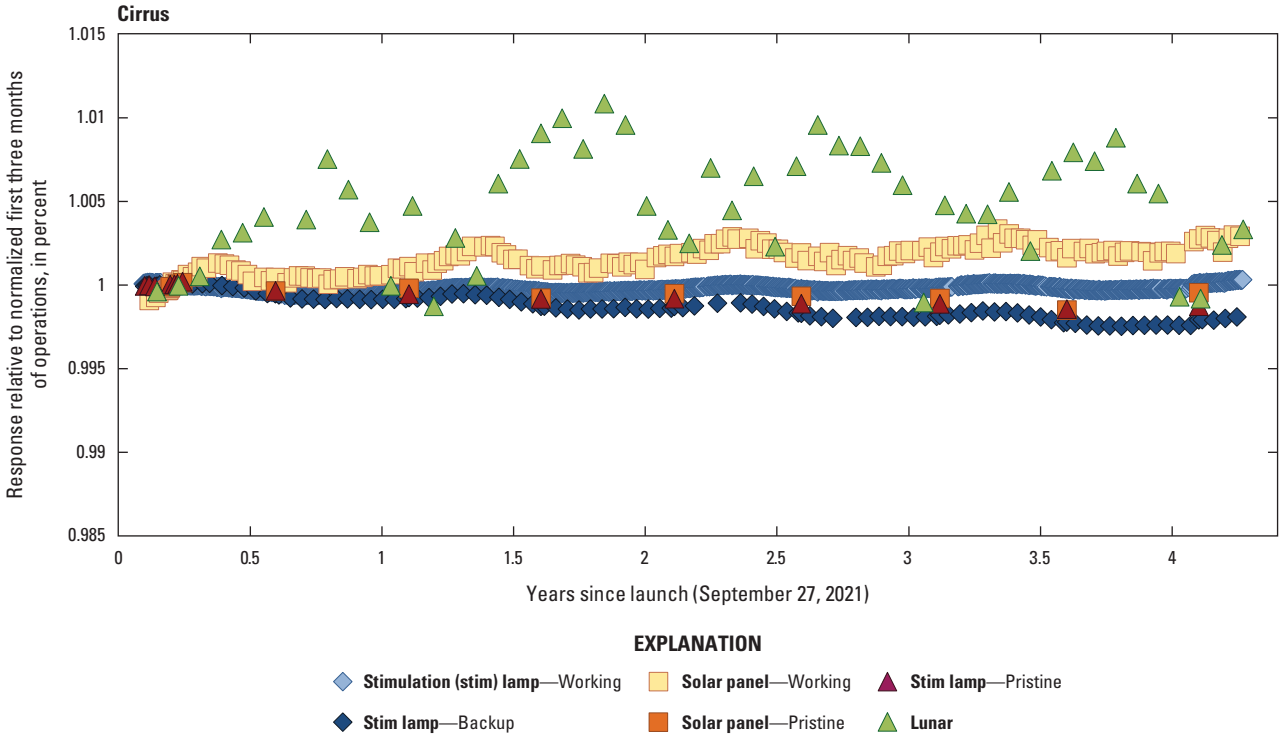

Figure 21. Graph showing Landsat 9 Operational Land Imager cirrus band lifetime radiometric stability.

0.43 percent for bands 10 and 11, respectively (Haque and others, 2024). This change is corrected during data product generation and is transparent to the data users. After the reset event, there has been a slight degradation in TIRS responsivity over time, and an update to the band-average absolute gain parameters in the CPF was released for quarter 3, 2025, as shown in figures 22 and 23. This CPF update corrected a 0.36 and 0.55 percent post-reset event degradation for bands 10 and 11, respectively.

Landsat 9 Relative Gains

Relative gains account for the differences in responsivity between detectors within a spectral band. OLI relative gains are monitored using solar diffuser acquisitions, side slither acquisitions (which entail a 90-degree yaw maneuver over an invariant site to flatten the data), and scene statistics. Quarterly updates are completed using data from the solar diffuser acquisitions from the previous quarter (quarter 3, 2025).

Typical per-detector changes in relative gains between the previous quarter (quarter 3, 2025) and this quarter (quarter 4, 2025) for several bands are shown in figures 24, 25, 26, and 27 by analyzing data from within each quarter. In each figure, the x-axis indicates the detector index, and the y-axis indicates the change in relative gain between quarter 3 and quarter 4 as a ratio. These changes in responsivity are accounted for in the L1 product by updating the following quarter's CPF.

The Landsat 9 OLI detectors that have indicated a sudden change in responsivity of 0.5 percent or greater in the shortwave infrared (SWIR) 1 and SWIR 2 bands since launch are shown in figures 28 and 29. The x-axis indicates the date of the jump in responsivity, and the y-axis signifies the detector number. The observed responsivity jumps seem to be randomly scattered in time and location on the focal plane and do not seem to be associated with an instrument event or failure. These jumps are only observed in the SWIR bands (SWIR 1, SWIR 2, and cirrus); the visible and near infrared band detectors have not indicated any jump behavior over the whole mission.

Landsat 9 to Landsat 8 Operational Land Imager Radiometric Cross Comparison

The instruments onboard Landsat 9 are improved replicas of those currently collecting data onboard Landsat 8. Landsat 9 improvements include higher OLI radiometric resolution with a 14-bit quantization, increased from 12 bits for Landsat 8 (USGS, 2019b). Cross comparison quantitative analysis between the Landsat 9 and Landsat 8 L1 TOA reflectance acquisitions over a pseudoinvariant calibration site (PICS) is performed to determine interoperability between Landsat 9 OLI and Landsat 8 OLI.

The TOA reflectance values observed over the Libya 4 PICS site (lat 28.55° N., long 23.39° E.) using the Centre National D'Etudes Spatiales (CNES) region of interest are shown in figure 30. The reflectance measurements indicate good agreement between both sensors, and the similar trends by both sensors indicate consistent calibration.

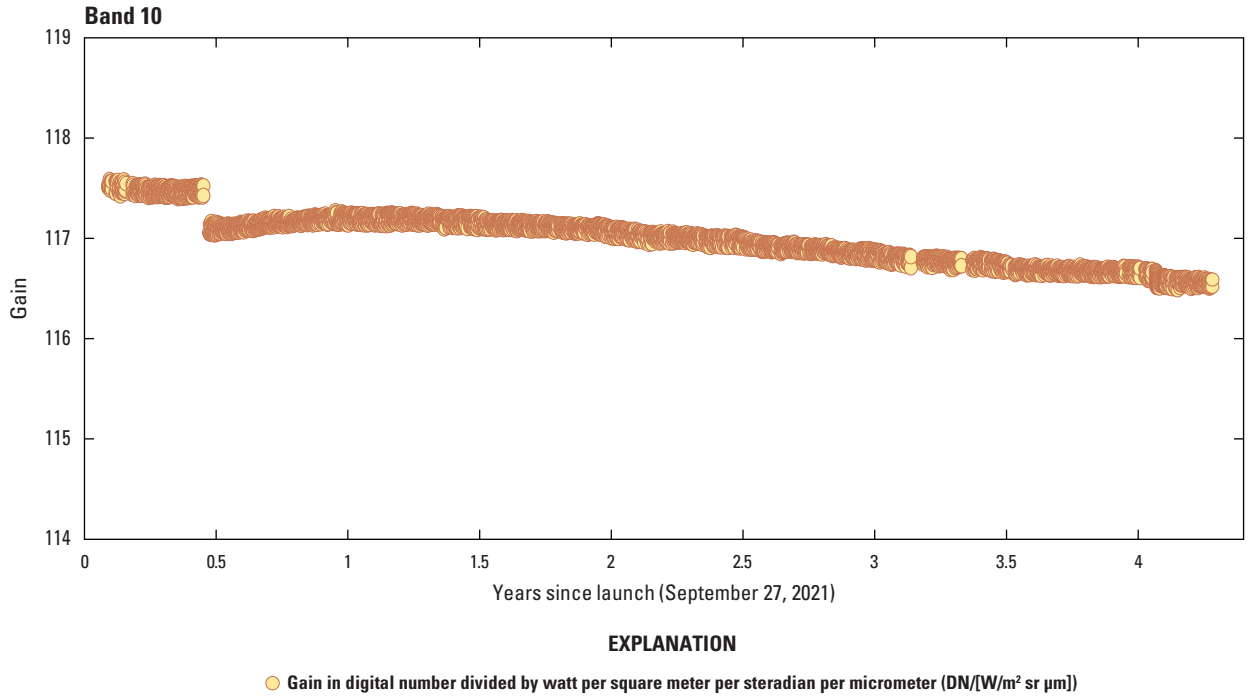

Figure 22. Graph showing Landsat 9 Thermal Infrared Sensor band 10 lifetime radiometric stability.

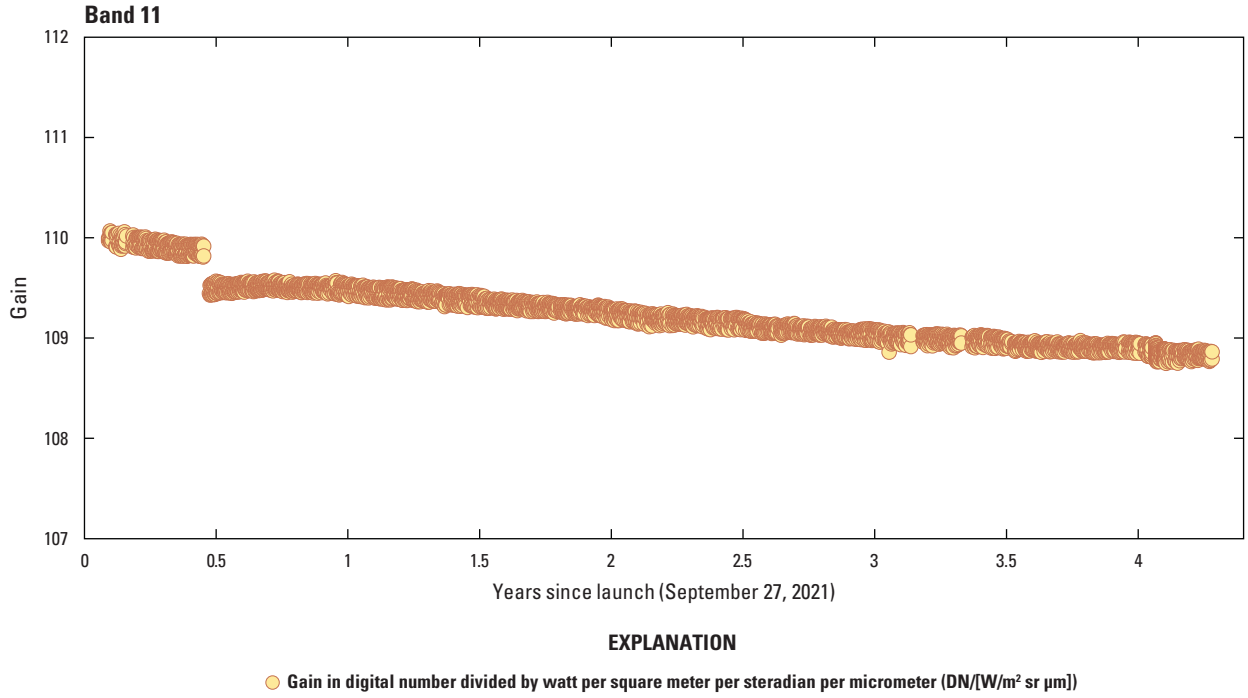

Figure 23. Graph showing Landsat 9 Thermal Infrared Sensor band 11 lifetime radiometric stability.

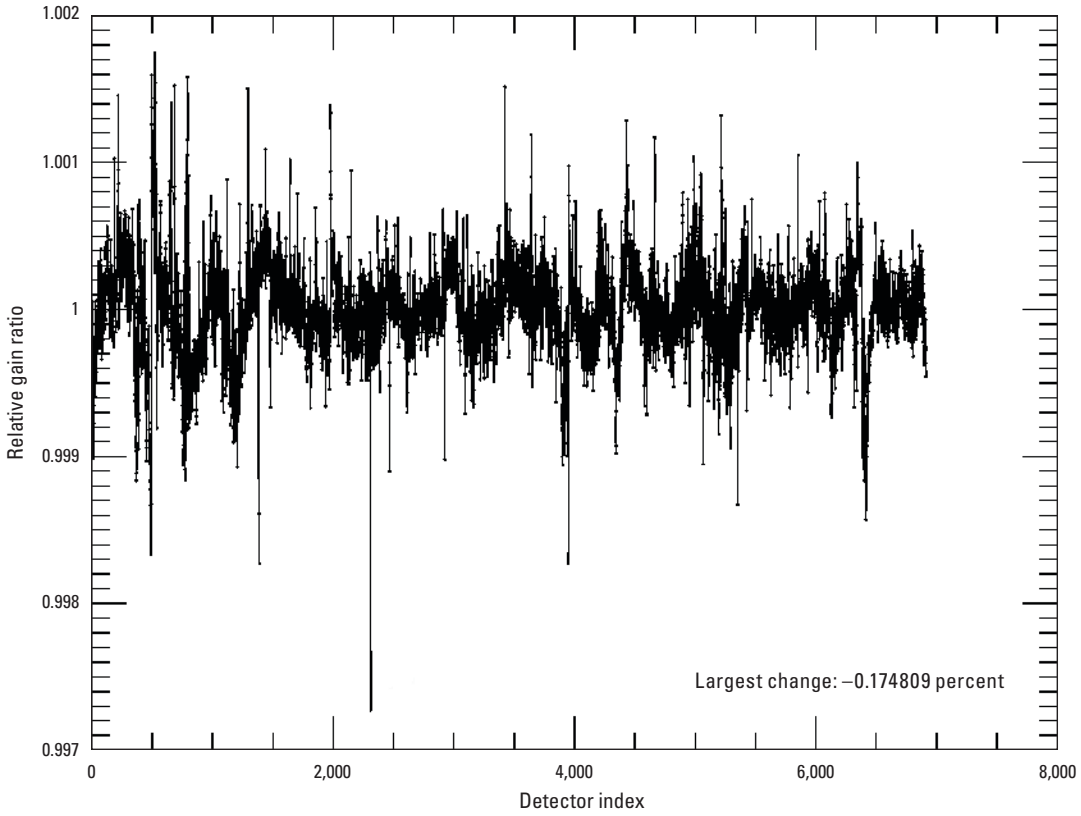

Figure 24. Graph showing Landsat 9 Operational Land Imager coastal/aerosol band per-detector change in relative gains between quarter 3 (July–September) and quarter 4 (October–December), 2025.

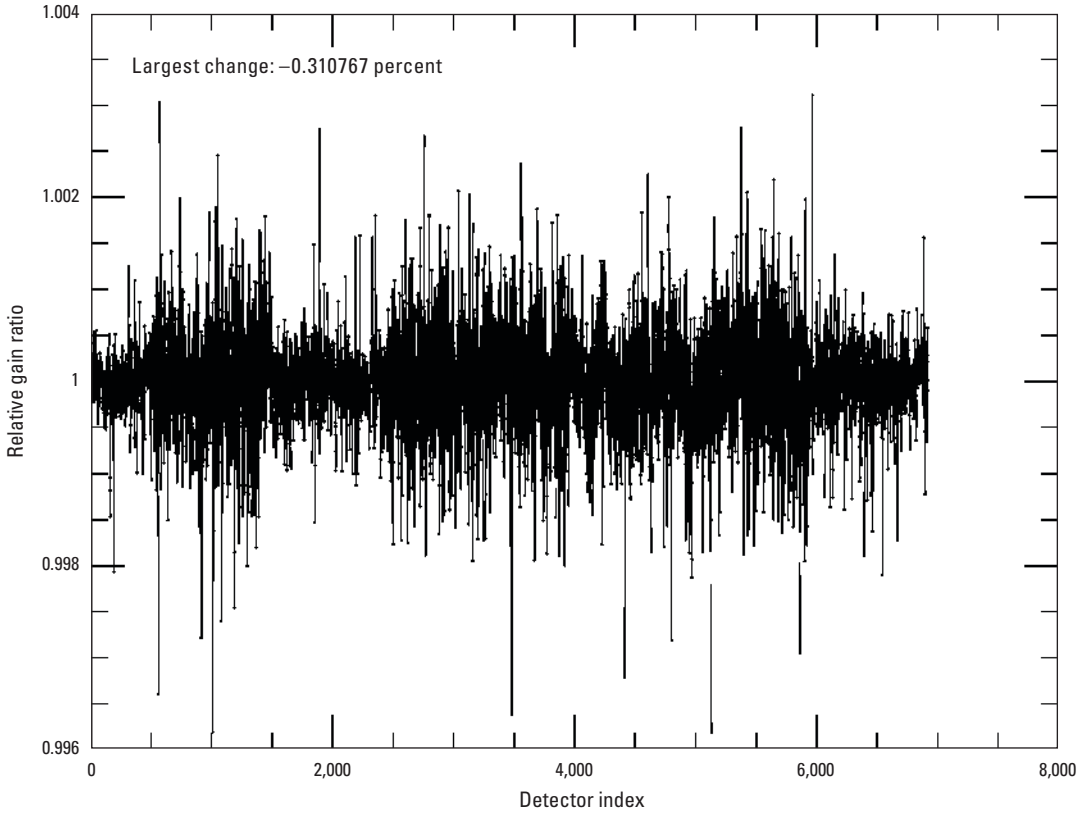

Figure 25. Graph showing Landsat 9 Operational Land Imager shortwave infrared 1 band per-detector change in relative gains between quarter 3 (July–September) and quarter 4 (October–December), 2025.

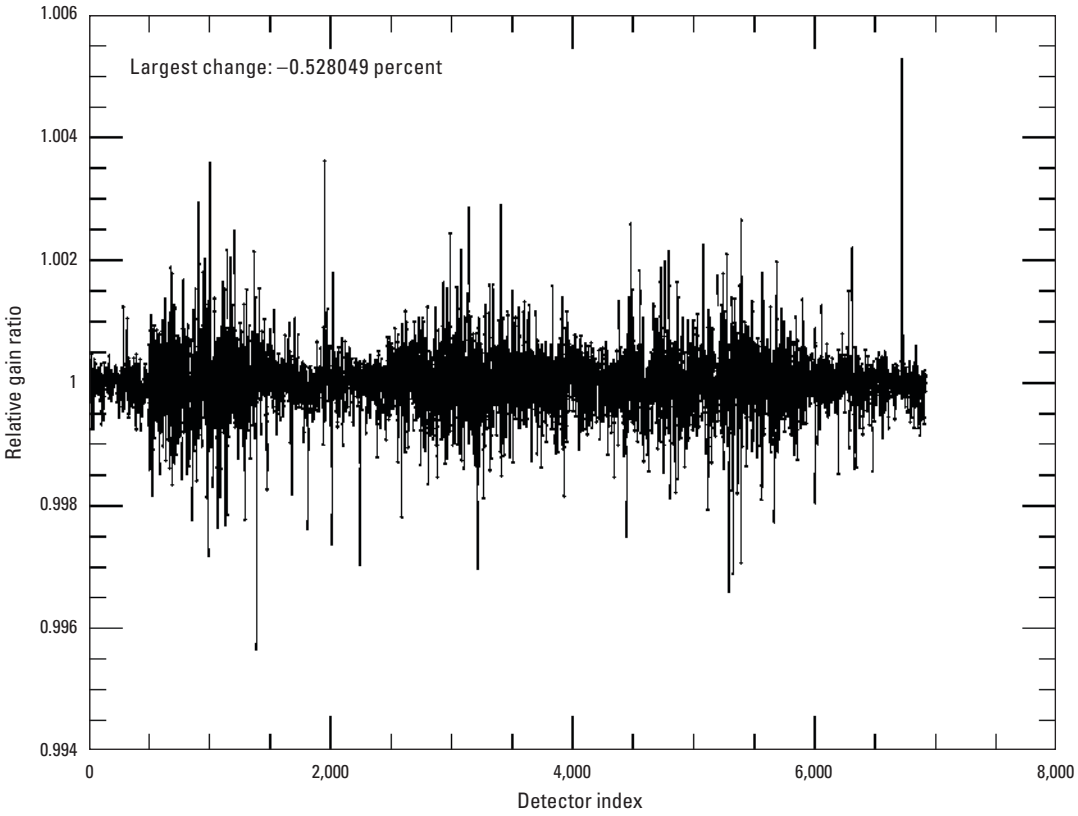

Figure 26. Graph showing Landsat 9 Operational Land Imager shortwave infrared 2 band per-detector change in relative gains between quarter 3 (July–September) and quarter 4 (October–December), 2025.

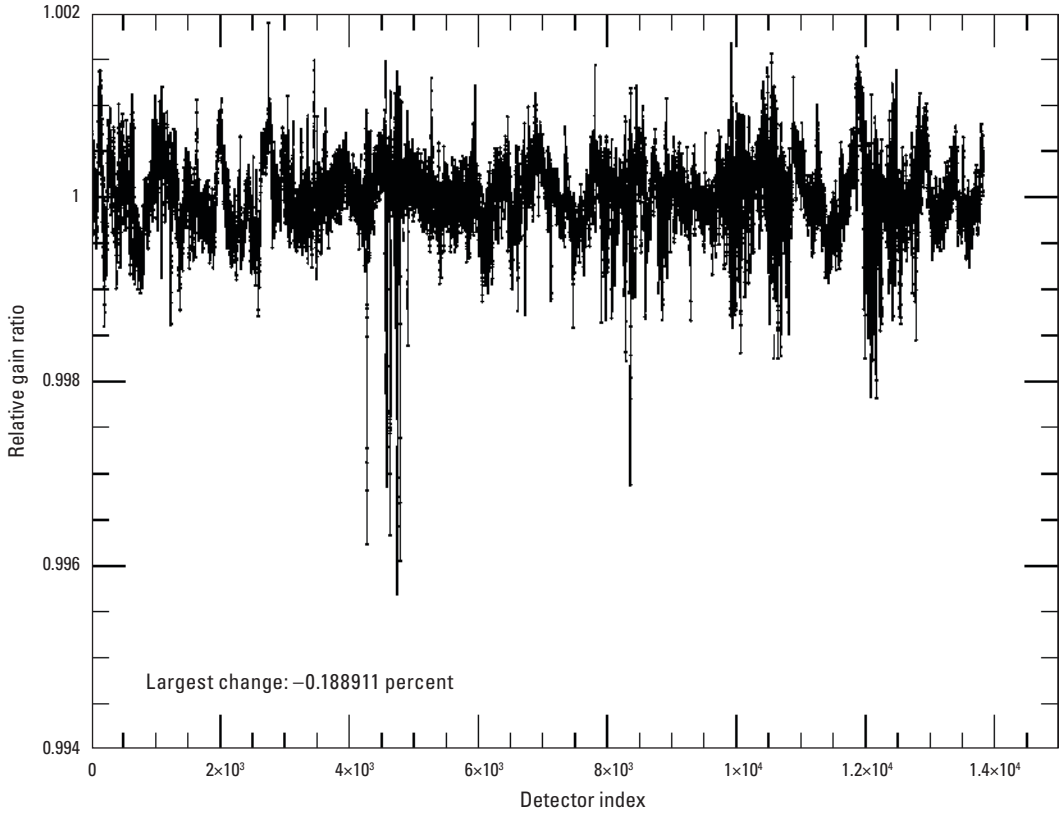

Figure 27. Graph showing Landsat 9 Operational Land Imager panchromatic band per-detector change in relative gains between quarter 3 (July–September) and quarter 4 (October–December), 2025.

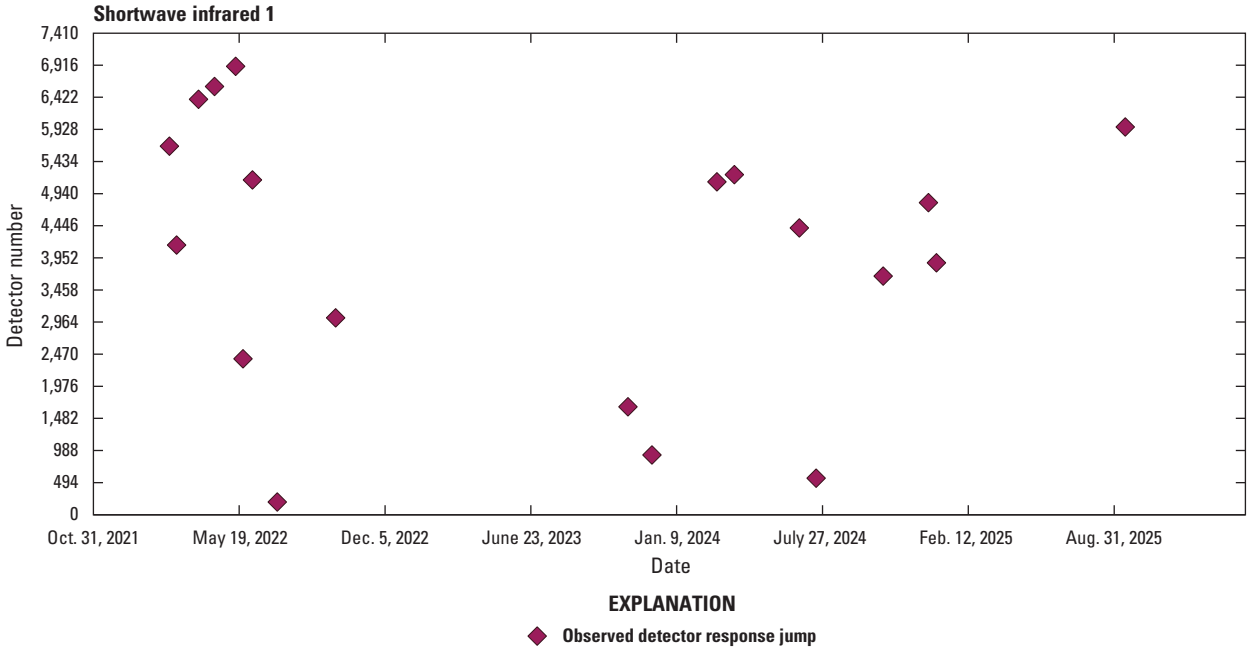

Figure 28. Graph showing Landsat 9 Operational Land Imager shortwave infrared 1 lifetime jumps in detector responsivity.

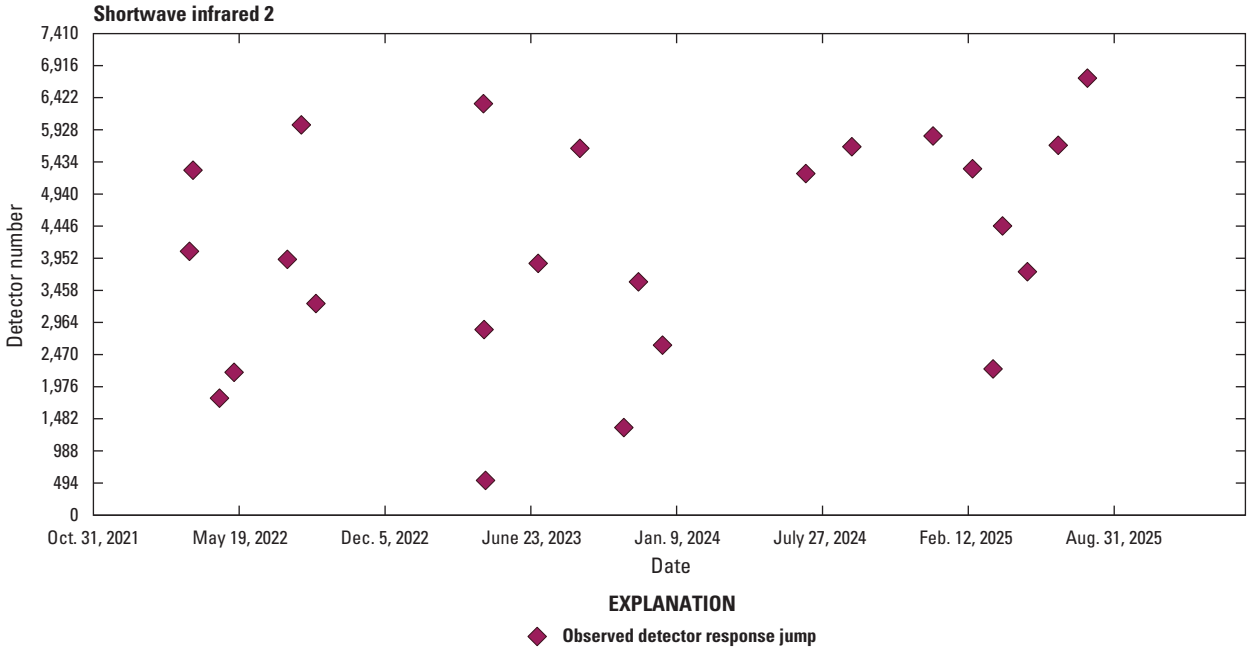

Figure 29. Graph showing Landsat 9 Operational Land Imager shortwave infrared 2 lifetime jumps in detector responsivity.

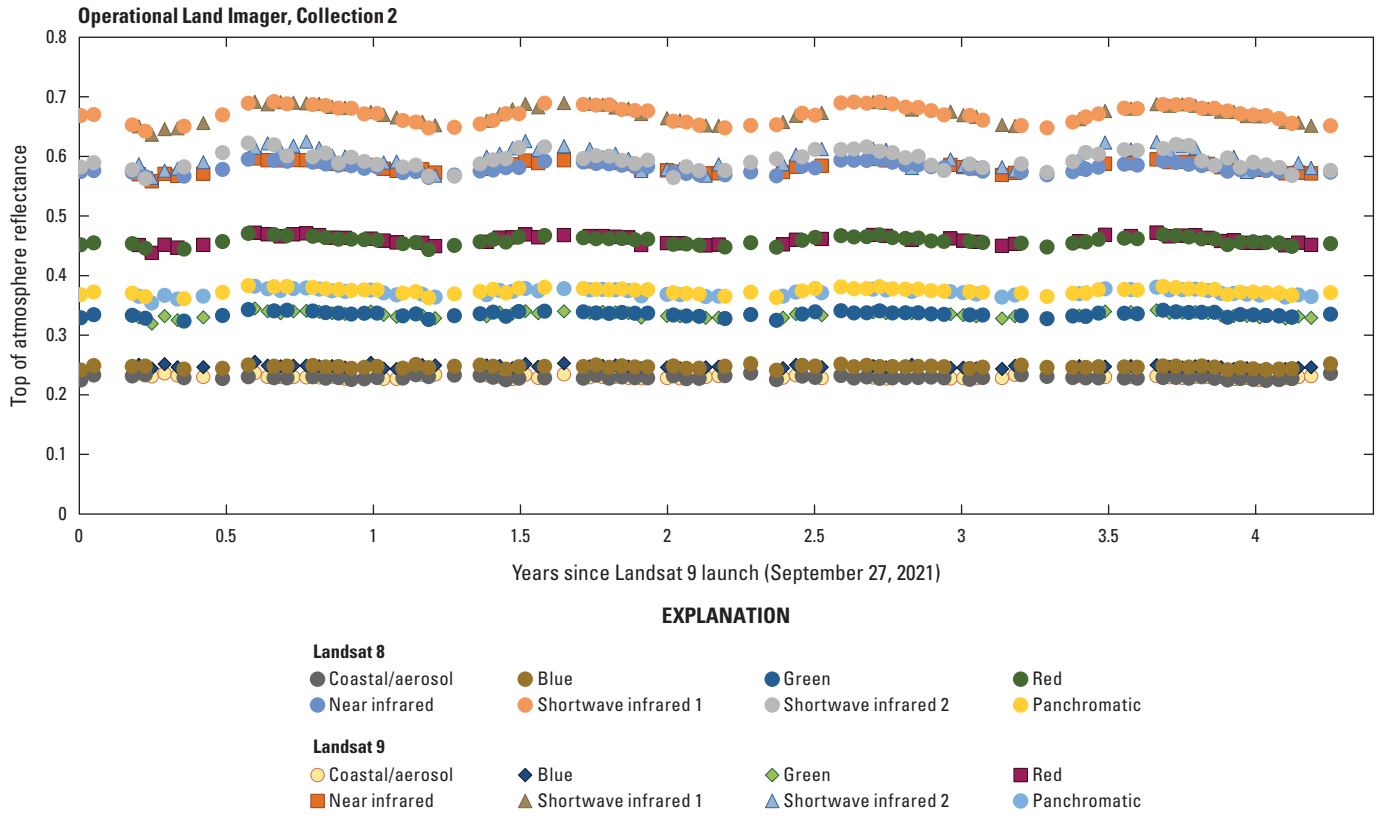

Figure 30. Graph showing Landsat 9 to Landsat 8 Operational Land Imager Libya 4 pseudoinvariant calibration site top of atmosphere reflectance cross comparison.

Landsat 9 Geometric Performance Summary

The Landsat 9 on-orbit geometric performance for the reporting quarter (quarter 4, 2025) meets all requirements as outlined in USGS (2022). The quarterly results summary is provided in table 4.

Landsat 9 Band Registration Accuracy

Internal band registration measures how accurately the various Landsat 9 spectral bands are geometrically aligned to each other. The assessment provides a numerical evaluation of the accuracy of the band registration within an image using automated cross correlation techniques between the bands to be assessed (USGS, 2021c).

Landsat 9 OLI band registration performance has been stable over time. Quarterly band-to-band maximum registration accuracy for each band combination except for the cirrus band is shown in figure 31. Within the figure, blue bars indicate maximum registration accuracy in the line direction, and green bars indicate maximum registration accuracy in the sample direction. Lifetime OLI band registration accuracy for all bands is 4.44 meters (not shown), and lifetime OLI band registration accuracy for all bands, excluding cirrus, is 3.18 meters, which is well within the instrument specification accuracy. OLI band registration accuracy for all bands during quarter 4, 2025, is 4.21 meters, and OLI band registration accuracy for all bands, excluding the cirrus band, during quarter 4, 2025, is 3.28 meters (table 4).

TIRS band registration performance has been stable throughout the instrument's lifetime. Behavior is well within specification, as shown in figure 32, and quarter 4, 2025, results are consistent with past performance. Within the figure, blue bars indicate maximum registration accuracy in the line direction, and green bars indicate maximum registration accuracy in the sample direction. Lifetime TIRS band registration accuracy is 8.8 meters, and during quarter 4, 2025, the accuracy is 8.7 meters.

Lifetime TIRS to OLI band registration accuracy by quarter is shown in figure 33. Behavior has been stable throughout the instrument's lifetime and well within specification. Within the figure, blue bars indicate maximum registration accuracy in the line direction, and green bars indicate maximum registration accuracy in the sample direction. Lifetime TIRS to OLI registration accuracy (excluding the cirrus band) is 18.2 meters in the line direction and 18.1 meters in the sample direction. Quarter 4, 2025, TIRS to OLI registration accuracy (excluding the cirrus band) is 18.3 meters in the line direction and 18.6 meters in the sample direction.

Table 4. Landsat 9 geometric performance summary, quarter 4 (October–December), 2025.

[The previous quarter is quarter 3 (July–September), 2025. OLI, Operational Land Imager; <, less than; LE90, linear error with 90 percent confidence; CE90, circular error with 90 percent confidence; L1T, Level 1 terrain-corrected product; >, greater than; TIRS, Thermal Infrared Sensor]

Requirement	Measured value from this quarter	Measured value from previous quarter[1]	Required value	Unit
OLI band registration accuracy (all bands)	4.21	4.40	<4.5	Meter (LE90)
OLI band registration accuracy (no cirrus)	3.28	3.24	<4.5	Meter (LE90)
Absolute geodetic accuracy	21.72	18.51	<65	Meter (CE90)
Relative geodetic accuracy	7.7	7.7	<25	Meter (CE90)
Geometric (L1T) accuracy	3.5	3.3	<12	Meter (CE90)
OLI edge slope	0.030	0.029	>0.027	1 per meter
TIRS band registration accuracy	8.7	8.9	<18	Meter (LE90)
TIRS to OLI registration accuracy	18.6	17.9	<30	Meter (LE90)

[1]From Haque and others (2026).

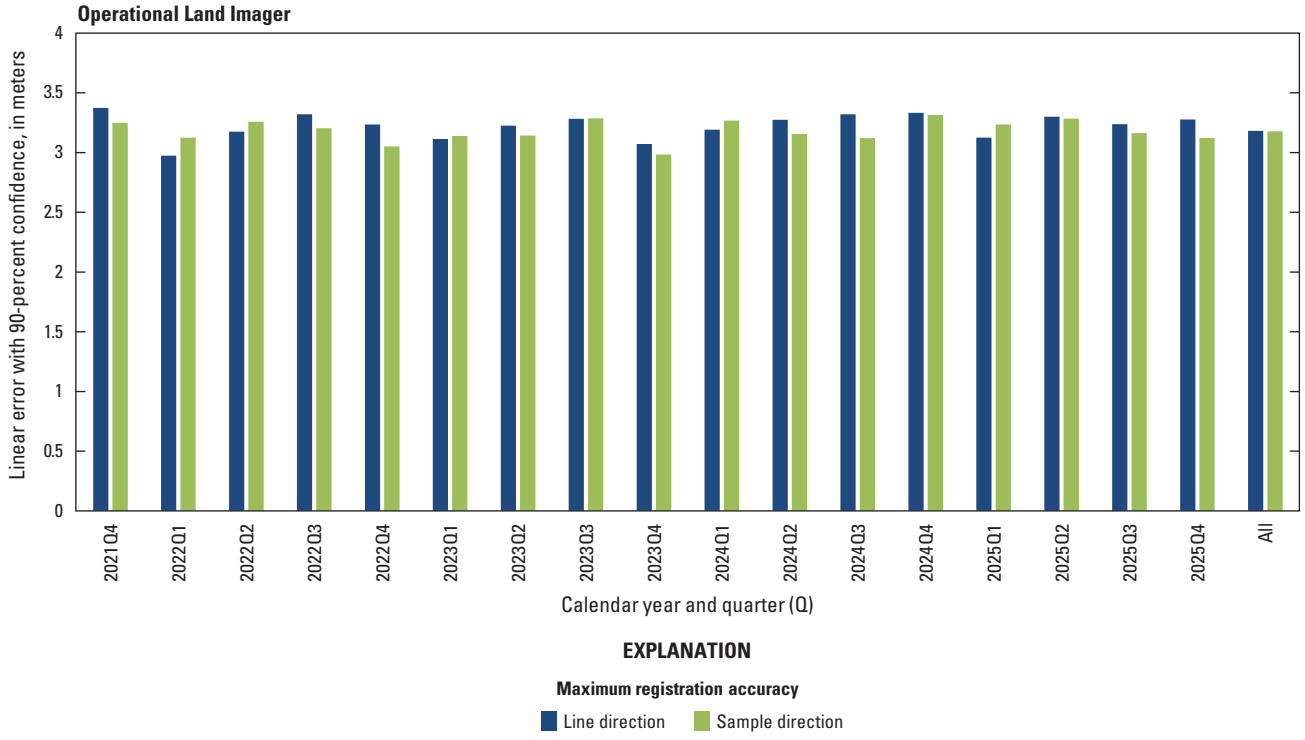

Figure 31. Graph showing Landsat 9 Operational Land Imager lifetime band (excluding cirrus) registration accuracy by quarter.

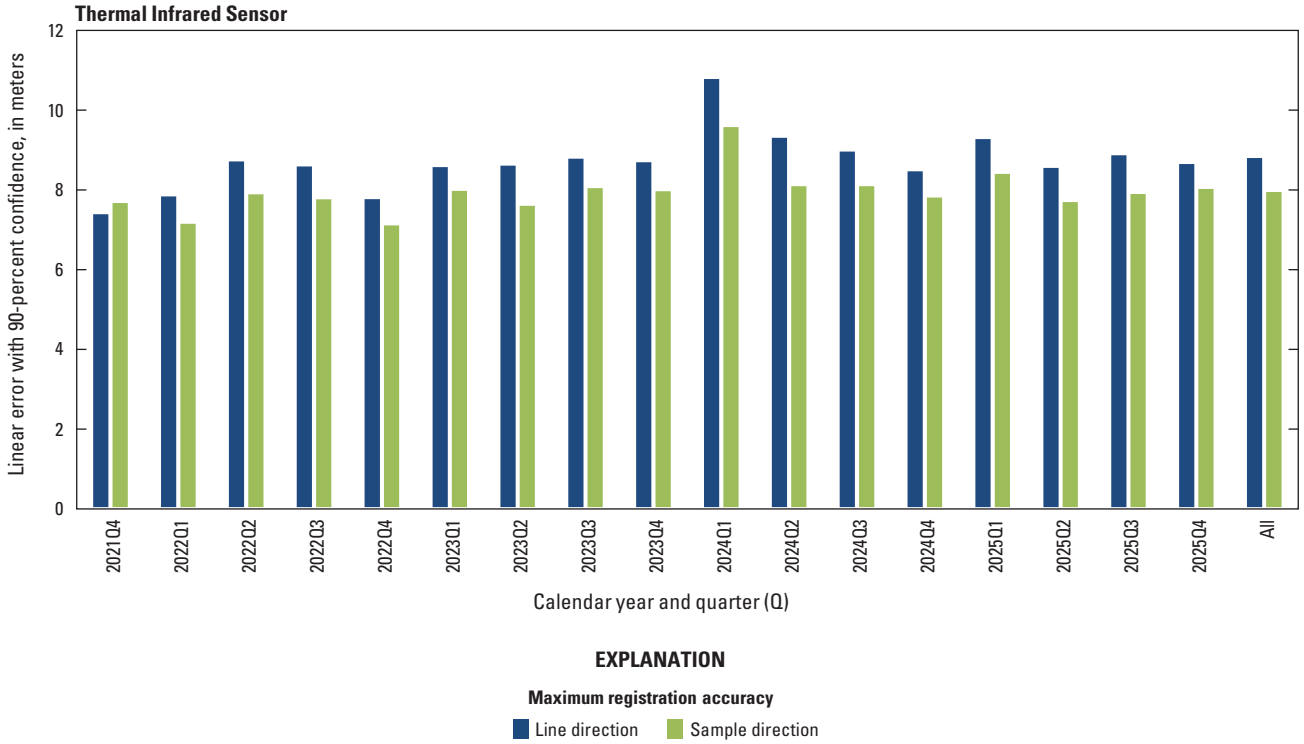

Figure 32. Graph showing Landsat 9 Thermal Infrared Sensor lifetime band registration accuracy by quarter.

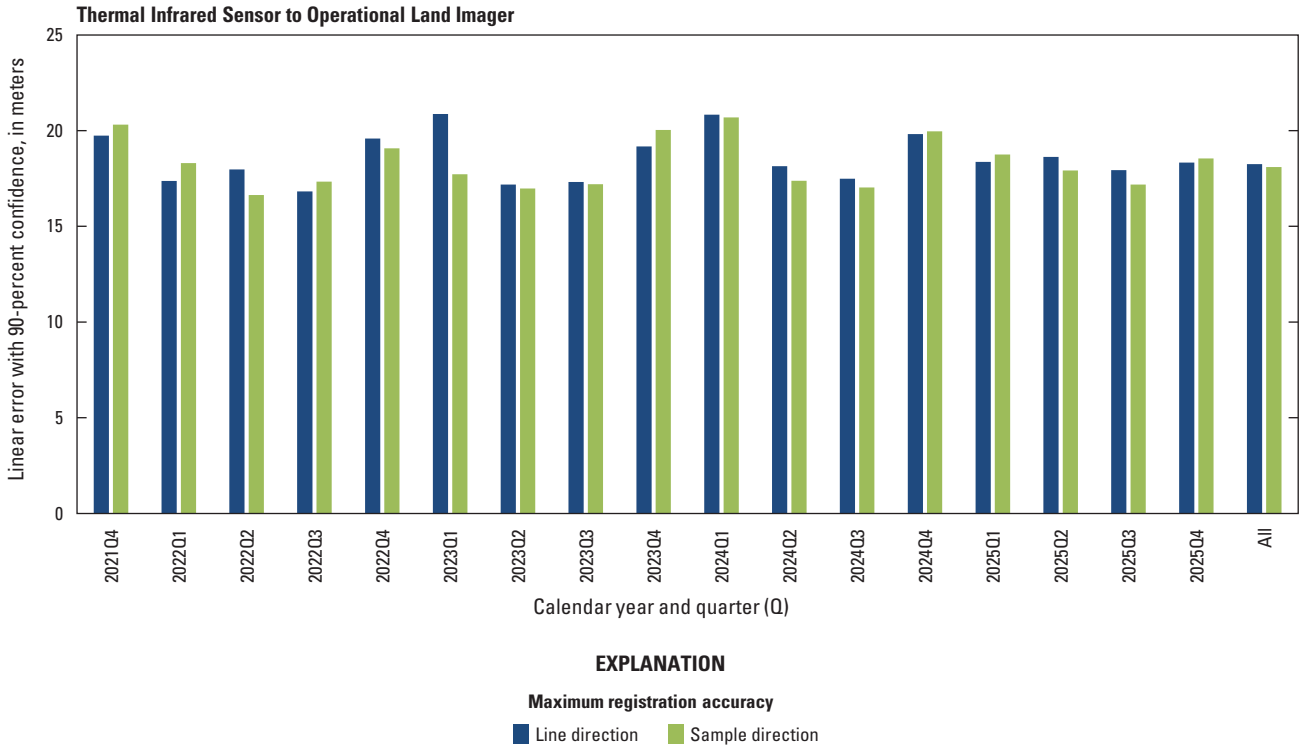

Figure 33. Graph showing Landsat 9 Thermal Infrared Sensor to Operational Land Imager lifetime band (excluding cirrus) registration accuracy by quarter.

Landsat 9 Operational Land Imager to Thermal Infrared Sensor Alignment

Landsat 9 OLI to TIRS alignment knowledge is critical to ensure that the L1 product accuracy requirements can be met. The alignment between OLI and TIRS instruments is periodically measured using correlation-based methods to ensure that the band-to-band alignment requirements for all Landsat 9 bands can be met (USGS, 2021c). The alignment estimates are used to update the calibration parameters in the CPFs when the observed changes are determined to affect the performance requirements.

TIRS to OLI pitch alignment measurements over instrument lifetimes are shown in figure 34. Although still in the early stages of the Landsat 9 mission, a seasonal pattern has been observed along with a slight downward trend. The predictive estimate for quarter 1 (January–March), 2026, was determined based on these observed trends. The lifetime TIRS to OLI roll alignment is shown in figure 35, and the lifetime TIRS to OLI yaw alignment is shown in figure 36. Each light blue symbol on these figures represents one calibration scene, the dark blue solid lines indicate quarterly alignment averages, and the orange dashed lines indicate applied Collection 2 CPF correction values.

Landsat 9 Geometric Accuracy

The Landsat 9 geometric assessment evaluates the absolute positional accuracy of the image products with respect to a ground (geometric) reference. The geometric accuracy assessment estimates the geometric error between the L1TP products and GCPs using automated cross correlation techniques (USGS, 2021c).

Based on analysis results, relative accuracy of the Collection 2 GCPs is comparable to the digital orthophoto quadrangle (DOQ) supersites, which are sites created from a mosaic of highly accurate high-resolution terrain-corrected aerial data. Comparatively, relative accuracy of the Collection 2 GCPs is substantially better than the internal consistency of the Collection 1 GCPs. Overall, results based on cloud-contaminated scenes are the primary contributor to substandard geometric accuracy from L1TP products. Lifetime quarterly geometric accuracy at a circular error with 90 percent confidence at a CE90 is shown in figure 37. Blue bars indicate the geometric accuracy estimated over DOQ supersite paths/rows (calibration sites) with cloud-free scenes, yellow bars indicate geometric accuracy estimated over supersite paths/rows with no cloud constraints using Collection 2 GCPs, and green bars indicate geometric accuracy estimated over all L1TP scenes processed in Collection 2 using Collection 2 GCPs with no cloud constraints. All results for this quarter are within the accuracy specification.

Lifetime and quarter 4, 2025, geometric accuracies for L1TP products are 3.6 and 3.5 meters when compared against cloud-free scenes over supersite paths/rows (using DOQ GCPs), 5.9 and 6.5 meters when compared against all L1TP scenes over supersite paths/rows only, and 11.1 and 11.3 meters when analyzing all the L1TP scenes processed in Collection 2, respectively. Note that seasonal effect is a factor in accuracy results.

Landsat 9 Geodetic Accuracy

The purpose of the geodetic accuracy assessment is to ensure that the Landsat 9 L0Rp data can be successfully processed into L1 systematic products that meet the system requirement of 65 meters at a CE90 horizontal accuracy. To measure the accuracy, calibration scenes are automatically correlated with data from the panchromatic band to measure the discrepancy between the known ground location and the position predicted by the OLI geometric model (USGS, 2021c).

Based on analysis results, absolute accuracy of the Collection 2 GCPs is comparable to the DOQ supersites and is substantially better compared to the Collection 1 GCPs (Rengarajan and others, 2020). Lifetime quarterly geodetic accuracy at a CE90 is shown in figure 38. Blue bars indicate the accuracy estimated using DOQ supersite paths/rows (calibration sites), and green bars indicate accuracy estimated from all L1TP scenes processed in Collection 2 using Collection 2 GCPs. As with the geometric accuracy, a wide variety of scene types (cloud-contaminated, islands, desert, snow covered, ice sheets, and so on) are the primary contributor to the substandard geodetic accuracy for Collection 2 GCP-based results. Lifetime geodetic accuracies for systematic products are 14.7 meters when compared using DOQ GCPs over supersites and 26.1 meters when compared using Collection 2 GCPs over all the scenes processed in Collection 2, respectively.

Geodetic accuracy is a direct indicator of sensor pointing performance. Therefore, any systematic bias observed in geodetic accuracy—particularly when examined in the along-track and (or) across-track components of the geodetic trends—is typically attributed to residual sensor misalignment. When such biases are identified, sensor alignment updates are evaluated and, if warranted, incorporated into the quarterly CPF updates to mitigate these effects in a timely manner.

During the early mission lifetime of Landsat 9, following approximately 1 year of operations, a focused reprocessing campaign was conducted covering the period from quarter 1, 2022, through quarter 4, 2022. As part of this effort, sensor alignment updates were applied to the affected quarters to reduce alignment-related geodetic biases identified in the lifetime trending analysis. Subsequent monitoring indicated the emergence of a small but measurable bias in the along-track direction, and a sensor alignment update was issued beginning in quarter 1, 2023, to mitigate this effect.

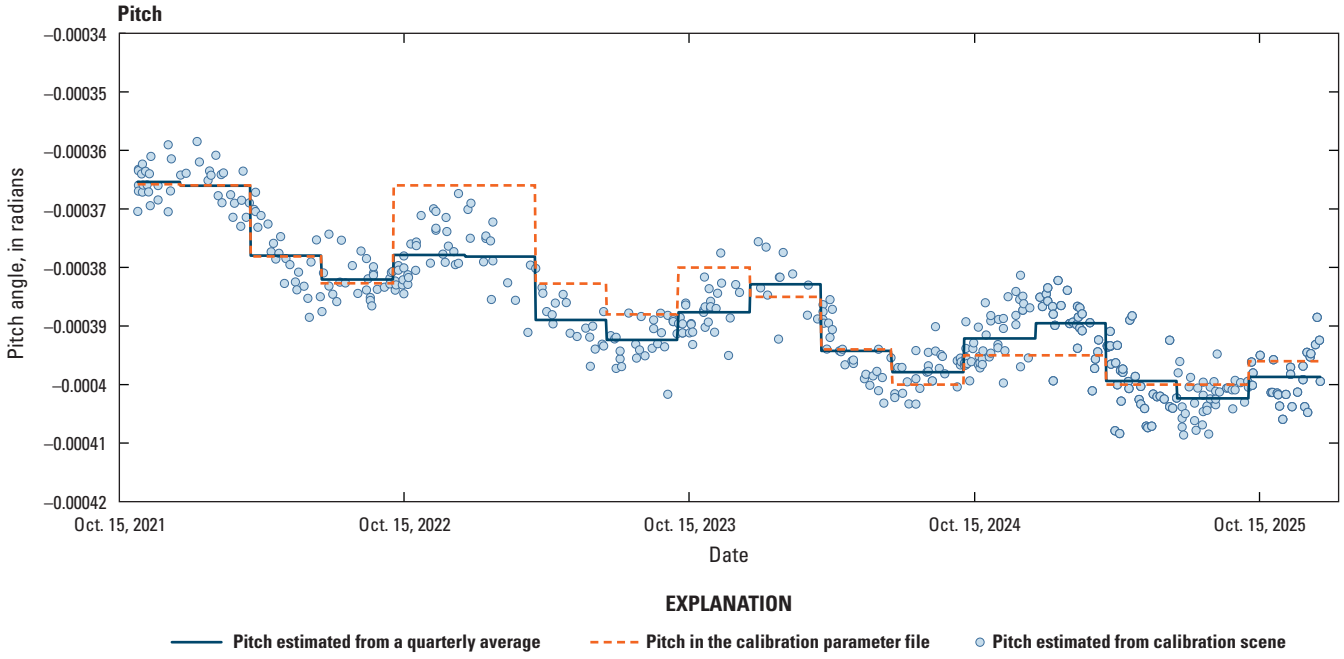

Figure 34. Graph showing Landsat 9 Thermal Infrared Sensor to Operational Land Imager lifetime pitch alignment.

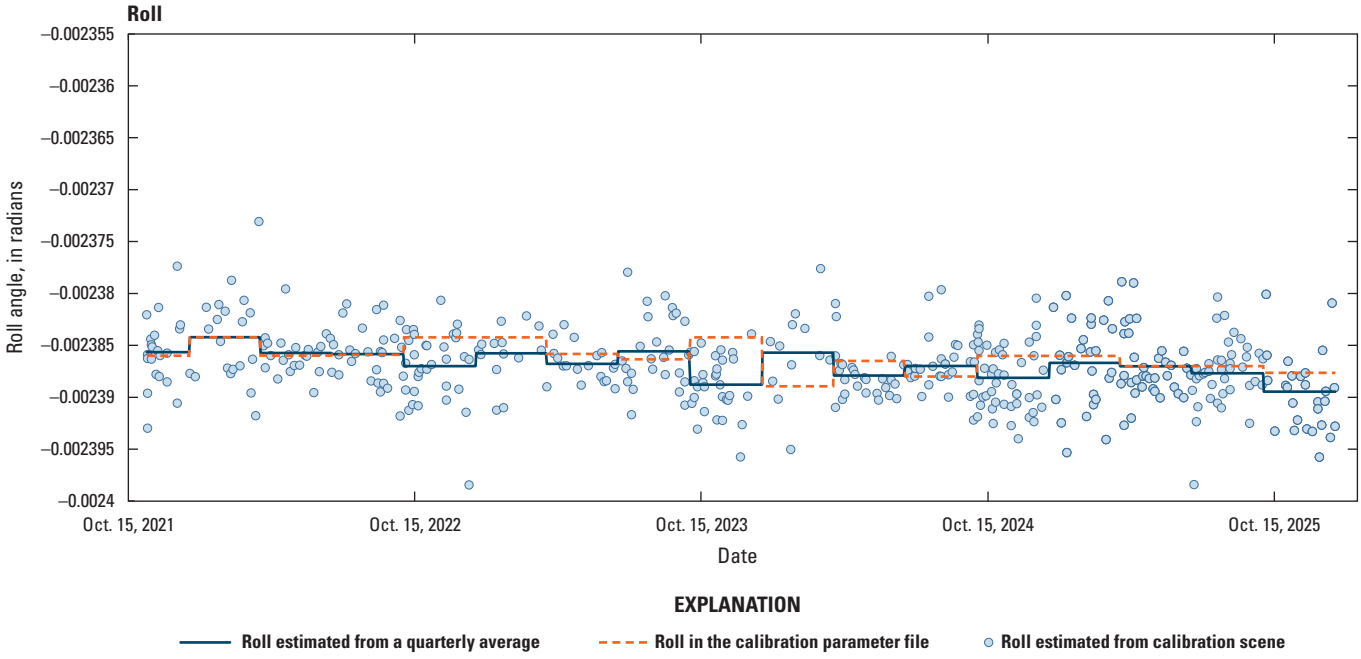

Figure 35. Graph showing Landsat 9 Thermal Infrared Sensor to Operational Land Imager lifetime roll alignment.

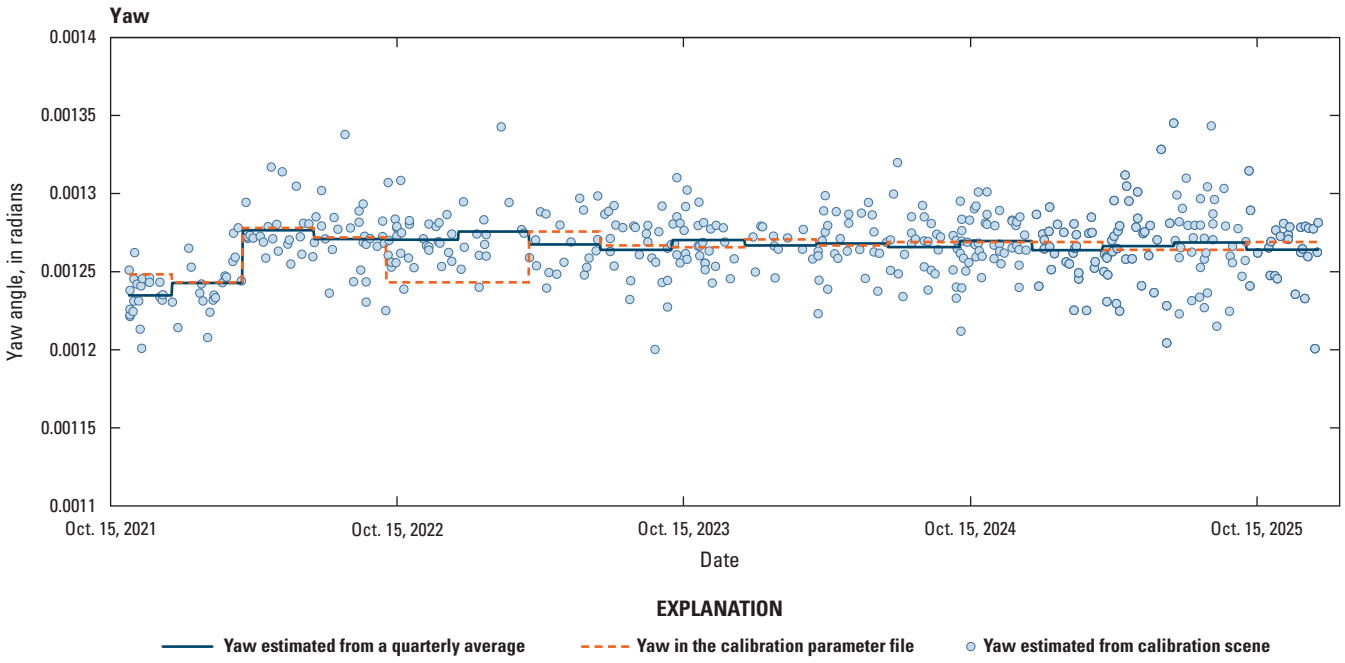

Figure 36. Graph showing Landsat 9 Thermal Infrared Sensor to Operational Land Imager lifetime yaw alignment.

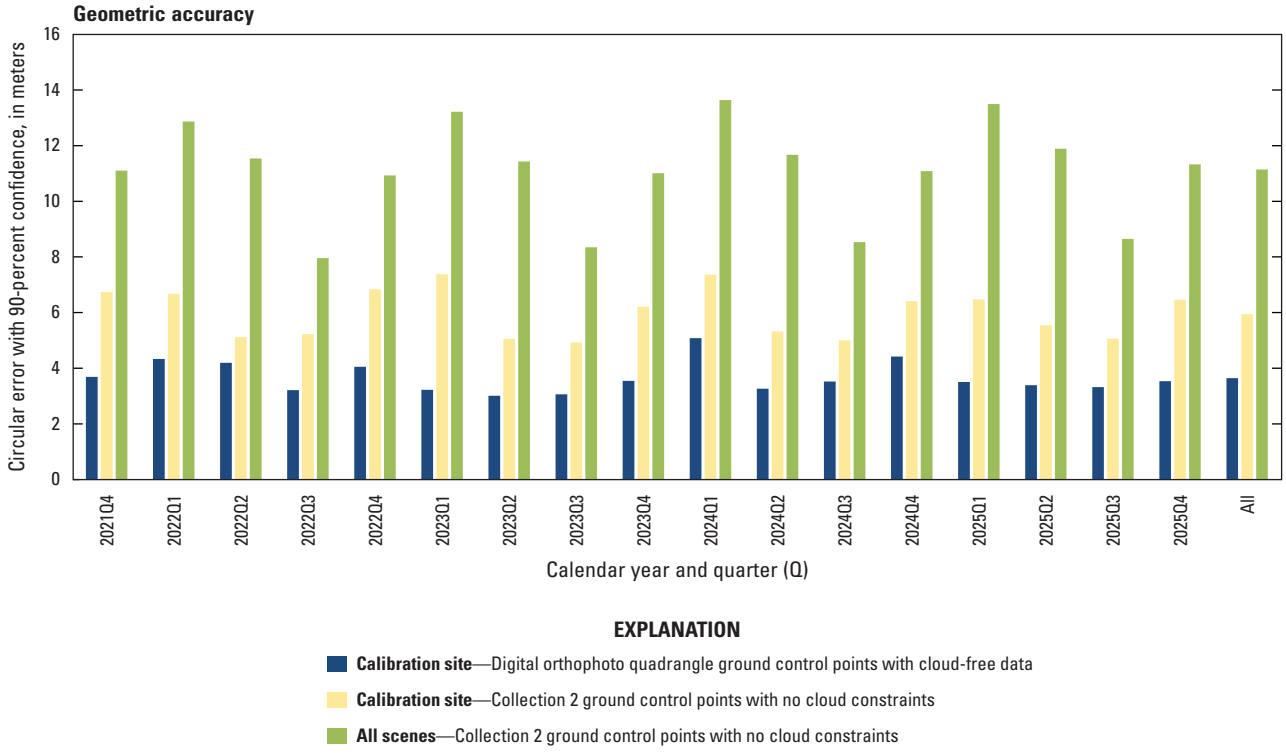

Figure 37. Graph showing Landsat 9 lifetime geometric accuracy by quarter.

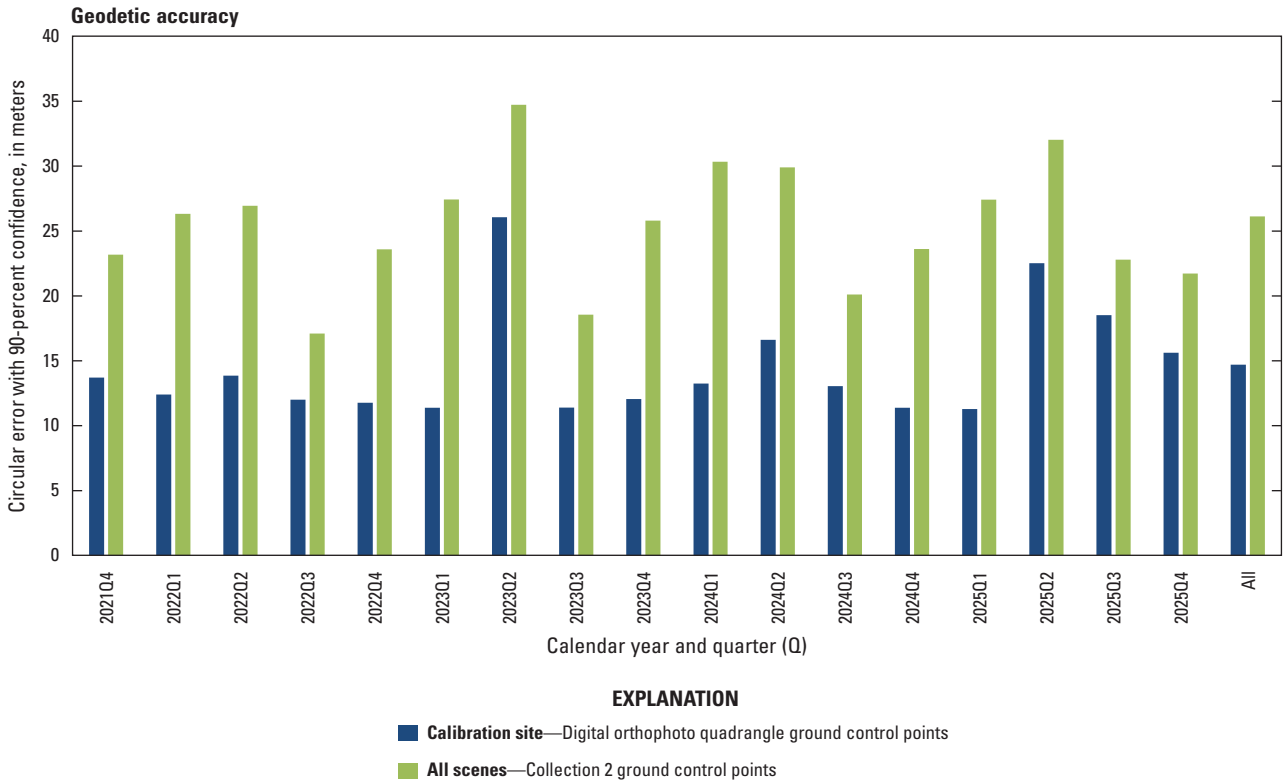

Figure 38. Graph showing Landsat 9 lifetime geodetic accuracy by quarter.

More recently, additional geodetic biases were observed beginning in quarter 2, 2025, and continuing through quarter 3, 2025. In response to these trends, a sensor alignment update was implemented beginning in quarter 4, 2025, to correct the observed biases and improve geodetic performance. Continued monitoring of post-update geodetic accuracy is ongoing to verify the effectiveness of the applied correction. The October 2025 Landsat 9 SADA anomaly did not affect the geodetic accuracy.

Landsat 9 to Landsat 8 Operational Land Imager Geometric Coregistration

The Landsat 9 and Landsat 8 OLI sensors provide identical spectral and spatial characteristics. To measure the geometric coregistration, image-to-image comparisons between Landsat 9 and Landsat 8 L1TP products were assessed, and the results are shown in figure 39. The image-to-image registration accuracy characterization is performed between panchromatic band image products using a correlation-based mensuration process (Choate and others, 2022). While measuring the image-to-image registration between two sensors, scene pairs were selected in such a way that temporal distance between the two scenes was no more than 32 days. The observed coregistration error between Landsat 9 and Landsat 8 L1TP products is indicated with the magenta dots. Based on analysis results, the Landsat 9 and Landsat 8 L1TP products are coregistered to within 3 meters of the CE90 (Rengarajan and others, 2024).

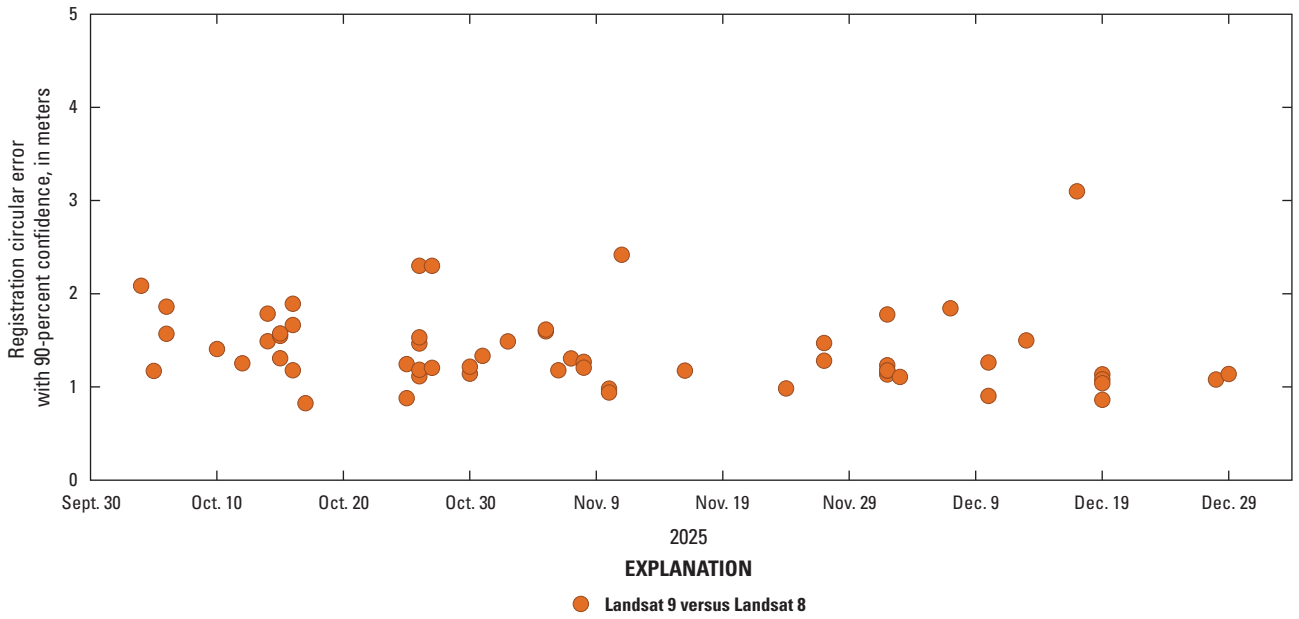

Figure 39. Graph showing coregistration error between Landsat 9 and Landsat 8 Level 1 terrain-corrected products, quarter 4, 2025.

Landsat 8 Radiometric Performance Summary

The Landsat 8 on-orbit radiometric performance for this reporting quarter (quarter 4, 2025) meets all requirements outlined in USGS (2019a). The quarterly OLI and TIRS radiometric performance summaries are provided in tables 5 and 6, respectively.

Landsat 8 Operational Land Imager Signal-to-Noise Ratio

The SNR for each of the OLI spectral bands is characterized at a prescribed band-specific $L_{typical}$ level, as described in table 3. The SNR of a detector at a given radiance level is defined as the mean of the measured pixel radiances acquired over a homogenous target divided by their standard deviation. A curve is fit to the SNR at the measured radiance levels and is evaluated at the prescribed $L_{typical}$ level. The SNR is characterized at multiple stages of the instrument build, culminating in the testing of the fully integrated instrument.

The Landsat 8 OLI SNR is evaluated on orbit each month. It remains consistently two to three times better than requirements and about eight times better than the Landsat 7 ETM+ SNR. The Collection 2 SNR slightly increased because of improvement in the bias calculation, further exceeding requirement thresholds. The per-band OLI median SNR at the $L_{typical}$ level (yellow bars) for December 2025, which easily exceeds the OLI SNR requirements (blue bars) by more than 50 percent for all bands, is shown in figure 40. Lifetime SNR stability at $L_{typical}$ for each OLI band is represented in figures 41, 42, 43, 44, 45, 46, 47, 48, and 49; monthly SNR values (for the detectors that have median SNRs for all bands) are denoted by the diamonds, and the uncertainties in the monthly SNR model are denoted by the error bars. The SNR for each band has remained stable over time (within the uncertainty of the models and much greater than the required levels).

Landsat 8 Thermal Infrared Sensor Noise Performance

Noise can be defined as variation in the detected signal over time when observing a stable source of radiation. For thermal sensors, noise is usually expressed in terms of a change in brightness temperature (that is, NEΔT). NEΔT is estimated as the standard deviation of detector data acquired over a uniform radiance source and then converted to temperature. Noise performance is completed on blackbody and deep space TIRS data (Montanaro and others, 2014).

All Landsat 8 TIRS detectors have similar NEΔT. At 300 K, band-average noise performance for both thermal bands is about eight times better than the requirement (less than 0.4 K) and about four times better than the NEΔT of the Landsat 7 ETM+ thermal band at that same temperature. Lifetime averages of NEΔT at 300 K for TIRS band 10 are shown in figure 50, and the same averages for TIRS band 11 are shown in figure 51. In both figures, colored diamonds are used to indicate the observed NEΔT values as measured over time.

Table 5. Landsat 8 Operational Land Imager radiometric performance summary, quarter 4 (October–December), 2025.

[The previous quarter is quarter 3 (July–September), 2025. OLI, Operational Land Imager; <, less than; SNR, signal-to-noise ratio; $L_{typical}$, typical radiance; -, not applicable; L_{high}, high radiance; RMS, root mean square; stdev, standard deviation; ≤, less than or equal to; W/m² sr µm, watt per square meter per steradian per micrometer; σ, sigma; spec, specification]

Requirement	Measured value from this quarter	Measured value from previous quarter[1]	Required value	Unit
OLI ghosting	Meets	Meets	Varies	Percent
OLI absolute radiance uncertainty	4	4	<5	Percent
OLI absolute reflectance uncertainty	<3	<3	<3	Percent
OLI median SNR $L_{typical}$	Meets	Meets	Varies	-
OLI median SNR L_{high}	Meets	Meets	Varies	-
OLI uniformity full field of view	0.35	0.35	<0.5	Percent
OLI uniformity banding RMS	0.80	0.80	<1	Percent
OLI uniformity banding stdev	0.15	0.15	<0.25	Percent
OLI uniformity streaking	0.5	0.5	≤0.5, 1	Percent
OLI coherent noise	Meets	Meets	Less than coherent noise threshold curve	-
OLI saturation radiances	Meets	Meets	Varies	W/m² sr µm
OLI 16-day radiometric stability	0.12	0.12	<1	Percent (2σ)
OLI 60-second radiometric stability	0.1	0.1	<0.5	Percent (2σ)
OLI inoperable detectors	0	0	<0.1	Percent
OLI out-of-spec detectors	0.06	0.06	<0.25	Percent

[1]From Haque and others (2026).

Table 6. Landsat 8 Thermal Infrared Sensor radiometric performance summary, quarter 4 (October–December), 2025.

[The previous quarter is quarter 3 (July–September), 2025. TIRS, Thermal Infrared Sensor; ~, approximately; <, less than; NEΔT, noise equivalent change in temperature; K, Kelvin; TBD, to be determined; RMS, root mean square; stdev, standard deviation; -, not applicable; >, greater than; W/m² sr µm, watt per square meter per steradian per micrometer; σ, sigma; spec, specification]

Requirement	Measured value from this quarter	Measured value from previous quarter[1]	Required value	Unit
TIRS absolute radiance uncertainty	~1	~1	<2	Percent
TIRS NEΔT (at 300 K)	0.05	0.05	<0.4	K
TIRS uniformity full field of view	TBD	TBD	<0.5	Percent
TIRS uniformity banding RMS	TBD	TBD	<0.5	Percent
TIRS uniformity banding stdev	TBD	TBD	<0.5	Percent
TIRS uniformity streaking	<0.5	<0.5	<0.5	Percent
TIRS coherent noise	Meets	Meets	Less than coherent noise threshold curve	-
TIRS saturation radiances	28.4, 19.2	28.4, 19.2	>20.5, >17.8	W/m² sr µm
TIRS 40-minute radiometric stability	0.1	0.1	<0.7	Percent (1σ)
TIRS inoperable detectors	0	0	<0.1	Percent
TIRS out-of-spec detectors	0.21	0.21	<0.25	Percent

[1]From Haque and others (2026).

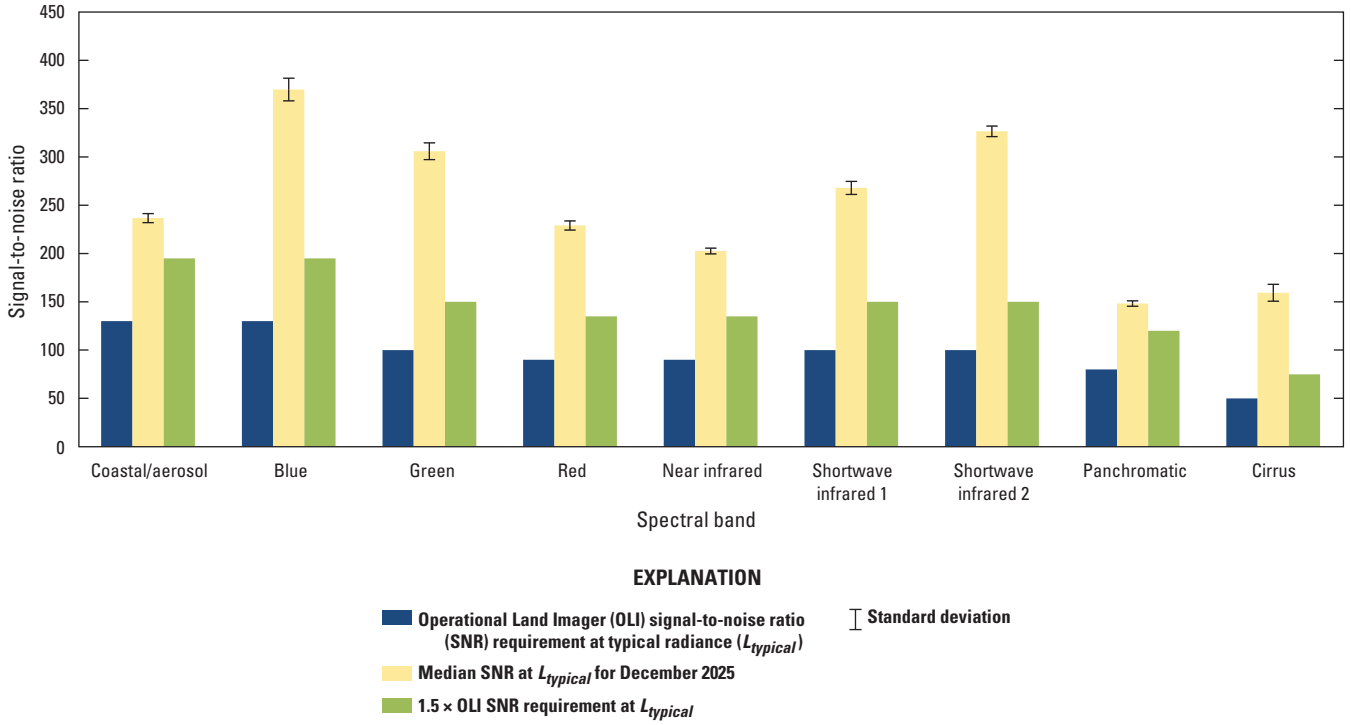

Figure 40. Graph showing Landsat 8 Operational Land Imager signal-to-noise ratio performance, December 2025.

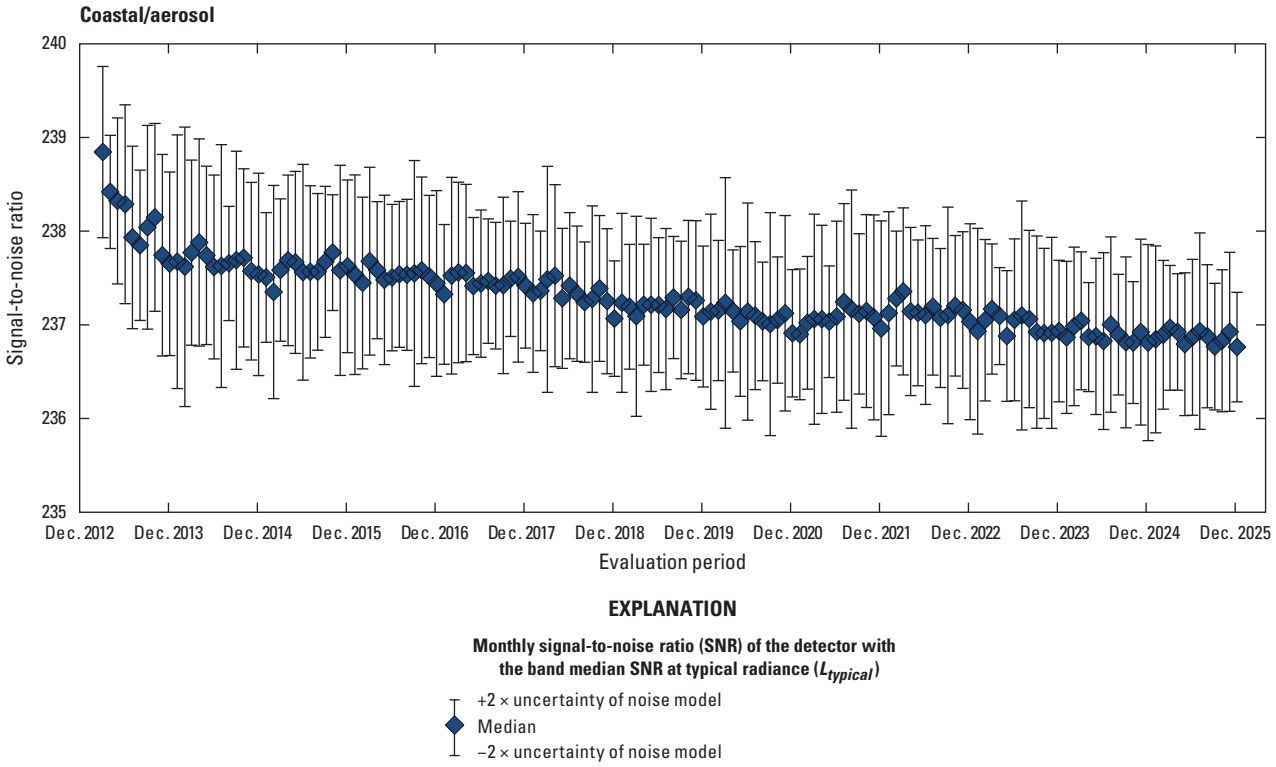

Figure 41. Graph showing Landsat 8 Operational Land Imager coastal/aerosol band lifetime signal-to-noise ratio stability.

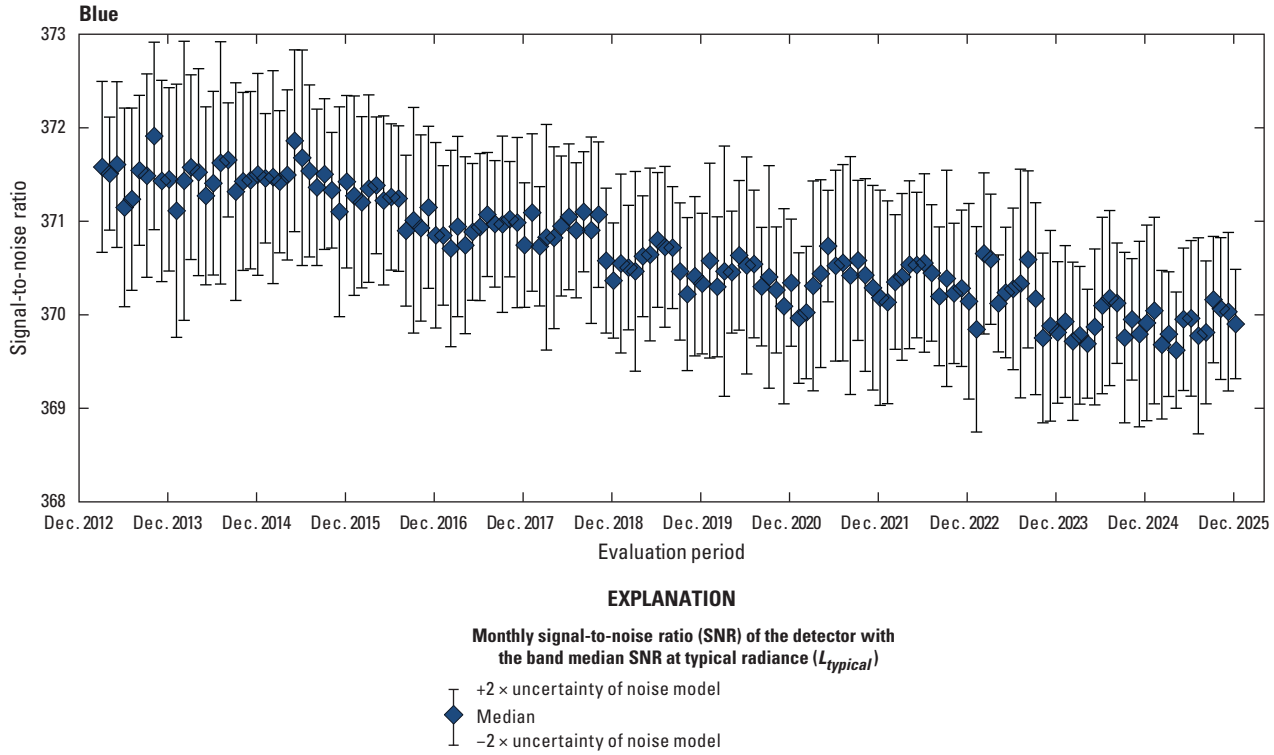

Figure 42. Graph showing Landsat 8 Operational Land Imager blue band lifetime signal-to-noise ratio stability.

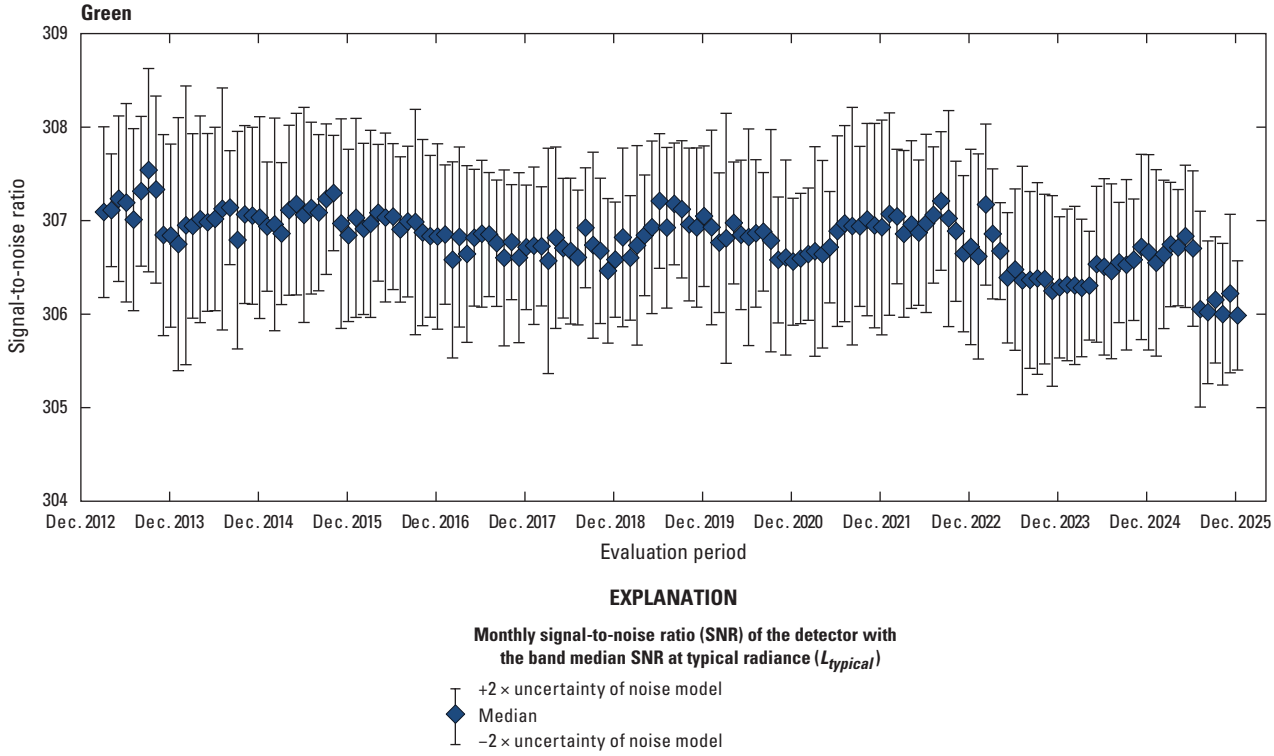

Figure 43. Graph showing Landsat 8 Operational Land Imager green band lifetime signal-to-noise ratio stability.

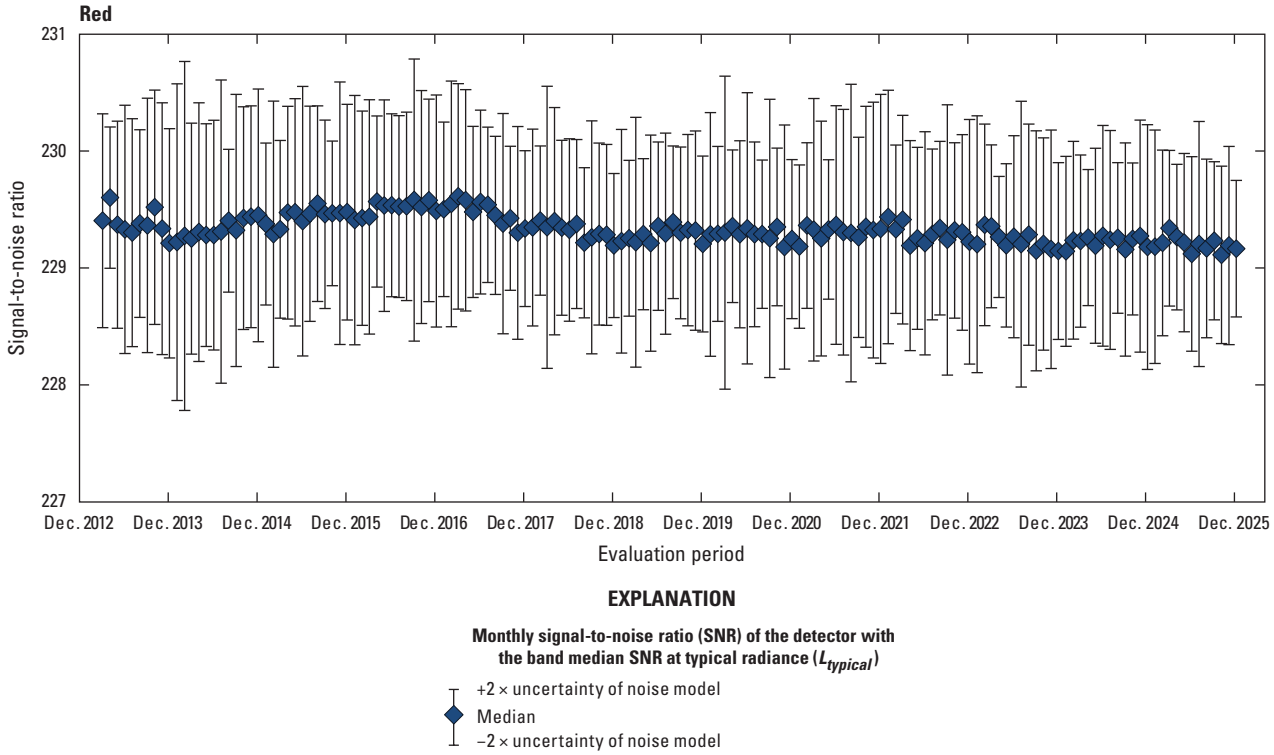

Figure 44. Graph showing Landsat 8 Operational Land Imager red band lifetime signal-to-noise ratio stability.

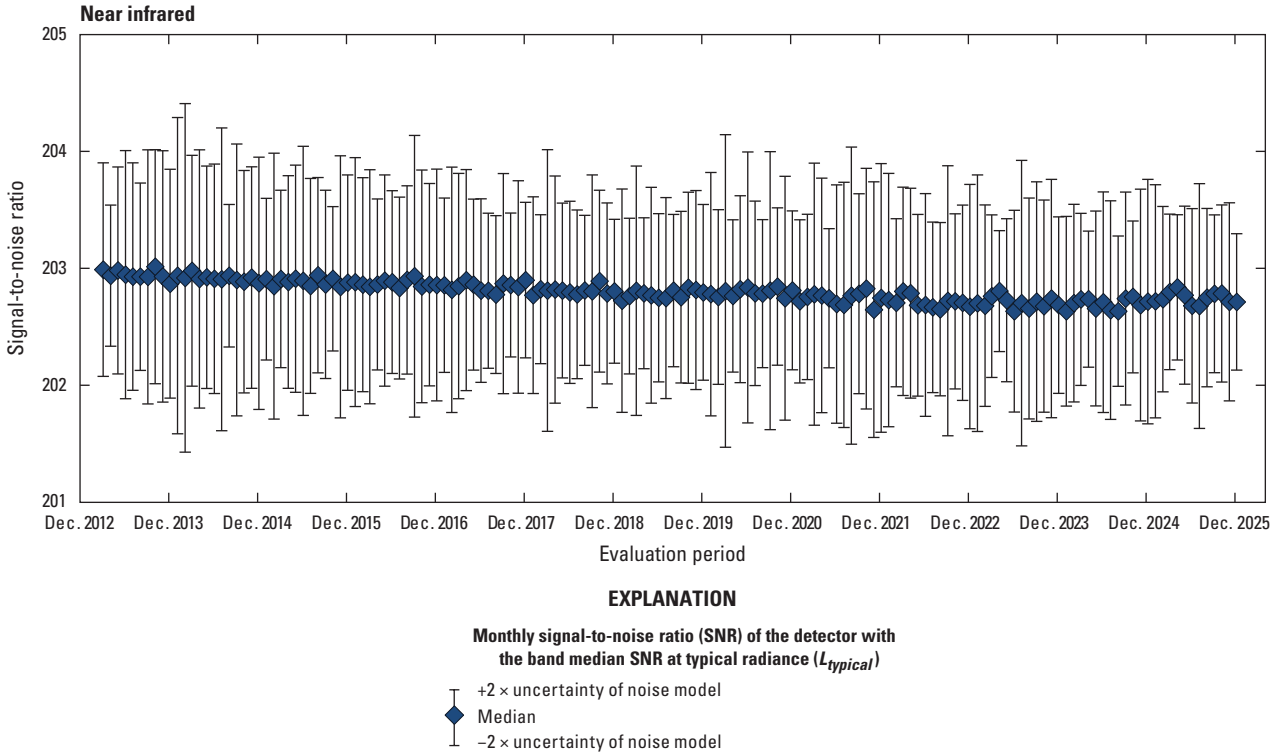

Figure 45. Graph showing Landsat 8 Operational Land Imager near infrared band lifetime signal-to-noise ratio stability.

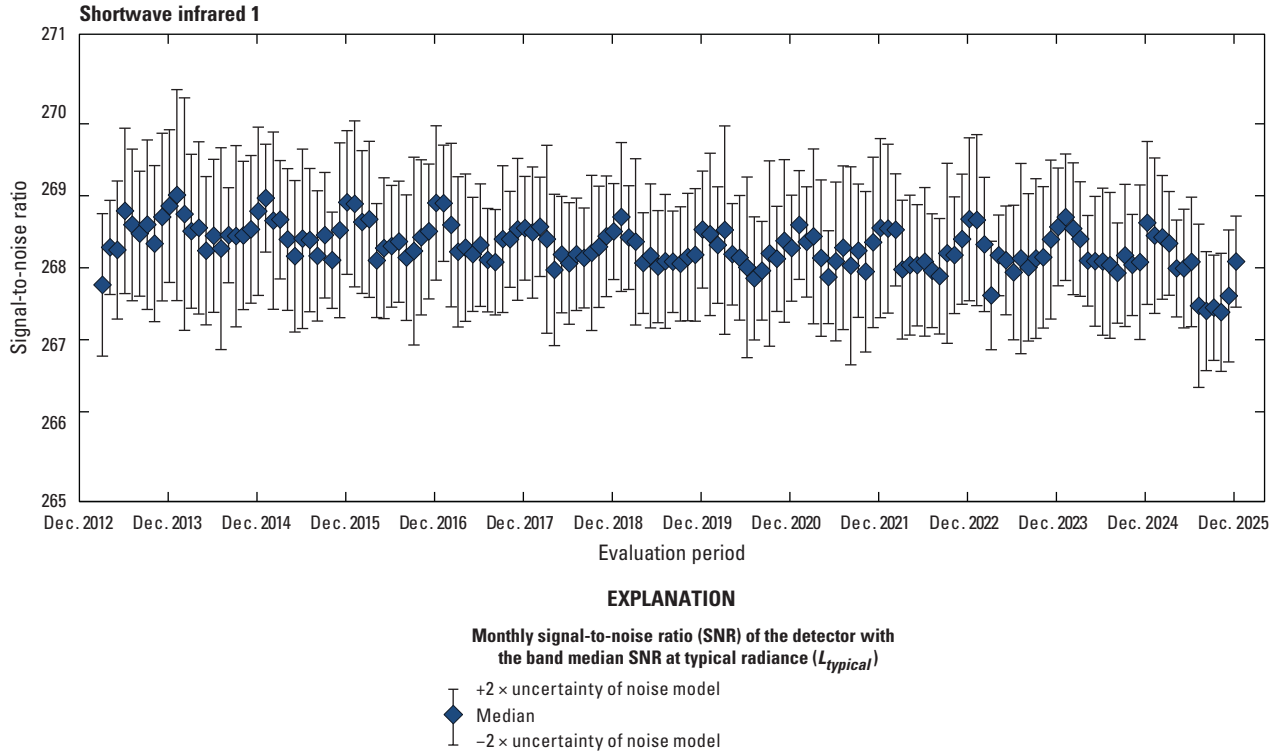

Figure 46. Graph showing Landsat 8 Operational Land Imager shortwave infrared 1 band lifetime signal-to-noise ratio stability.

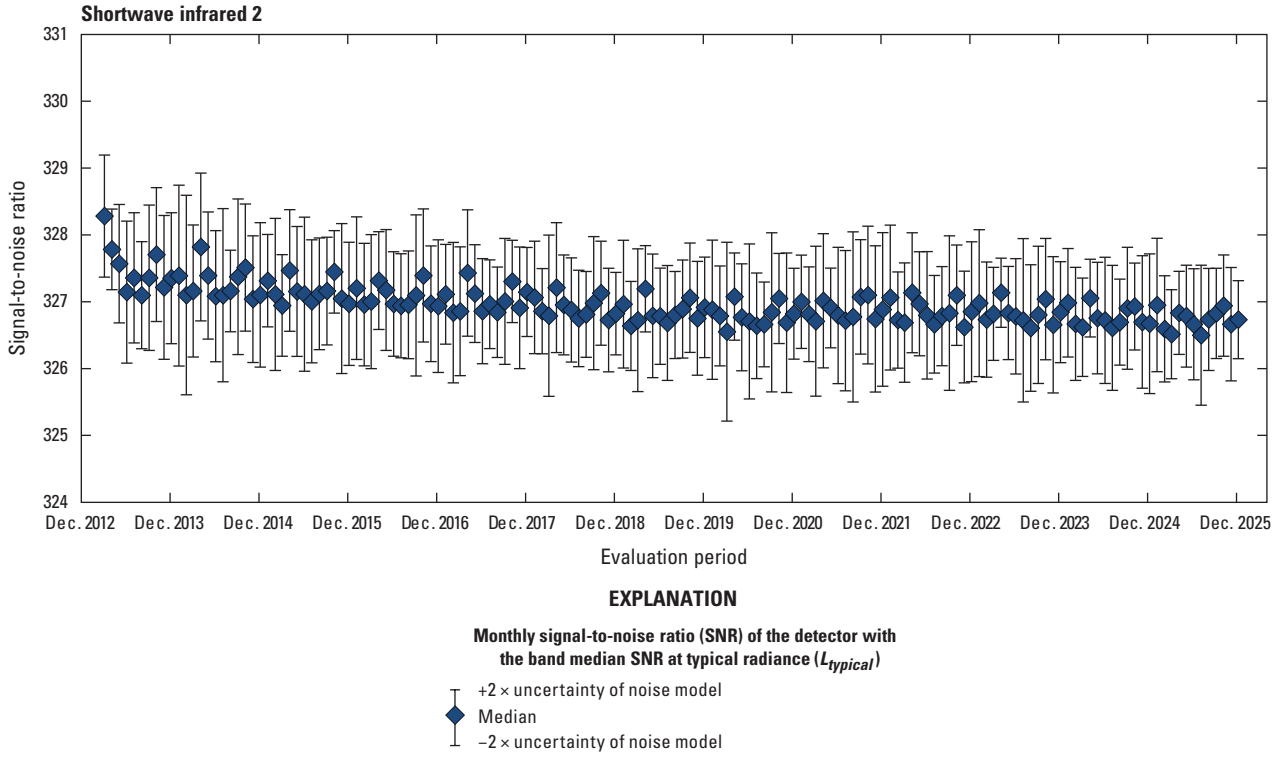

Figure 47. Graph showing Landsat 8 Operational Land Imager shortwave infrared 2 band lifetime signal-to-noise ratio stability.

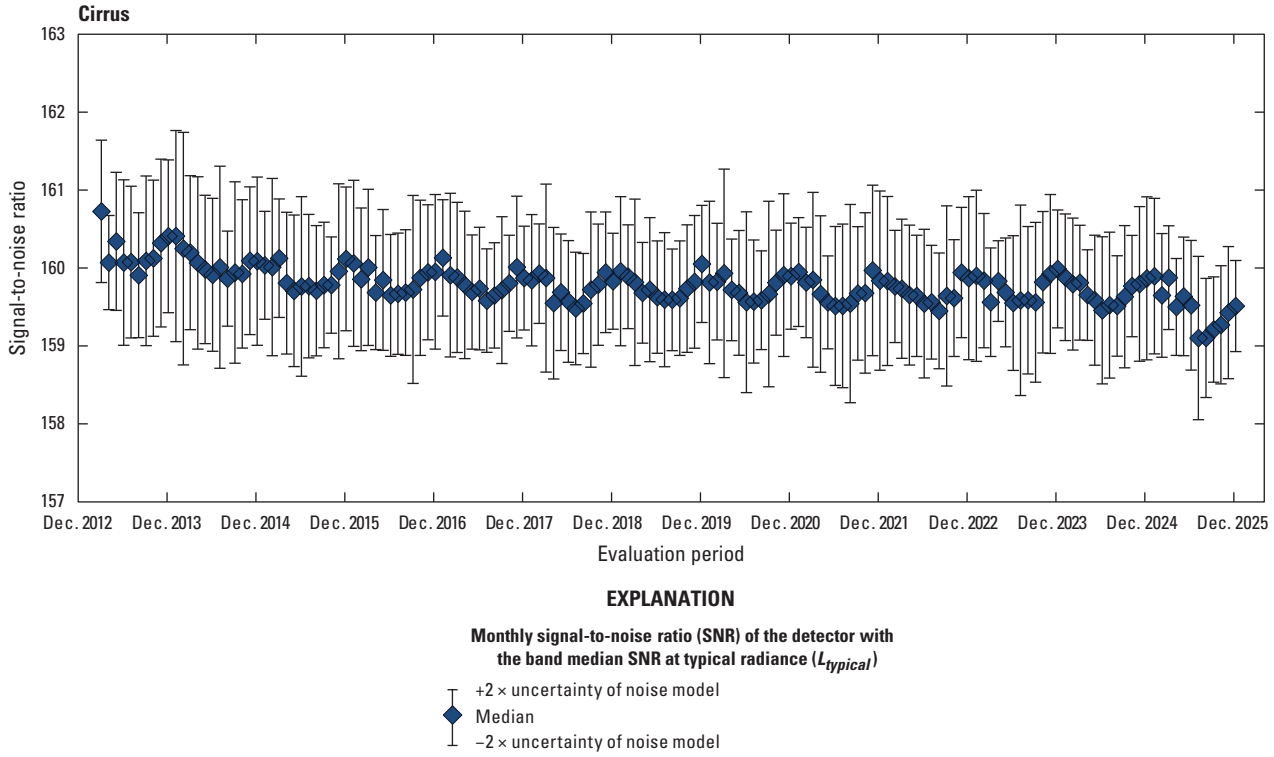

Figure 48. Graph showing Landsat 8 Operational Land Imager cirrus band lifetime signal-to-noise ratio stability.

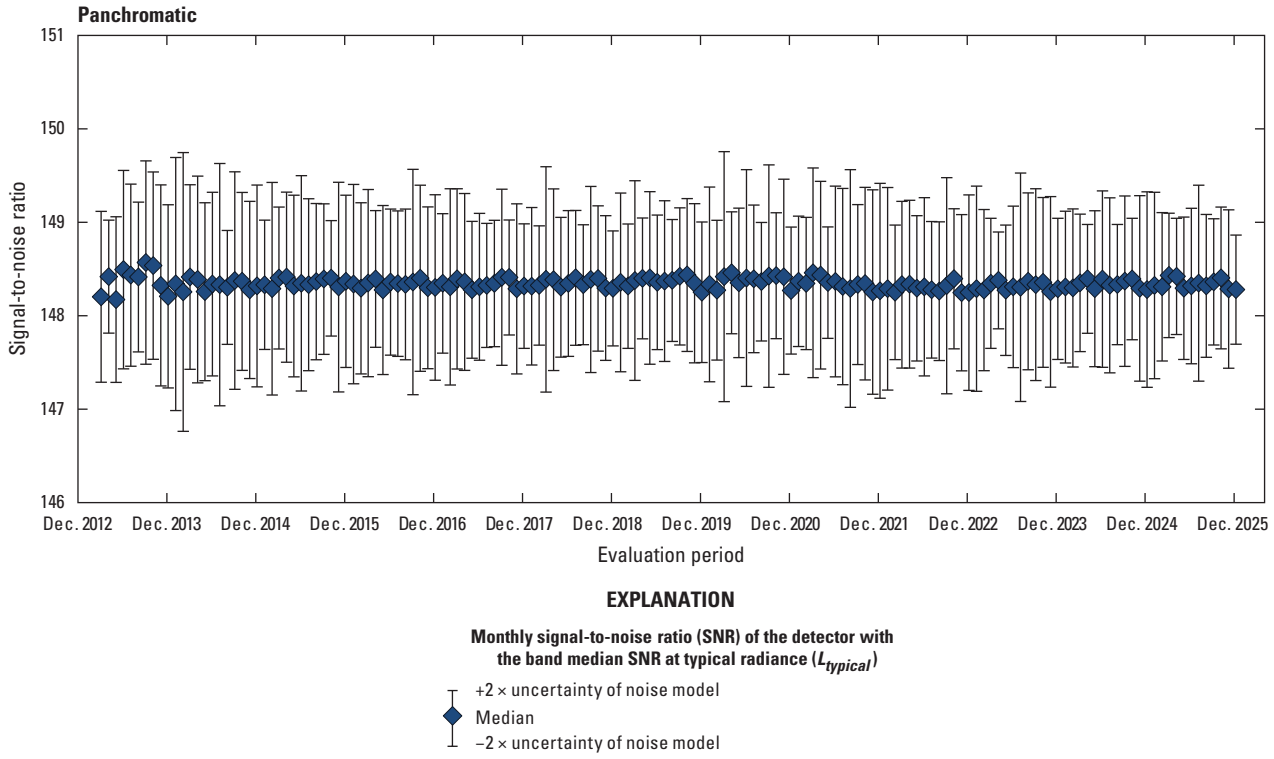

Figure 49. Graph showing Landsat 8 Operational Land Imager panchromatic band lifetime signal-to-noise ratio stability.

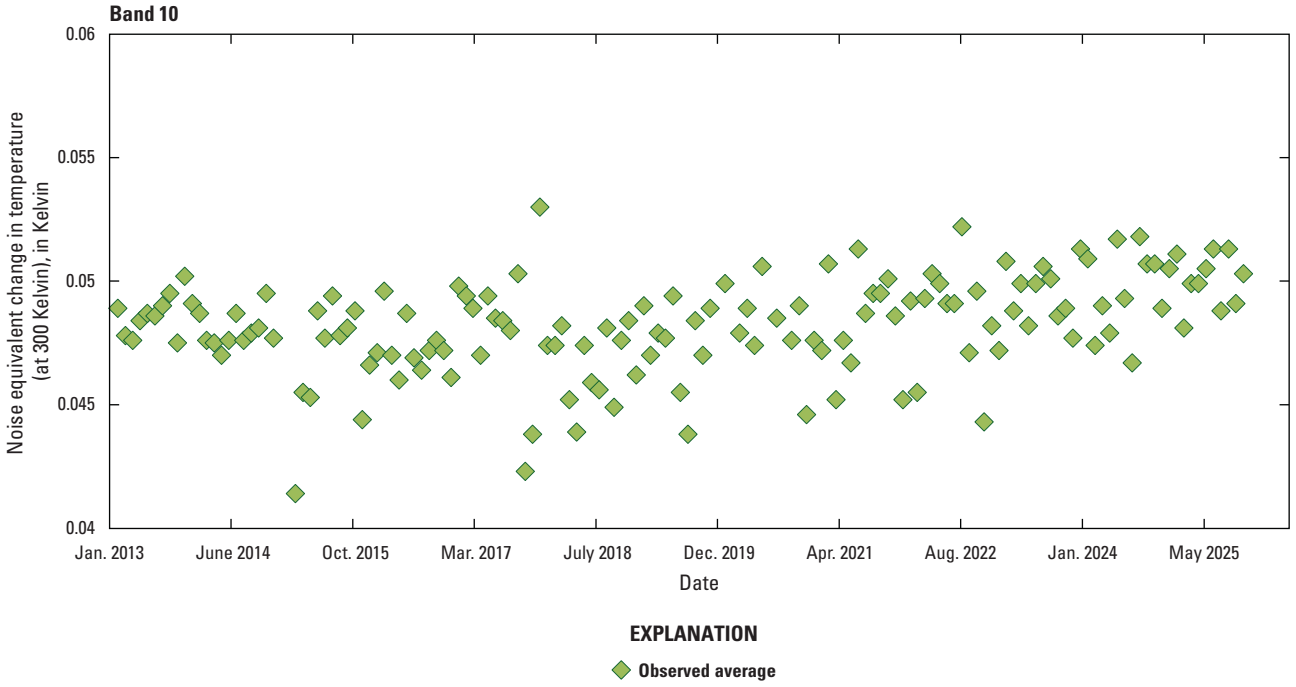

Figure 50. Graph showing Landsat 8 Thermal Infrared Sensor band 10 lifetime noise performance.

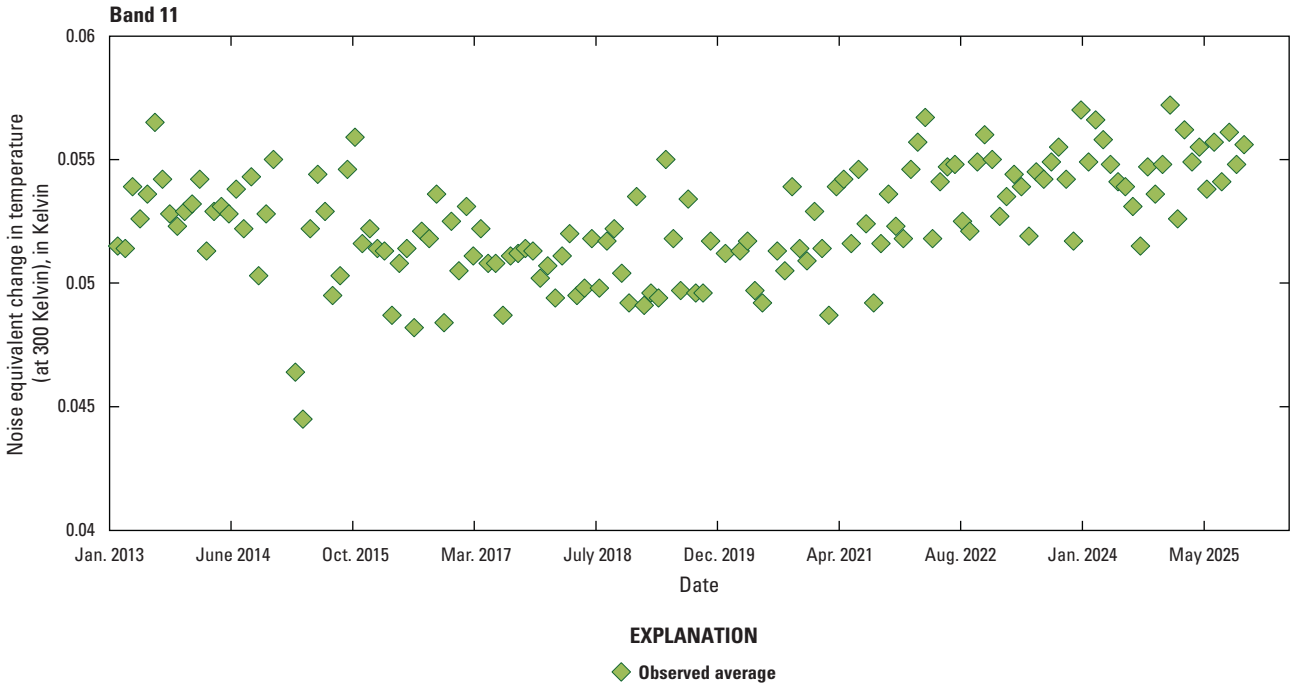

Figure 51. Graph showing Landsat 8 Thermal Infrared Sensor band 11 lifetime noise performance.

Landsat 8 Radiometric Stability

Radiometric stability of an instrument is fundamental to low uncertainty in the radiometric calibration of data products generated from its measurements. The radiometric response stability is characterized for all OLI and TIRS bands using the instruments' responses to signals from the onboard calibration devices collected over time (USGS, 2021c). The bias and gain stability of an instrument are contributing factors to variability within a radiometrically calibrated product.

The Landsat 8 per-band OLI radiometric stability over the lifetime of the instrument is shown in figures 52, 53, 54, 55, 56, 57, 58, 59, and 60. Within each figure, the x-axis represents years since launch (February 11, 2013), and the y-axis represents the response relative to mission day 40. The solid brown line (figs. 52, 53, 54, 57, and 60) represents the gain model used over time, which is derived from the OLI response to the stimulation lamps, solar panels, and lunar collects; it is only shown for the bands with responsivity (gain) determined to be slowly changing over time (CA, blue, green, SWIR 1, and cirrus bands) and exceeding 0.2 percent total degradation. For the remaining bands, response changes were minuscule until the safehold events in November 2020 and total responsivity degradation has not exceeded 0.2 percent. More information about the Landsat 8 safehold events is available at https://www.usgs.gov/landsat-missions/november-19-2020-landsat-8-data-availability-update-recent-safehold-events. These observations indicate high radiometric stability of the instrument over its lifetime. Data derived from bands that have changed responsivity are corrected during product generation, so final products are not affected.

From Micijevic and others (2021), the stability of the Landsat 8 TIRS bands 10 and 11 side A electronics that were used for the first ~700 days of the mission is shown in figures 61 and 62. During that period, TIRS gains changed by about 0.2 and 0.1 percent per year for bands 10 and 11, respectively. These trends reduced on the side B electronics to about 0.05 and 0.01 percent until the two safehold events in November 2020, as shown in figures 63 and 64, respectively. After the safehold events, TIRS responsivity has gradually decreased ~3.7 and ~7.2 percent for bands 10 and 11, respectively. Note that the response degradation is modeled and corrected to within 0.5 percent uncertainty in the L1 products.

Since January 2021, Landsat 8 TIRS onboard calibrator acquisitions have been collected on a weekly basis (instead of once every ~2 weeks) to better monitor the degradation in response observed after the safehold events. Weekly calibration acquisitions are planned into the future if the response degradation trend continues and if geometric and radiometric accuracies are not negatively affected by the increased acquisition frequency.

Landsat 8 Absolute Radiometric Calibration

Absolute radiometric calibration is established on the ground before launch and transferred to orbit using the solar diffuser for OLI and the blackbody for TIRS. Onboard calibrators and PICS (Committee on Earth Observation Satellites, 2021) are used to monitor changes in absolute calibration, and vicarious methods are used to check absolute calibration over time (USGS, 2021c). Updates can be made to the calibration parameters used in processing the data to L1 when a substantial change is detected in the calibrator trends.

The lifetime effect of Landsat 8 OLI gain updates is shown in figure 65. A slow decay in CA and blue band calibration response was observed (figs. 52 and 53, respectively). The absolute radiometric calibration for the CA band has been actively modeled since April 2015, and an update to the calibration parameters was implemented for the blue band in April 2017. In April 2018, it was determined that the response to the working stimulation lamp was diverging from the other calibrators, and the working stimulation lamp was removed from the model that generates the gain updates. Similarly, in October 2019, the working diffuser was removed from the gain model because of diverging trends. In both cases, the new estimates of the radiometric gain were only applied to newly acquired data. When the archive was reprocessed for Collection 2, the updated gains were applied to all data, which changed the calibrated response in the CA and blue bands by as much as 0.15 percent compared to the Collection 1 products (Micijevic and others, 2021). The safehold events in November 2020 caused small changes to the Landsat 8 OLI response, as reflected in figure 65 by the small, systematic error adjustments that were made to the gain models. In July 2021, the CPF was updated to account for as much as a 0.12 percent step change in OLI responsivity caused by the November 2020 safehold events (Micijevic and others, 2022). By quarter 3, 2025, the total responsivity degradation exceeded 0.2 percent for an additional three bands (green, SWIR 1, and cirrus). The CPF released for quarter 3, 2025, was updated to account for these degradations.

The effect of change in average gain for Landsat 8 TIRS bands 10 and 11 since the safehold event on November 1, 2020, is shown in figure 66. The orange line is a modeled gain trend for band 10 based on the internal calibrator data (fig. 63), and the blue line is the gain trend sampled into calibration parameters that ensure there is no more than a 0.5 percent band-average radiometric gain change over the CPF period in the L1 products. Likewise, for band 11, the magenta line in figure 66 is a modeled gain trend based on the internal calibrator data (fig. 64), and the yellow line is the gain trend sampled into calibration parameters. Because of the relatively sharp decrease in response shortly after the safehold events, when compared with the response before the safehold events, calibration parameters were issued more frequently to ensure high-quality L1 products. As the rate of degradation has slowed, updated calibration parameters have returned to quarterly issuance.

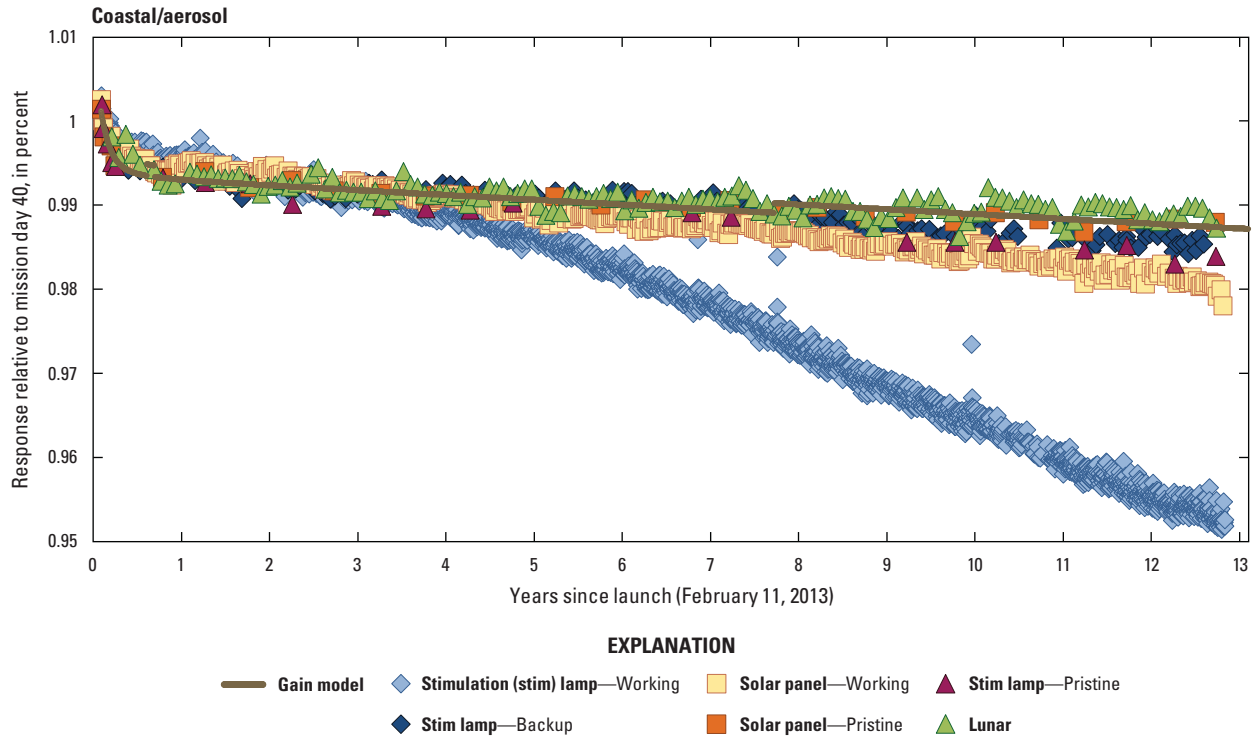

Figure 52. Graph showing Landsat 8 Operational Land Imager coastal/aerosol band lifetime radiometric stability.

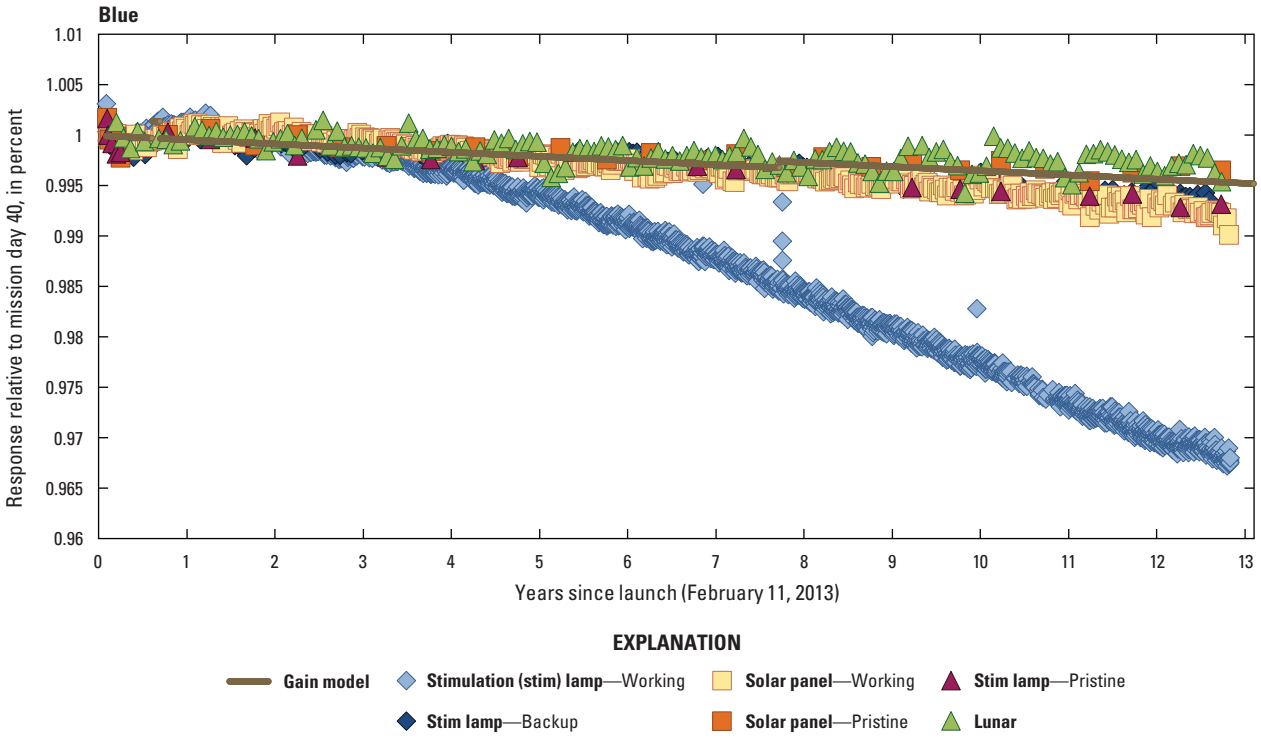

Figure 53. Graph showing Landsat 8 Operational Land Imager blue band lifetime radiometric stability.

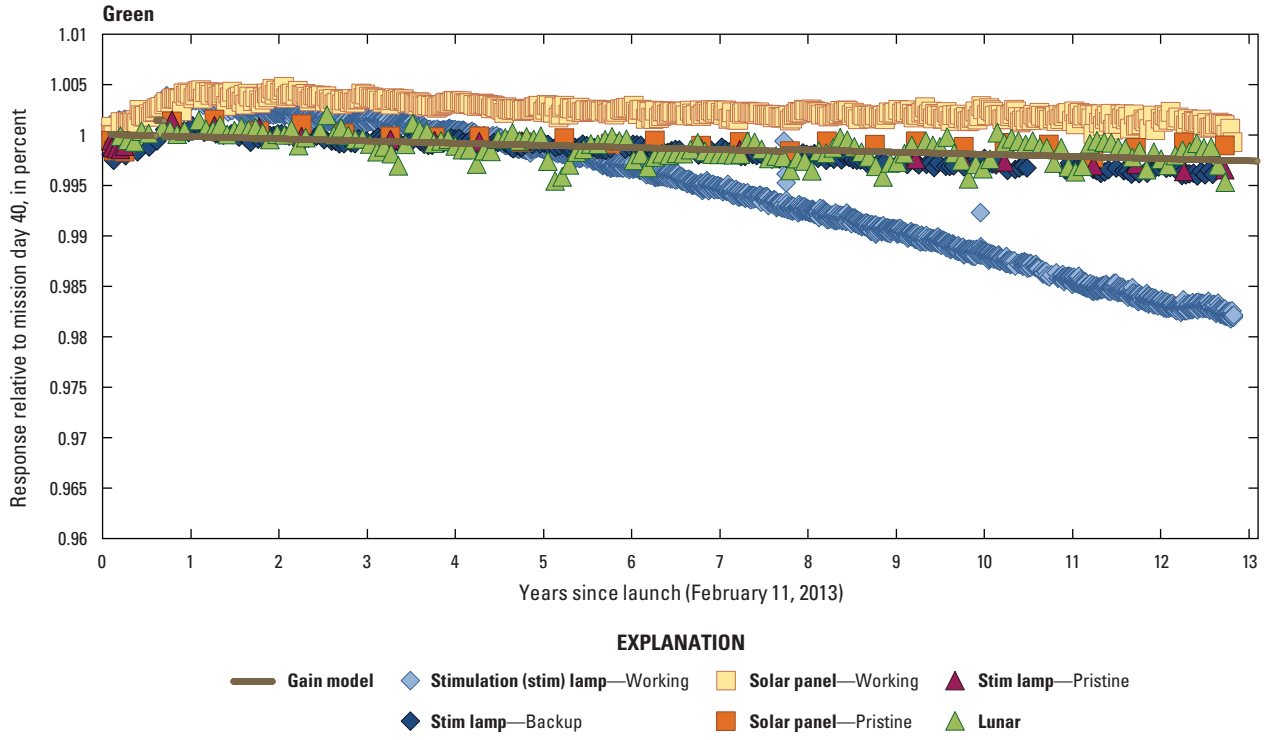

Figure 54. Graph showing Landsat 8 Operational Land Imager green band lifetime radiometric stability.

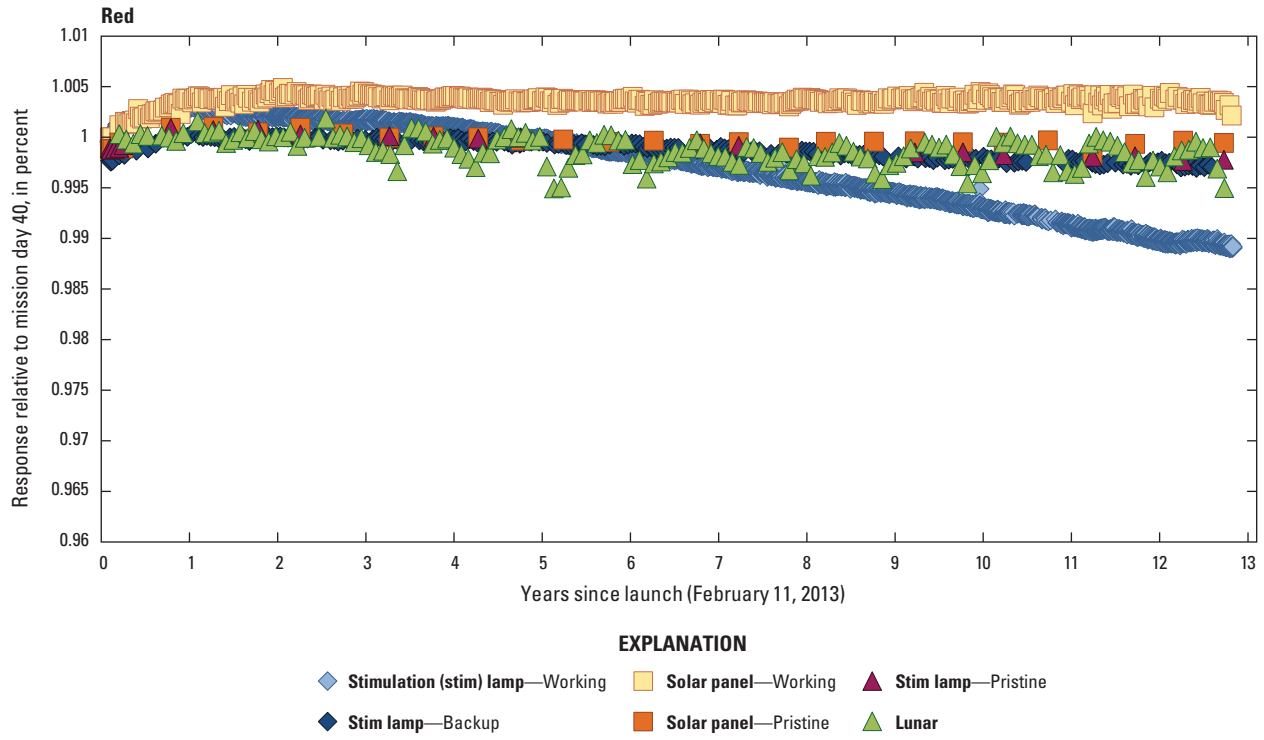

Figure 55. Graph showing Landsat 8 Operational Land Imager red band lifetime radiometric stability.

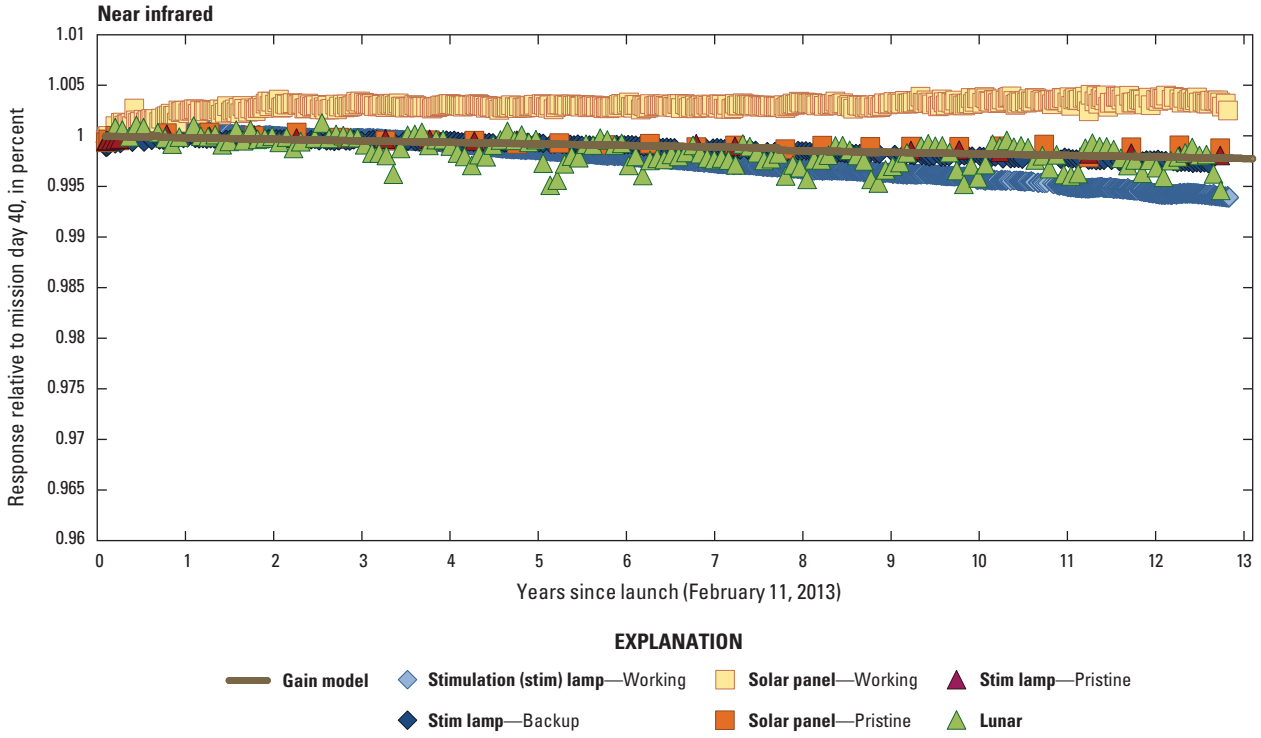

Figure 56. Graph showing Landsat 8 Operational Land Imager near infrared band lifetime radiometric stability.

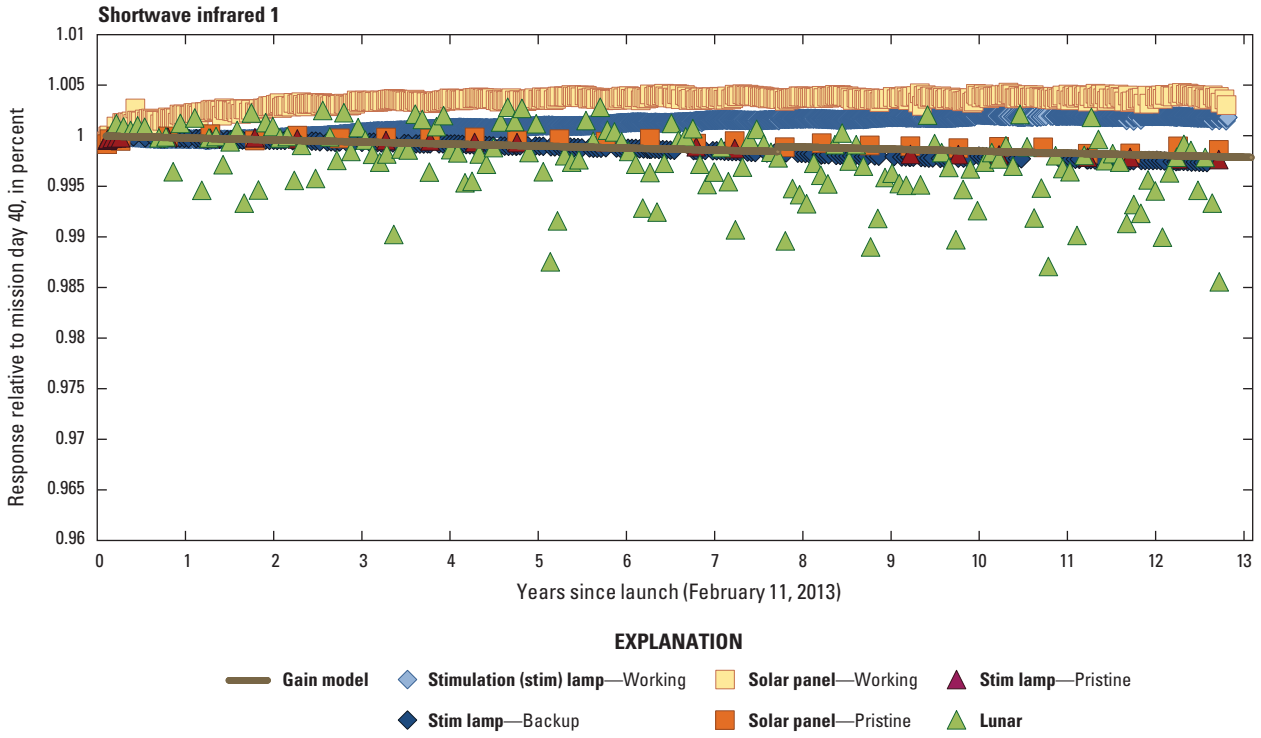

Figure 57. Graph showing Landsat 8 Operational Land Imager shortwave infrared 1 band lifetime radiometric stability.

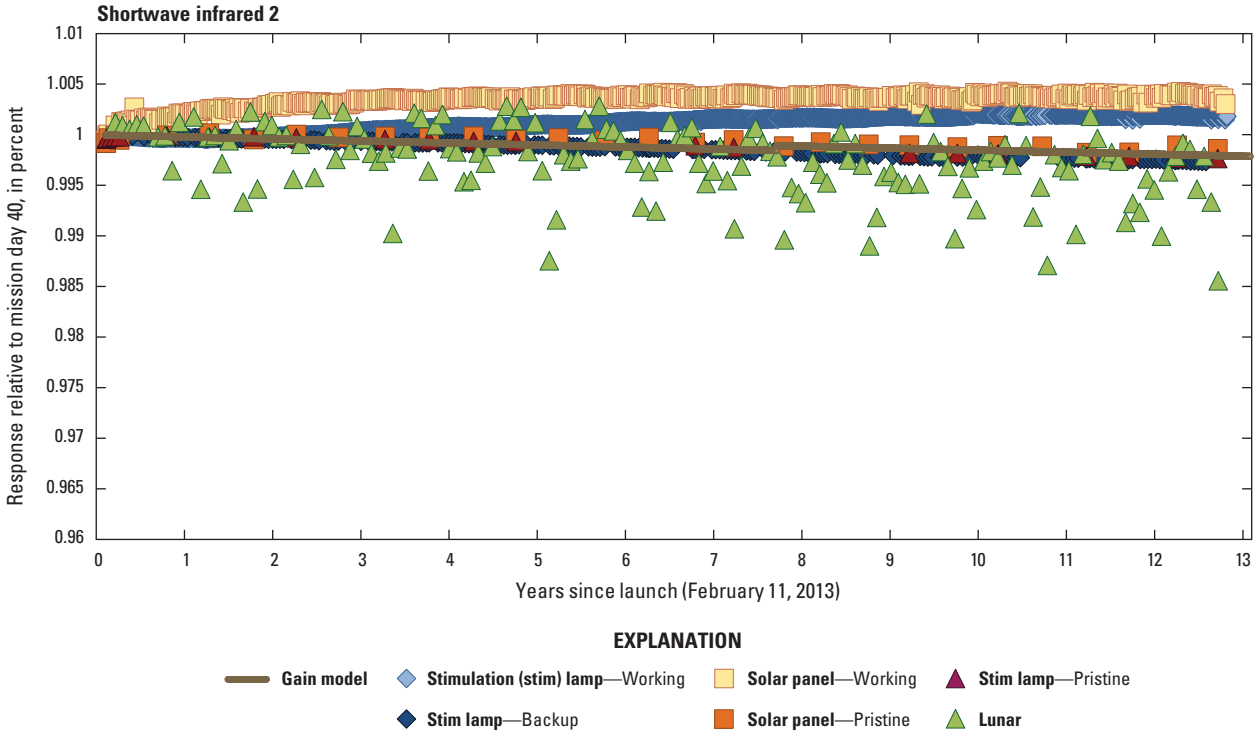

Figure 58. Graph showing Landsat 8 Operational Land Imager shortwave infrared 2 band lifetime radiometric stability.

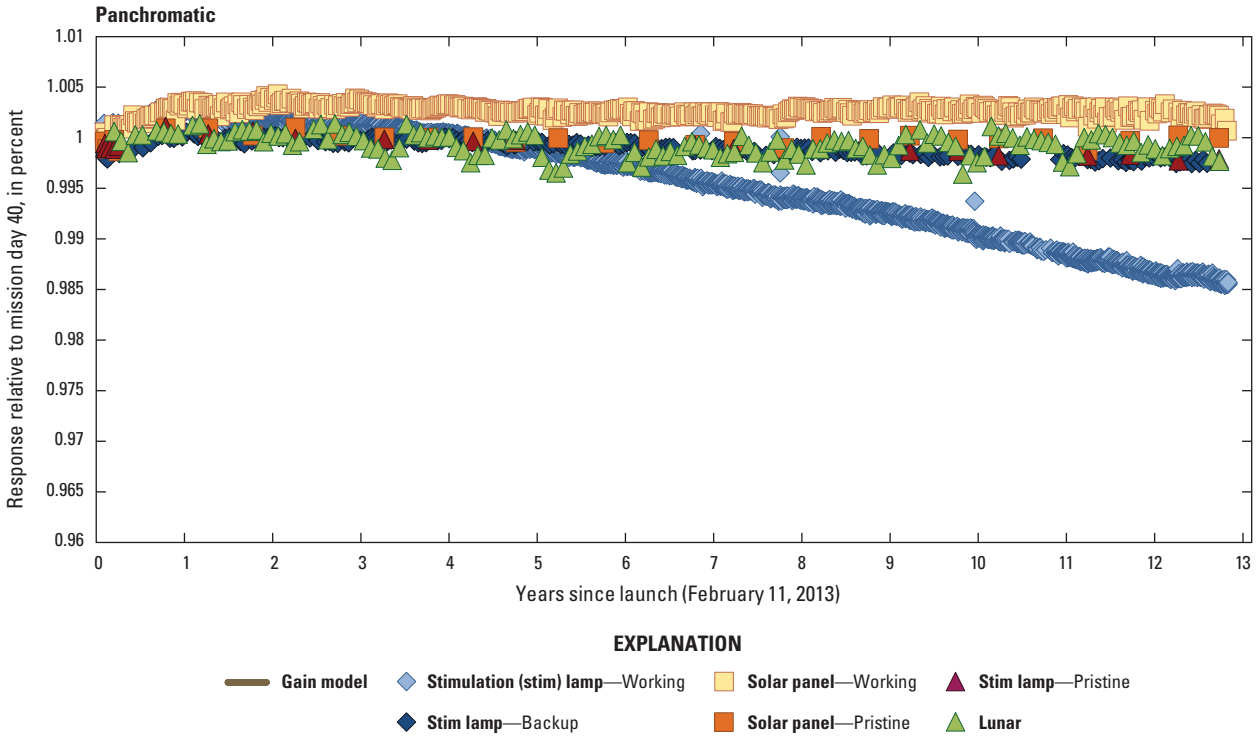

Figure 59. Graph showing Landsat 8 Operational Land Imager panchromatic band lifetime radiometric stability.

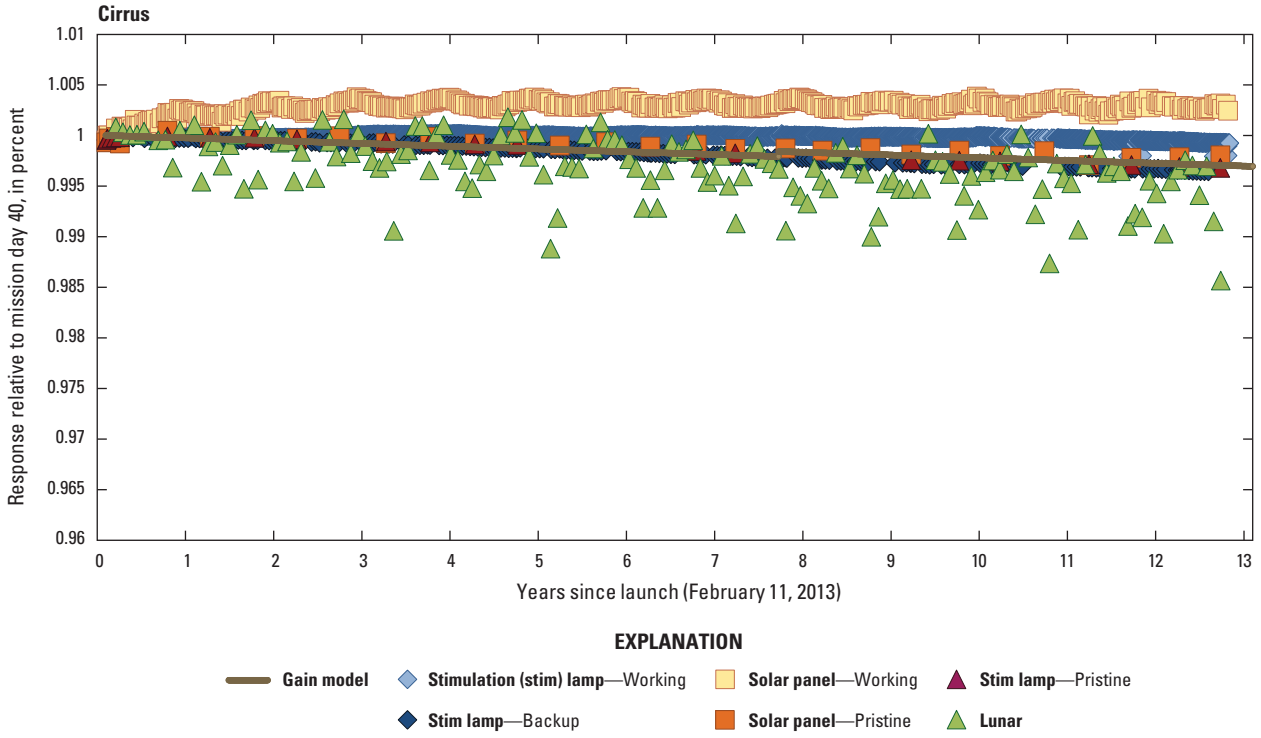

Figure 60. Graph showing Landsat 8 Operational Land Imager cirrus band lifetime radiometric stability.

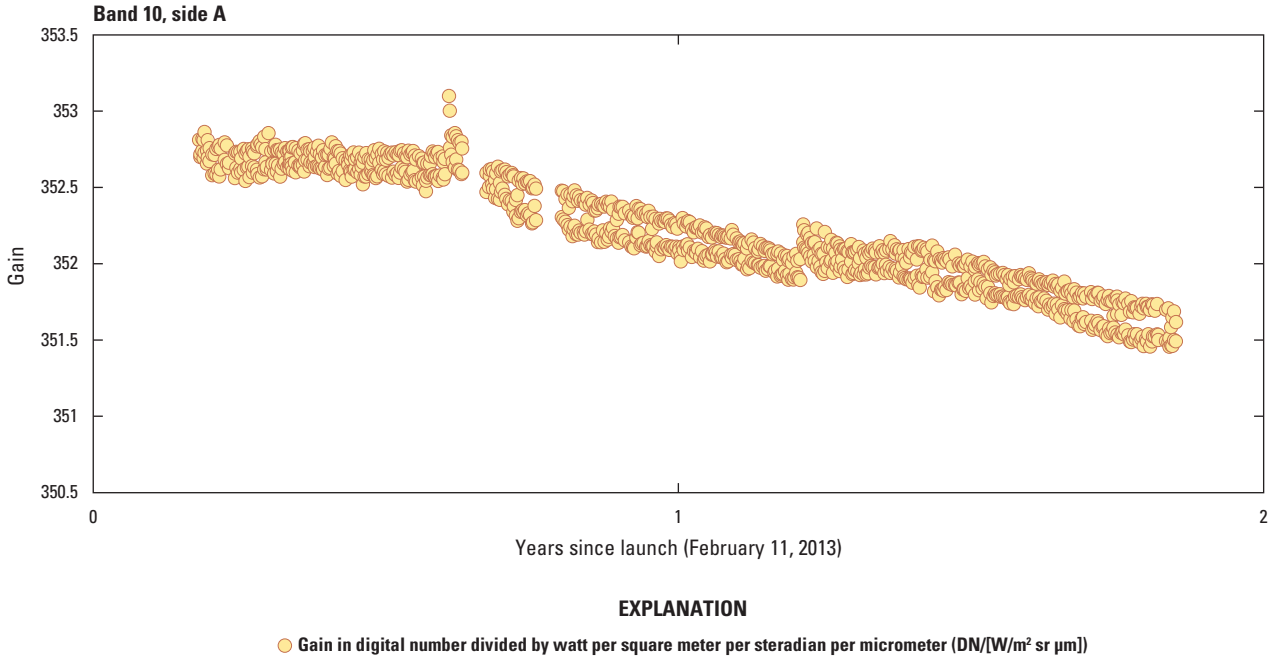

Figure 61. Graph showing Landsat 8 Thermal Infrared Sensor band 10 radiometric stability (side A) for the first approximately 700 days of the mission (from Micijevic and others, 2021).

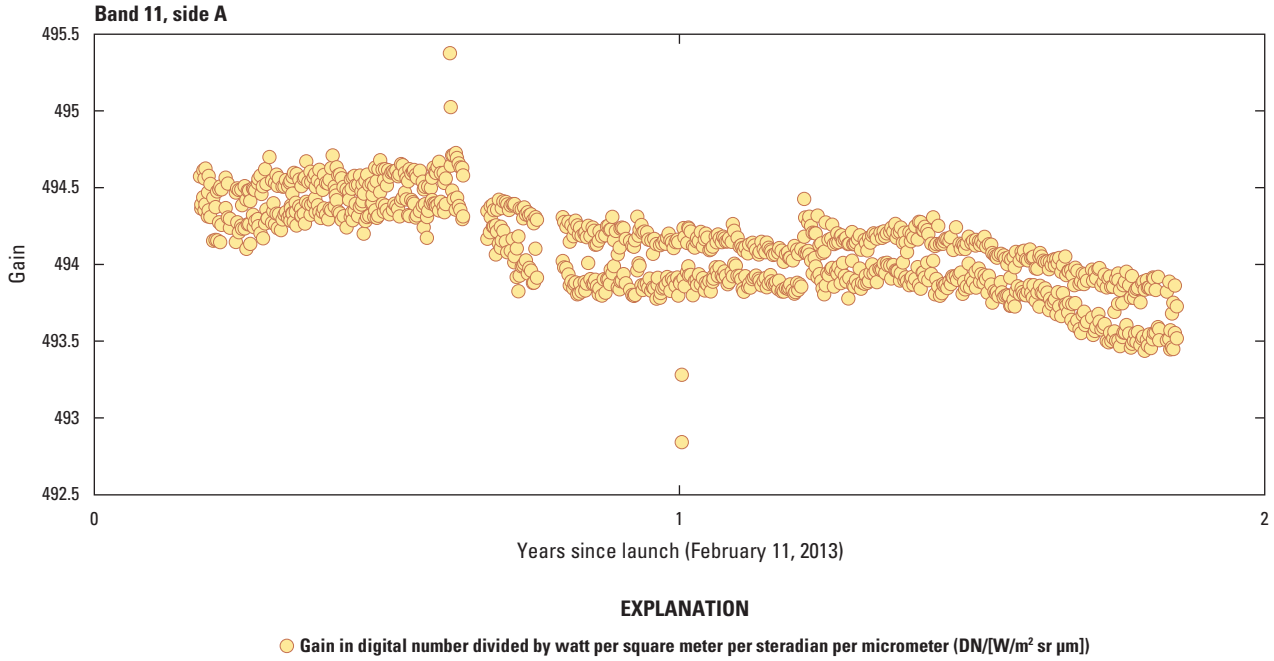

Figure 62. Graph showing Landsat 8 Thermal Infrared Sensor band 11 radiometric stability (side A) for the first approximately 700 days of the mission (from Micijevic and others, 2021).

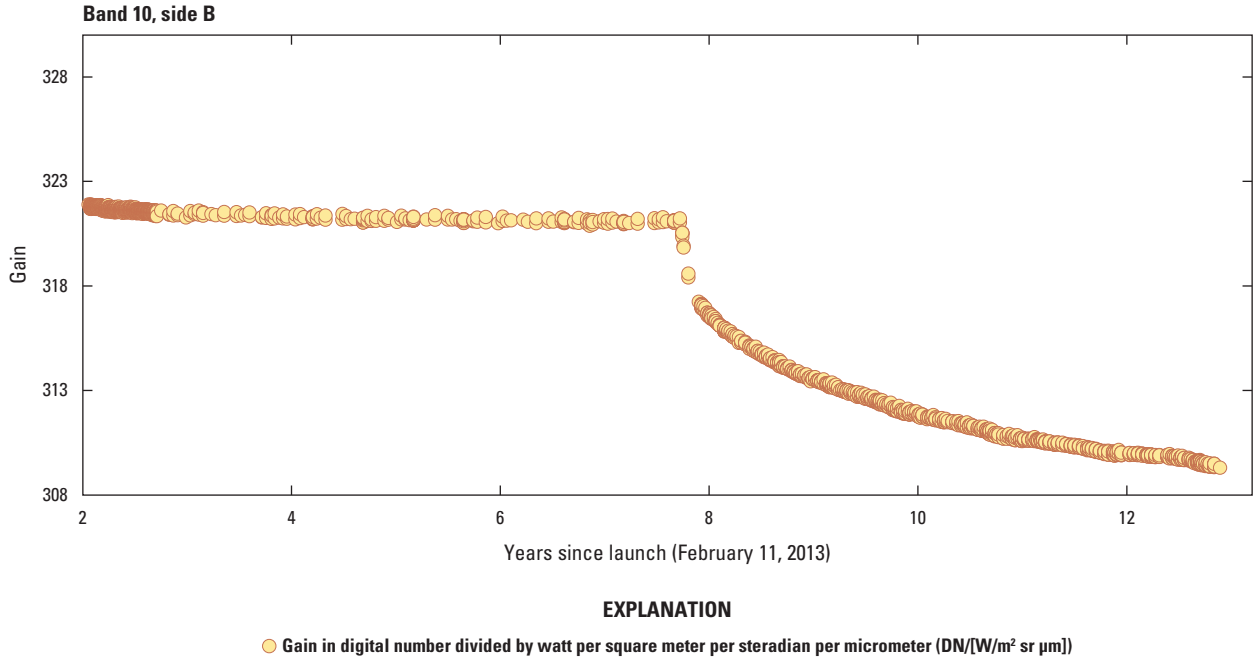

Figure 63. Graph showing Landsat 8 Thermal Infrared Sensor band 10 radiometric stability (side B).

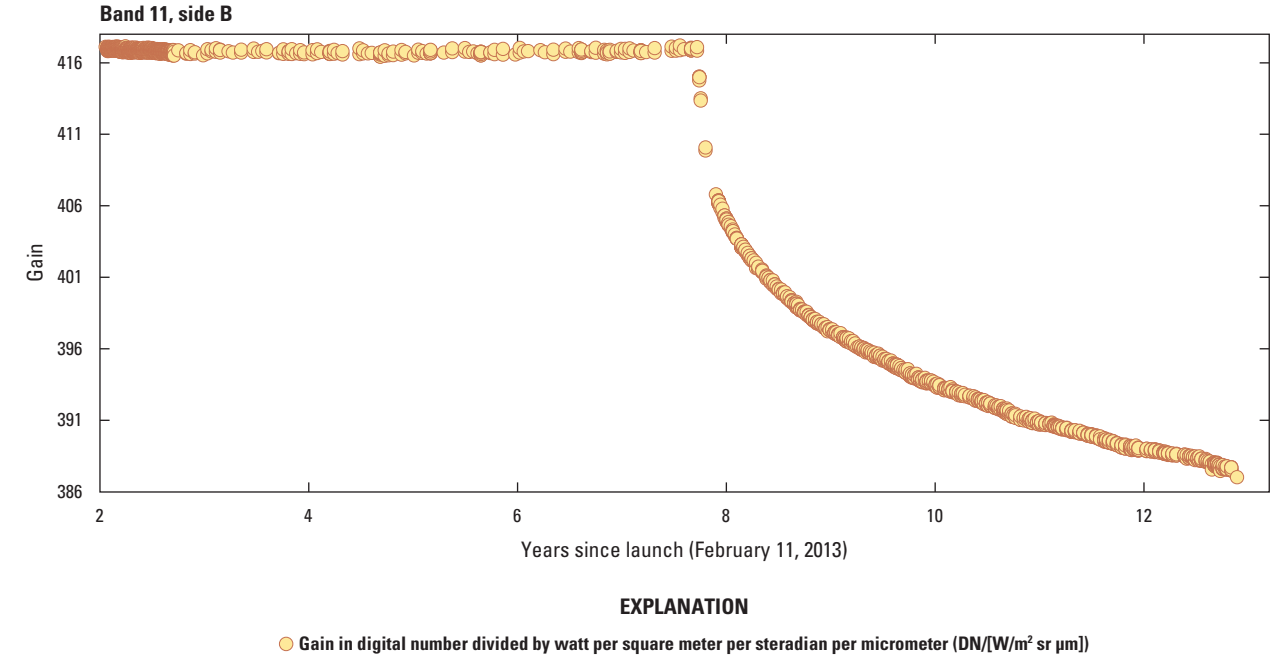

Figure 64. Graph showing Landsat 8 Thermal Infrared Sensor band 11 radiometric stability (side B).

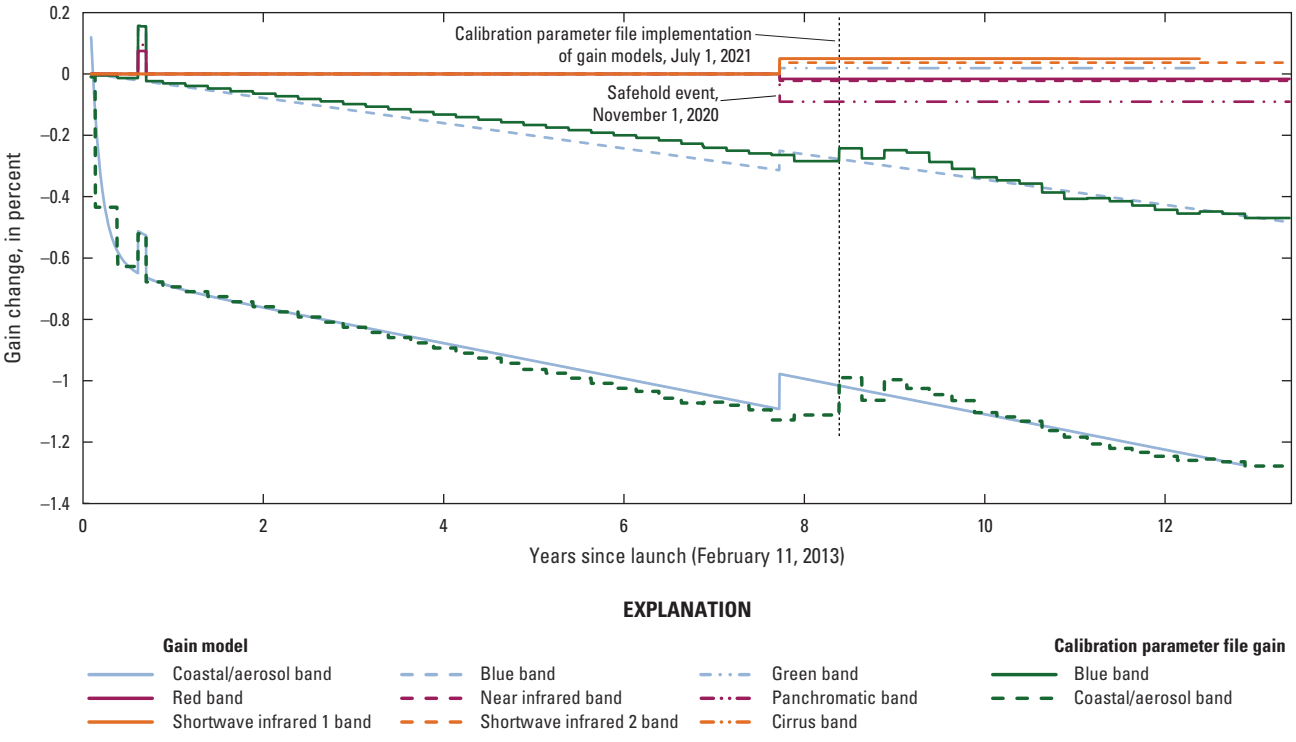

Figure 65. Graph showing Landsat 8 Operational Land Imager lifetime gain trends and calibration gain updates.

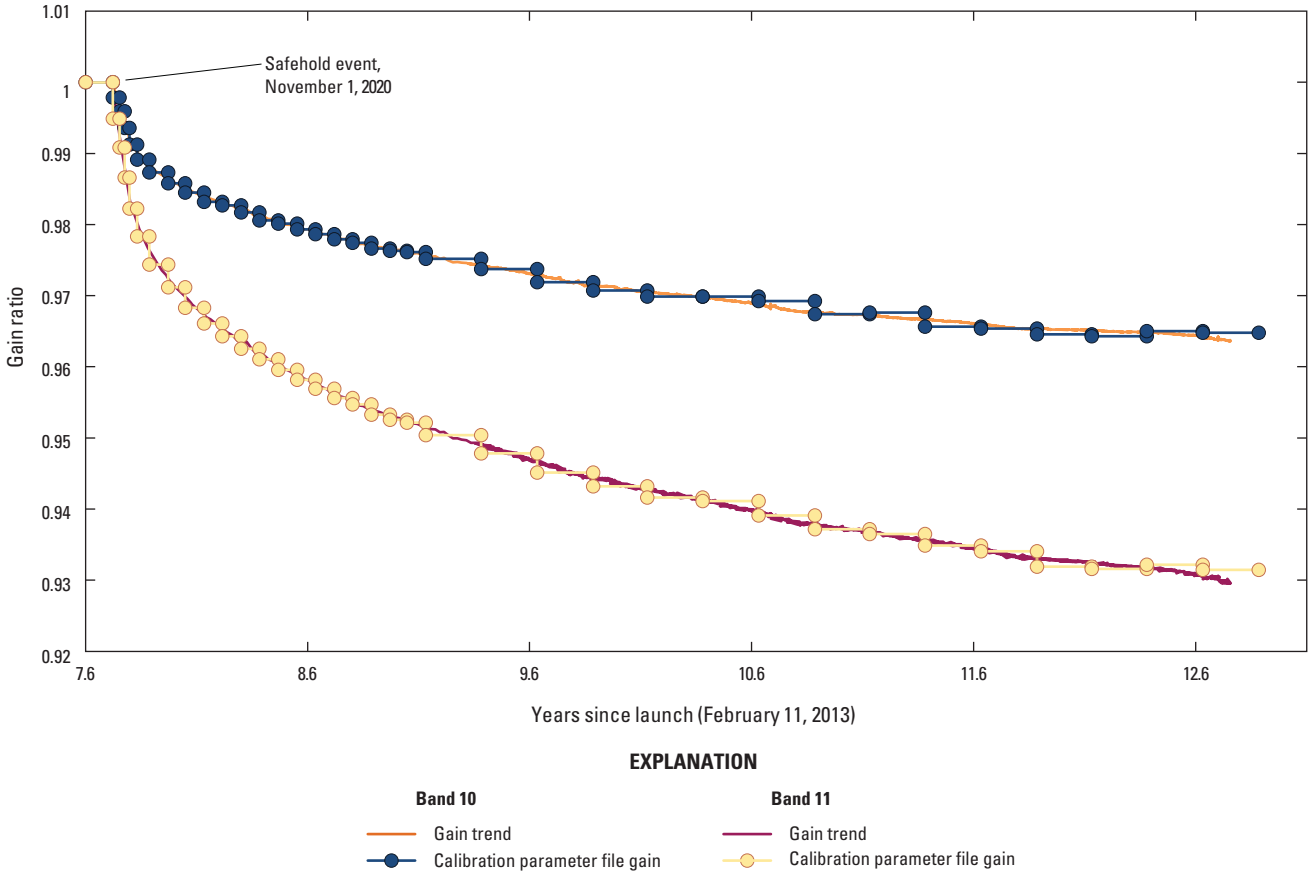

Figure 66. Graph showing Landsat 8 Thermal Infrared Sensor gain degradation since the safehold event on November 1, 2020.

Landsat 8 Relative Gains

Relative gains account for the differences in responsivity between detectors within a spectral band. OLI relative gains are monitored using solar diffuser acquisitions, side slither acquisitions (which entail a 90 degree yaw maneuver over an invariant site to flatten the data), and scene statistics. Quarterly updates are completed using data from the solar diffuser acquisitions from quarter 3, 2025. Starting with the release of Collection 2, TIRS relative gain calibration updates also were completed quarterly using blackbody collects from the previous quarter (USGS, 2021c). Beginning with quarter 3, 2025, TIRS relative gain calibration updates were performed using all blackbody collects acquired after the November 2020 safehold events. These updates effectively reduced detector-to-detector striping.

Typical per-detector changes in relative gains between the previous quarter and this quarter for several bands are shown in figures 67, 68, 69, and 70 by analyzing data from within each quarter. In each figure, the x-axis indicates the detector number, and the y-axis indicates the change in relative gain between the quarters as a ratio. These changes in responsivity are accounted for in the L1 product by updating the following quarter's CPF.

The OLI detectors that have indicated a sudden change in responsivity of 0.5 percent or greater in the SWIR 1 and SWIR 2 bands since launch are shown in figures 71 and 72. The x-axis indicates the date of the jump in responsivity, and the y-axis signifies the detector number. The observed responsivity jumps seem to be randomly scattered in time and location on the focal plane so do not seem to be associated with an instrument event or failure. These jumps are only observed in the SWIR bands (SWIR 1, SWIR 2, and cirrus); the visible and near infrared band detectors have not indicated any jump behavior over the whole mission.

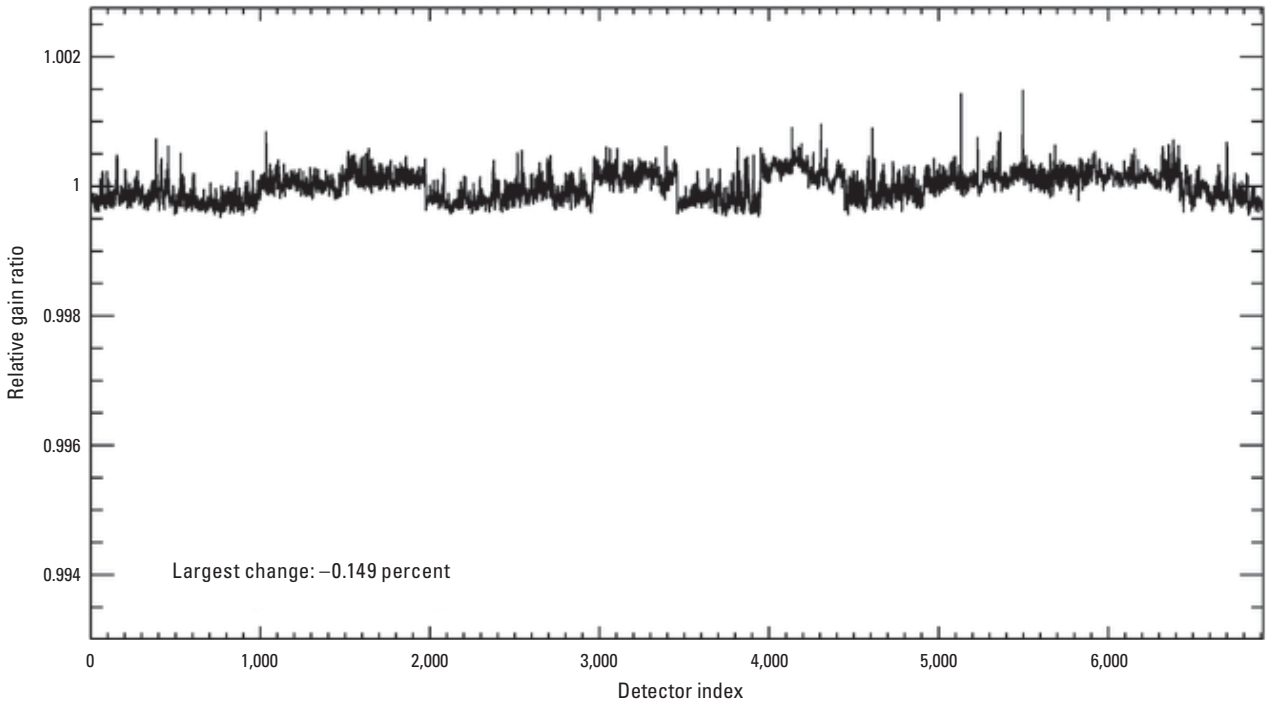

Figure 67. Graph showing Landsat 8 Operational Land Imager coastal/aerosol band per-detector change in relative gains between quarter 3 (July–September) and quarter 4 (October–December), 2025.

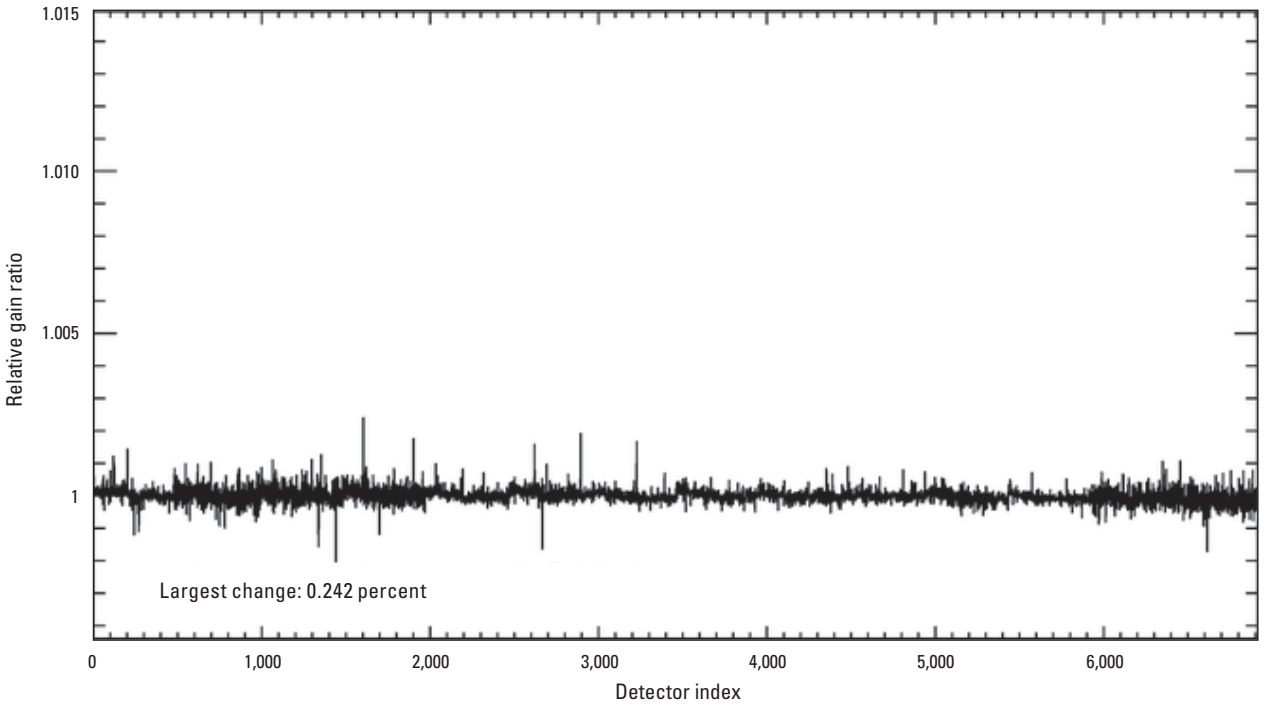

Figure 68. Graph showing Landsat 8 Operational Land Imager shortwave infrared 1 band per-detector change in relative gains between quarter 3 (July–September) and quarter 4 (October–December), 2025.

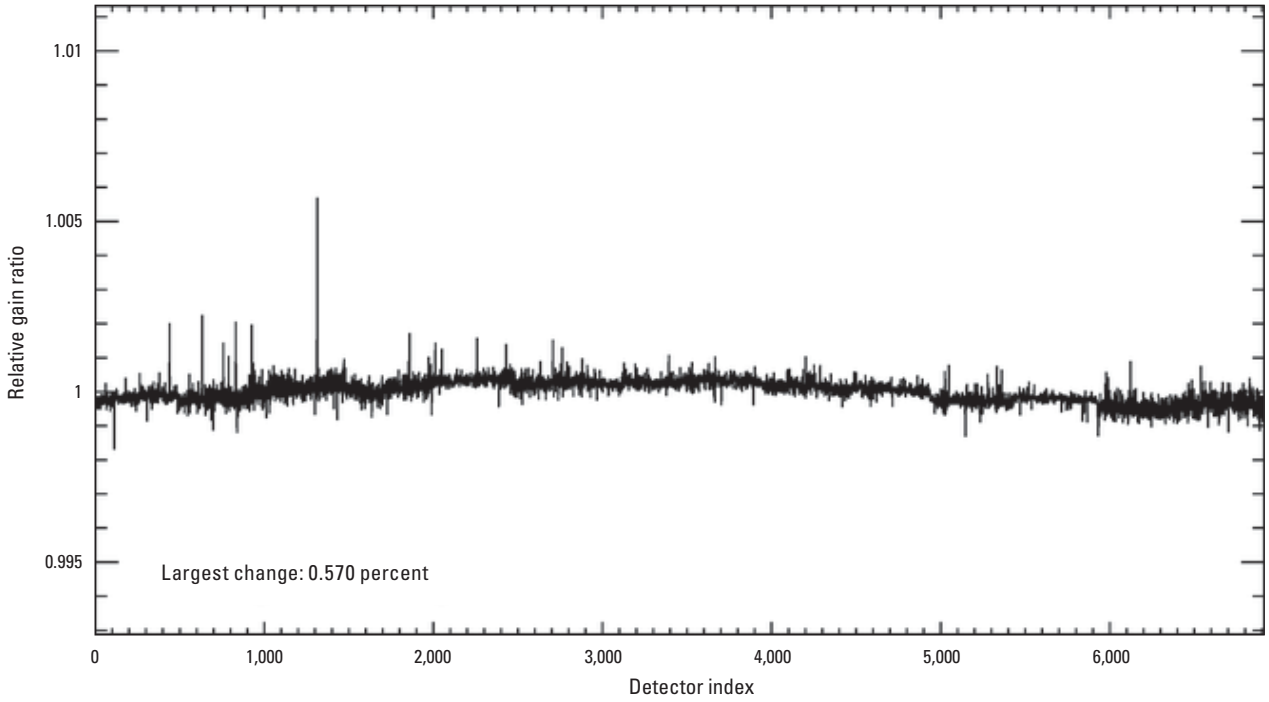

Figure 69. Graph showing Landsat 8 Operational Land Imager shortwave infrared 2 band per-detector change in relative gains between quarter 3 (July–September) and quarter 4 (October–December), 2025.

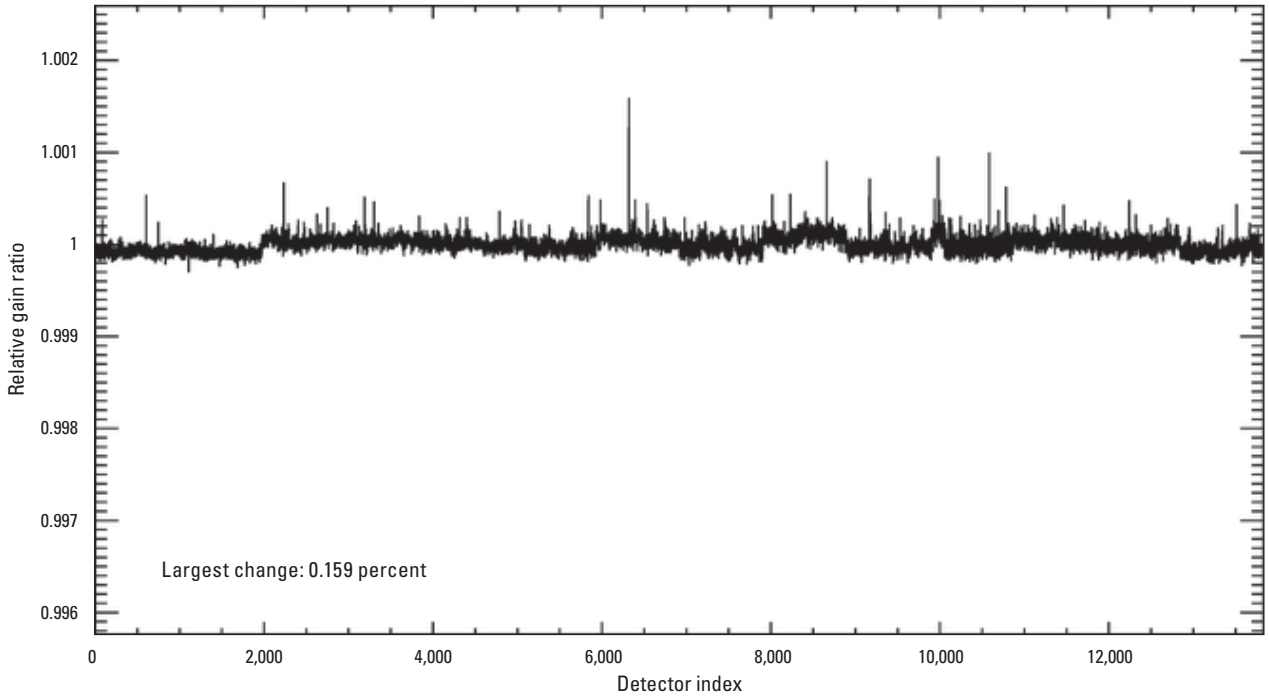

Figure 70. Graph showing Landsat 8 Operational Land Imager panchromatic band per-detector change in relative gains between quarter 3 (July–September) and quarter 4 (October–December), 2025.

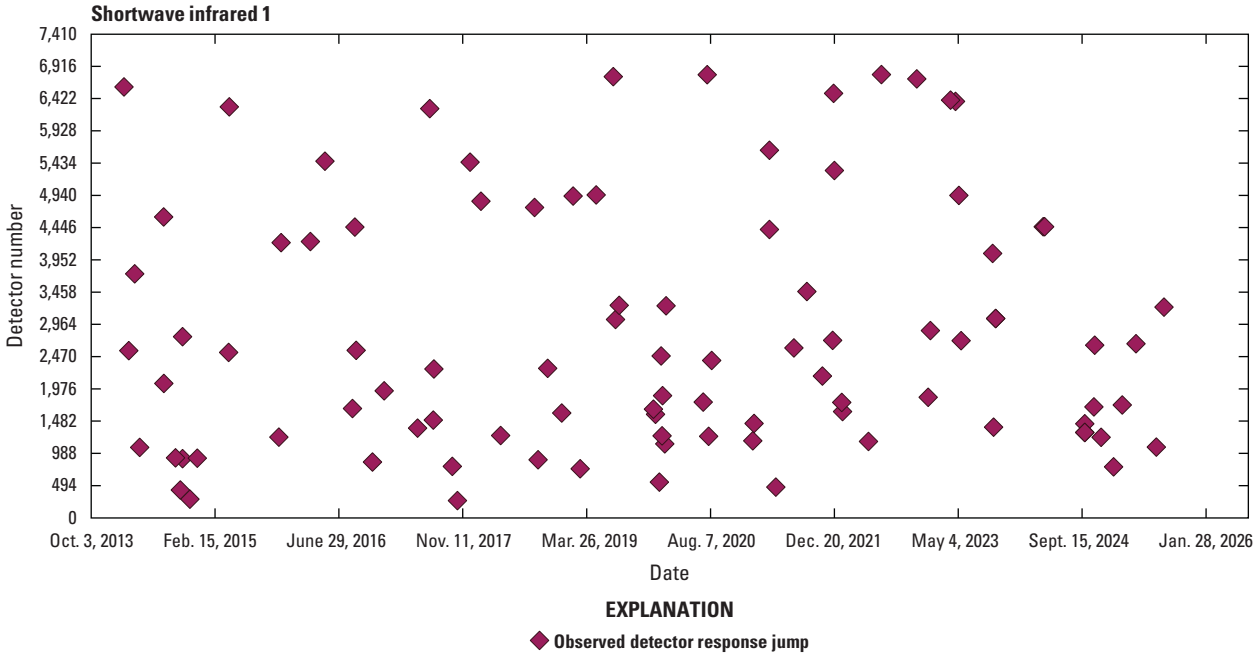

Figure 71. Graph showing Landsat 8 Operational Land Imager shortwave infrared 1 lifetime jumps in detector responsivity.

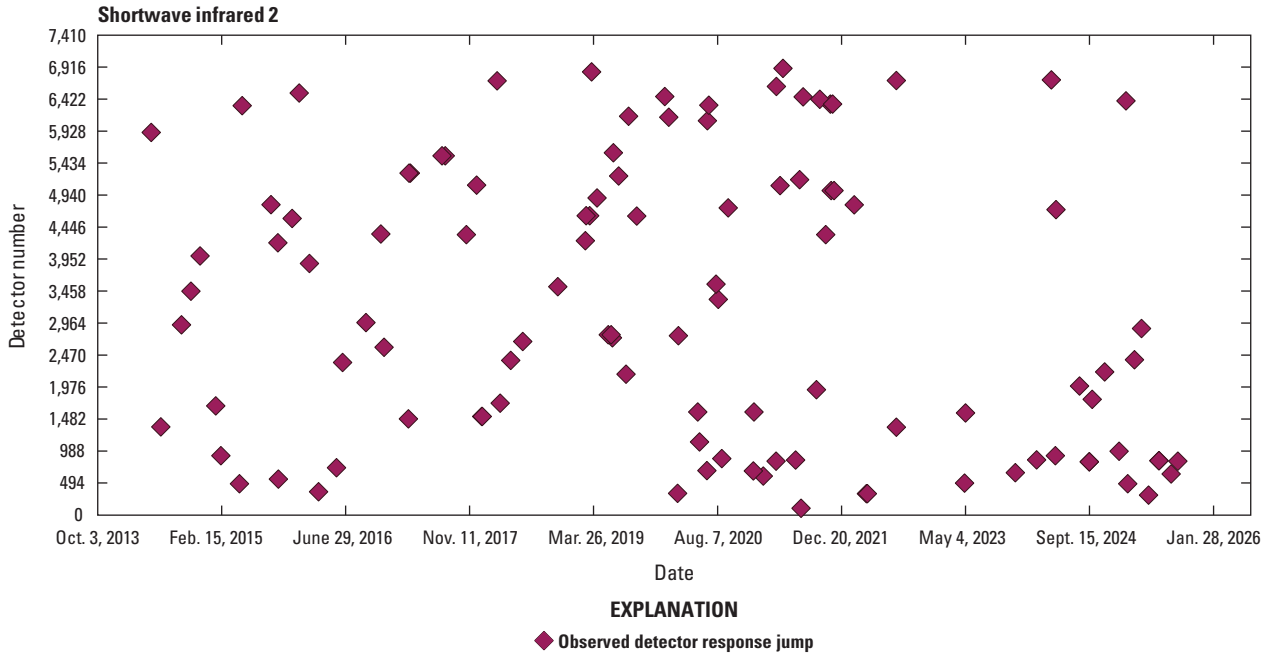

Figure 72. Graph showing Landsat 8 Operational Land Imager shortwave infrared 2 lifetime jumps in detector responsivity.

Landsat 8 Geometric Performance Summary

The Landsat 8 on-orbit geometric performance for the reporting quarter (quarter 4, 2025) meets all requirements outlined in USGS (2019a). The quarterly results summary is provided in table 7. Beginning with quarter 3, 2024, quarterly CPFs have been updated to improve the processing system's capability to generate L1TP products. The corrections introduced in the updated CPFs address sporadic errors with the Landsat 8 positioning information, ultimately resulting in more L1TP products.

Landsat 8 Band Registration Accuracy

Internal band registration measures how accurately the various Landsat 8 spectral bands are geometrically aligned to each other. The assessment provides a numerical evaluation of the accuracy of the band registration within an image using automated cross correlation techniques between the bands to be assessed (USGS, 2021c).

Landsat 8 OLI band registration performance has been stable over time. Quarterly band-to-band maximum registration accuracy for each band combination except for the cirrus band is shown in figure 73. Within the figure, blue bars indicate maximum registration accuracy in the line direction, and green bars indicate maximum registration accuracy in the sample direction. Lifetime OLI band registration accuracy for all bands is 4.14 meters (not shown), and lifetime OLI band registration accuracy for all bands, excluding cirrus, is 3.25 meters, which is well within the instrument specification accuracy. OLI band registration accuracy for all bands during quarter 4, 2025, is 4.09 meters (table 7), and OLI band registration accuracy for all bands, excluding cirrus, during quarter 4, 2025, is 3.18 meters (table 7).

Landsat 8 TIRS band registration performance has been stable throughout the instrument's lifetime, including after changes in Scene Select Mechanism (SSM) operation beginning in December 2014. Behavior is well within specification, as shown in figure 74, and quarter 4, 2025, results are consistent with past performance. Within the figure, blue bars indicate maximum registration accuracy in the line direction, and green bars indicate maximum registration accuracy in the sample direction. Lifetime TIRS band registration accuracy is 9.0 meters, and during quarter 4, 2025, the accuracy is 8.6 meters (table 7). Since quarter 3, 2020 (Collection 2 data), registration bias between the line and sample directions has reduced, which may be because of better SSM pointing stability, the TIRS relative gain update, or both.

Lifetime Landsat 8 TIRS to OLI band registration accuracy by quarter is shown in figure 75. Before the Collection 2 CPF update, seasonal effects are noticeable but leveled off after the release of Collection 2 in December 2020, as indicated by the closely aligned line (blue bars) and sample (green bars) accuracies. Lifetime Landsat 8 TIRS to OLI registration accuracy (excluding the cirrus band) is 19.5 meters in the line direction and 17.9 meters in the sample direction. Quarter 4, 2025, TIRS to OLI registration accuracy (excluding the cirrus band) is 19.9 meters in the line direction and 19.0 meters in the sample direction.

Landsat 8 Operational Land Imager to Thermal Infrared Sensor Alignment

Landsat 8 OLI to TIRS alignment knowledge is critical to ensure that the L1 product accuracy requirements can be met. The alignment between OLI and TIRS instruments is periodically measured using correlation-based methods to ensure that the band-to-band alignment requirements for all Landsat 8 bands can be met (USGS, 2021c). The alignment estimates are used to update the calibration parameters in the CPFs when the observed changes are determined to affect the performance requirements.

Landsat 8 TIRS to OLI pitch alignment measurements over instrument lifetimes are shown in figure 76. The November 2020 safehold events did substantially affect pitch alignment, but the ECCOE Landsat Cal/Val Team continues to monitor pitch alignment. From Haque and others (2022), in quarter 4, 2021, a small change in the TIRS to OLI pitch alignment was observed, which is similar to the seasonal trend observed in previous years; however, the magnitude of this trend was not the same as before, so it was unclear whether this new trend would continue. The trend continued in quarter 1, 2022, so a CPF update was issued in quarter 2 (April–June), 2022, for residual corrections to the alignment parameters. At this time, predictive estimates based on previous quarters, not knowing if the seasonal trend will be observed or not, made the CPF inconsistent with the seasonal pattern. With an intention to align the CPF more with the seasonal pattern for better prediction, subsequent predictive CPF updates for quarter 3, 2022; quarter 4, 2022; and quarter 1, 2023, were not changed. The April 2023 TIRS SSM excursion anomaly did not indicate any substantial effects in the TIRS to OLI pitch, roll, or yaw alignment. The lifetime TIRS to OLI roll alignment is shown in figure 77, and the lifetime TIRS to OLI yaw alignment is shown in figure 78. Each light blue symbol on these figures represents one calibration scene, the dark blue solid lines indicate quarterly alignment averages, and the orange dashed lines indicate applied Collection 2 CPF correction values.

Landsat 8 Geometric Accuracy

The Landsat 8 geometric assessment evaluates the absolute positional accuracy of the image products with respect to a ground (geometric) reference. The geometric accuracy assessment estimates the geometric error between the L1TP products and GCPs using automated cross correlation techniques (USGS, 2021c).

Table 7. Landsat 8 geometric performance summary, quarter 4 (October–December), 2025.

[The previous quarter is quarter 3 (July–September), 2025. OLI, Operational Land Imager; <, less than; LE90, linear error with 90 percent confidence; CE90, circular error with 90 percent confidence; L1T, Level 1 terrain-corrected product; >, greater than; TIRS, Thermal Infrared Sensor]

Requirement	Measured value from this quarter	Measured value from previous quarter[1]	Required value	Unit
OLI band registration accuracy (all bands)	4.09	4.31	<4.5	Meter (LE90)
OLI band registration accuracy (no cirrus)	3.18	3.24	<4.5	Meter (LE90)
Absolute geodetic accuracy	16.2	13.9	<65	Meter (CE90)
Relative geodetic accuracy	7.7	7.7	<25	Meter (CE90)
Geometric (L1T) accuracy	4.3	3.6	<12	Meter (CE90)
OLI edge slope	0.030	0.029	>0.027	1 per meter
TIRS band registration accuracy	8.6	8.1	<18	Meter (LE90)
TIRS to OLI registration accuracy	19.9	19.0	<30	Meter (LE90)

[1]From Haque and others (2026).

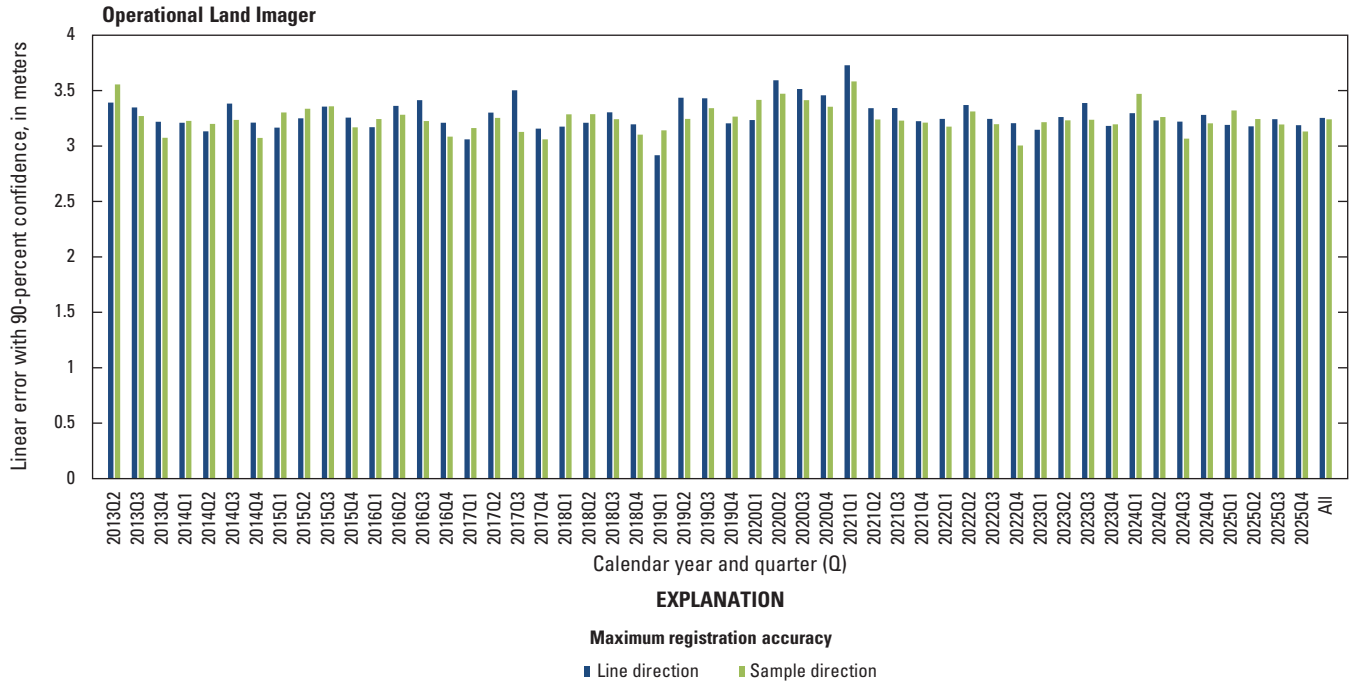

Figure 73. Graph showing Landsat 8 Operational Land Imager lifetime band (excluding cirrus) registration accuracy by quarter.

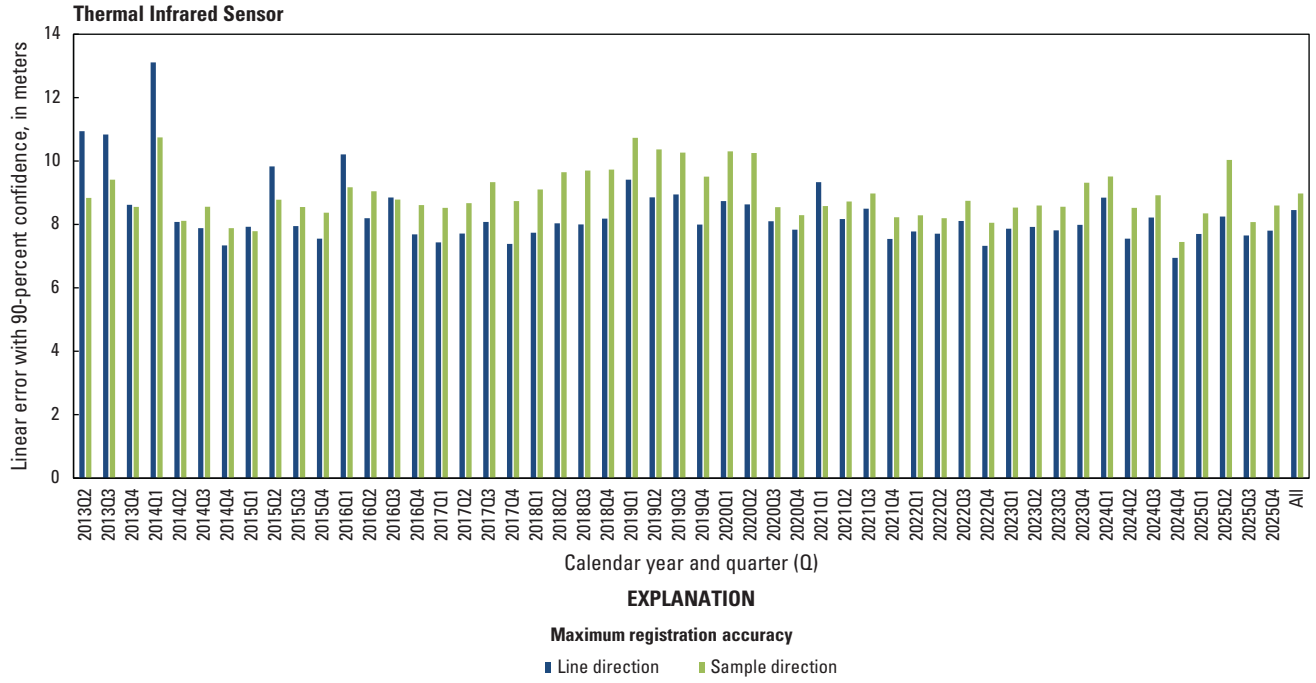

Figure 74. Graph showing Landsat 8 Thermal Infrared Sensor lifetime band registration accuracy by quarter.

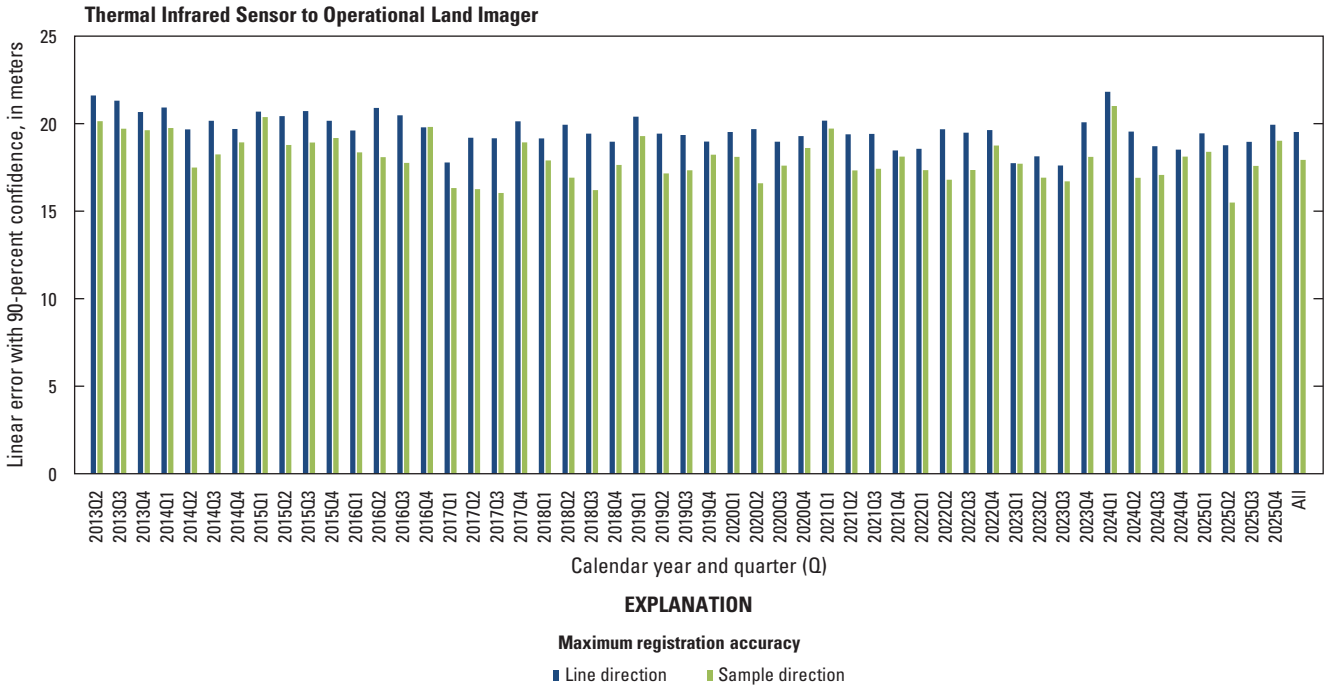

Figure 75. Graph showing Landsat 8 Thermal Infrared Sensor to Operational Land Imager lifetime band (excluding cirrus) registration accuracy by quarter.

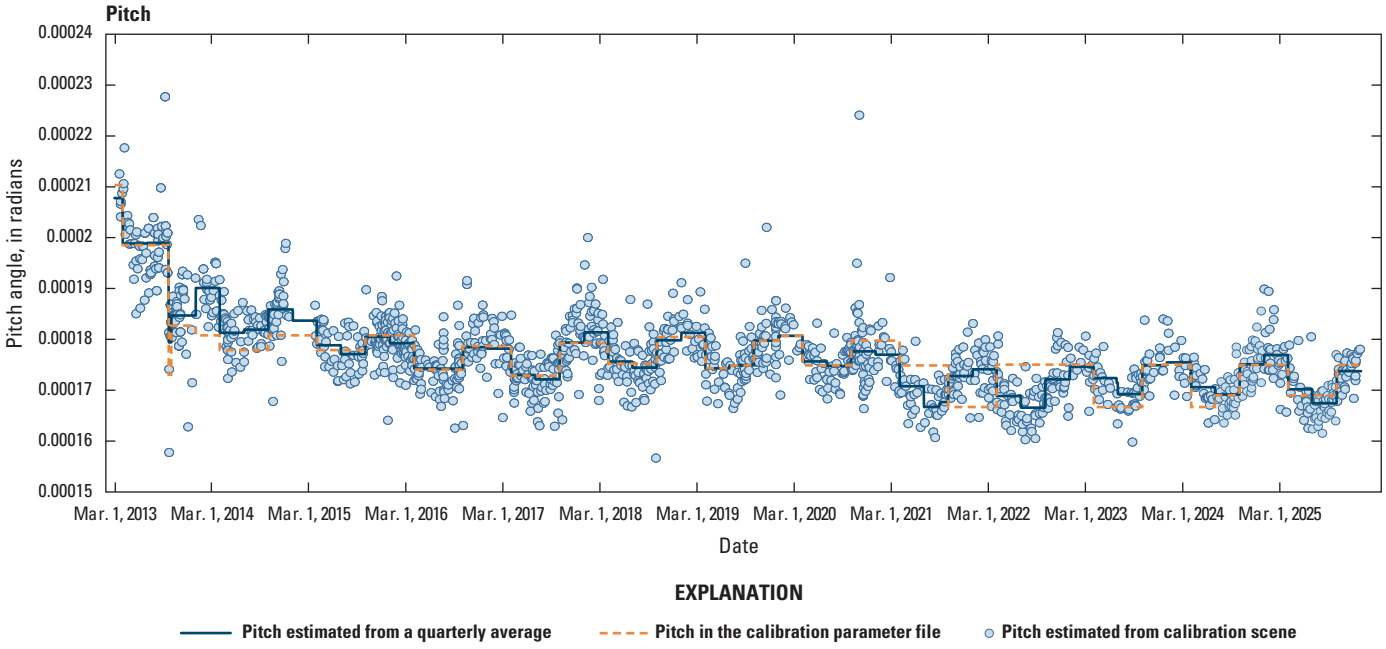

Figure 76. Graph showing Landsat 8 Thermal Infrared Sensor to Operational Land Imager lifetime pitch alignment.

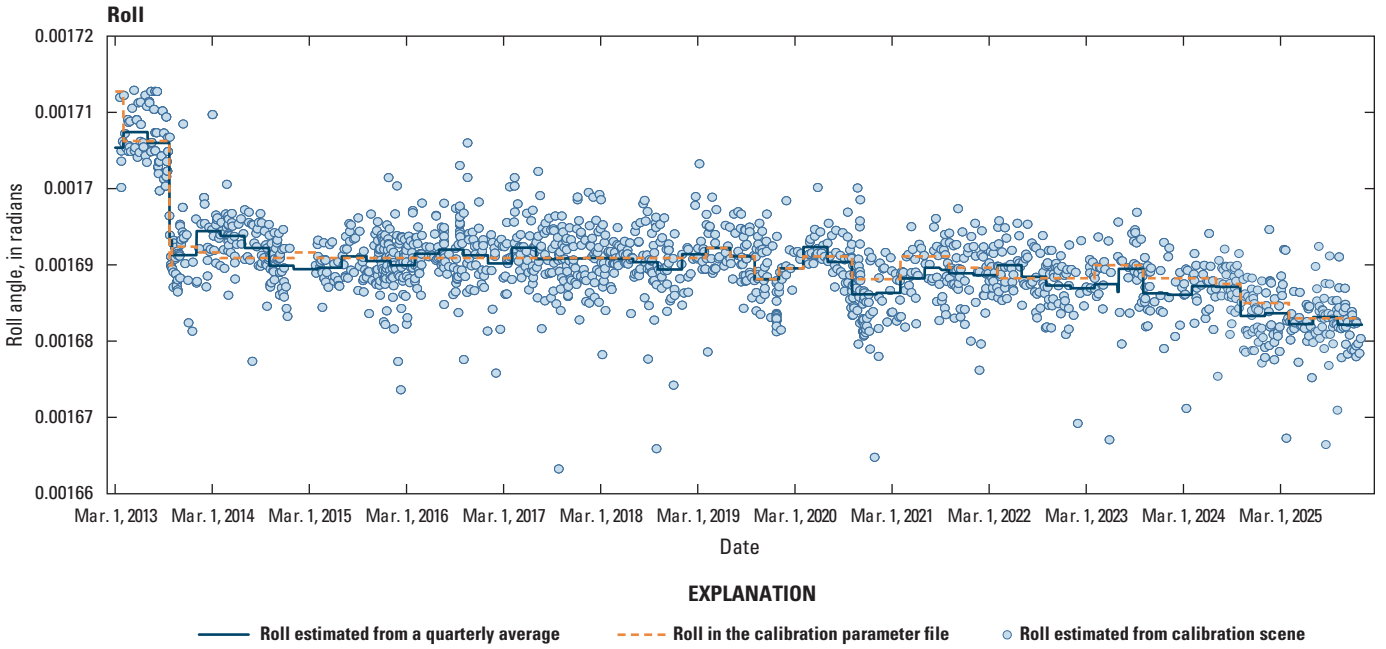

Figure 77. Graph showing Landsat 8 Thermal Infrared Sensor to Operational Land Imager lifetime roll alignment.

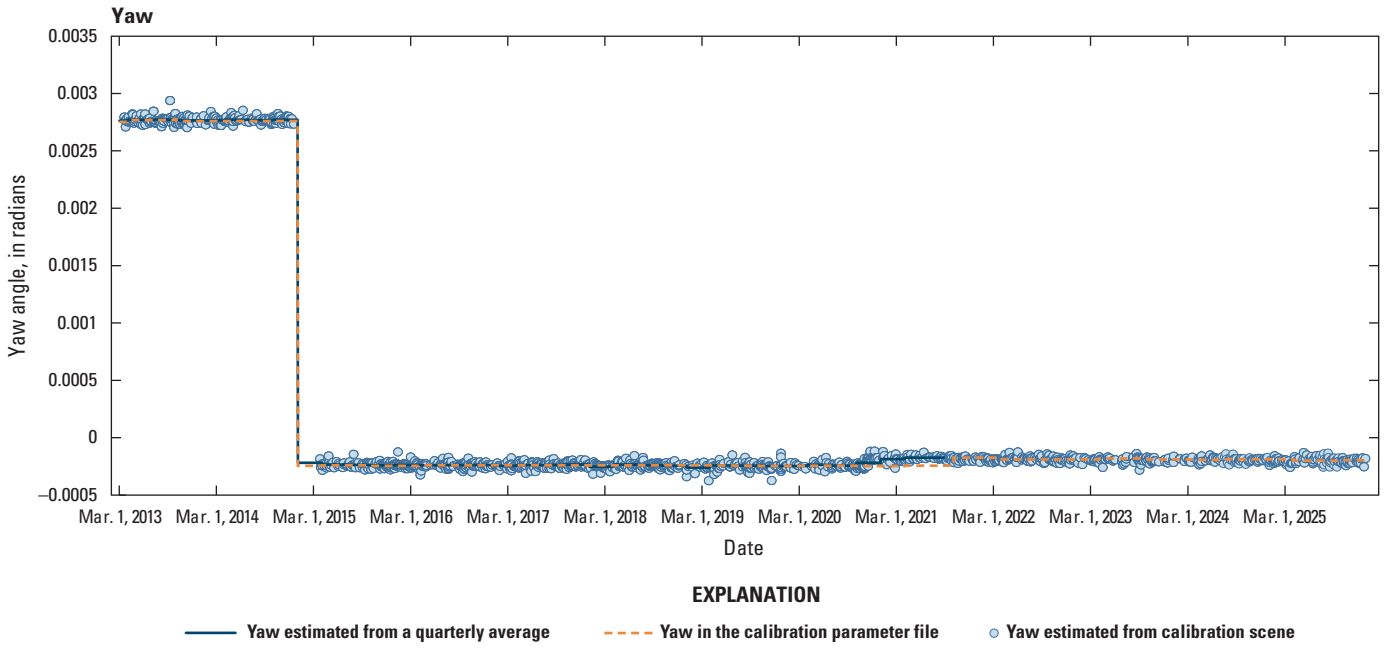

Figure 78. Graph showing Landsat 8 Thermal Infrared Sensor to Operational Land Imager lifetime yaw alignment.

Based on analysis results, relative accuracy of the Collection 2 GCPs is comparable to the DOQ supersites, which are sites created from a mosaic of highly accurate high-resolution terrain-corrected aerial data. Comparatively, relative accuracy of the Collection 2 GCPs is substantially better than the internal consistency of the Collection 1 GCPs. Overall, cloud-contaminated scene-based results are the primary contributor to substandard geometric accuracy from L1TP products. Lifetime quarterly Landsat 8 geometric accuracy at a CE90 is shown in figure 79. Blue bars indicate the geometric accuracy estimated over supersite paths/rows (calibration sites) with cloud-free scenes (using DOQ GCPs for the trend since quarter 1, 2022), yellow bars indicate geometric accuracy estimated over supersite paths/rows (calibration site scenes subsetting from all the L1TP scenes with no cloud constraints) using Collection 2 GCPs, and green bars indicate geometric accuracy estimated over all L1TP scenes processed in Collection 2 using Collection 2 GCPs (no cloud constraints). All results for this quarter are within the accuracy specification.

Lifetime and quarter 4, 2025, geometric accuracies for L1TP products are 3.7 and 4.3 meters when compared against cloud-free scenes over supersite paths/rows, 5.4 and 6.7 meters when compared against all L1TP scenes over supersite paths/rows only, and 10.5 and 11.4 meters when analyzing all the L1TP scenes processed in Collection 2, respectively. Note that seasonal effect is a factor in accuracy results.

Landsat 8 Geodetic Accuracy

The purpose of the geodetic accuracy assessment is to ensure that the Landsat 8 L0Rp data can be successfully processed into L1 systematic products that meet the system requirement of 65 meters at a CE90 horizontal accuracy. To measure the accuracy, calibration scenes are automatically correlated with data from the panchromatic band to measure the discrepancy between the known ground location and the position predicted by the OLI geometric model (USGS, 2021c).

Based on analysis results, absolute accuracy of the Collection 2 GCPs is comparable to the DOQ supersites and is substantially better compared to the Collection 1 GCPs (Rengarajan and others, 2020). Lifetime quarterly Landsat 8 geodetic accuracy at a CE90 is shown in figure 80. Blue bars indicate the accuracy estimated using DOQ supersite paths/rows (calibration site), and green bars indicate accuracy estimated from all L1TP scenes processed in Collection 2 using Collection 2 GCPs. As with the geometric accuracy, a wide variety of scene types (cloud-contaminated, islands, desert, snow covered, ice sheets, and so on) are the primary contributor to the poor geodetic accuracy for Collection 2 GCP-based results.

Although quarters 1, 2, and 3, 2021, indicated a slight increase in the geodetic accuracy offset, the lifetime results have been consistently well within the accuracy specification. The increase in the geodetic accuracy is because of a systematic bias in the along-track direction observed since the November 2020 safehold events. After the bias stabilized, an update to the sensor alignment parameters in the CPF was released in quarter 4, 2021, resulting in a decrease in the observed geodetic offsets. An additional sensor alignment update was released in quarter 2, 2022, in response to an along-track offset that was greater than 10 meters and continuing to increase (Haque and others, 2023). Geodetic accuracy has been within 10 meters (considering both along-track and across-track directions) since then, including after the April 2023 TIRS SSM excursion anomaly (USGS, 2023), and no sensor alignment update was necessary. Lifetime geodetic accuracies for systematic products are 16.2 meters when compared using DOQ GCPs over supersites and 26.0 meters when compared using Collection 2 GCPs over all the scenes processed in Collection 2, respectively.

Quarterly Level 2 Validation Results

In addition to L1 products, Landsat 8 and Landsat 9 surface reflectance PICS trending is completed by the ECCOE Landsat Cal/Val Team. The primary purpose of L2 surface reflectance PICS trending is to repeatedly characterize the temporal stability of the OLI sensors. The CNES region of interest has been chosen for completing the analysis, and the results are summarized in this section.

Level 2 Surface Reflectance Pseudoinvariant Calibration Site Trending

The Collection 2, L22 lifetime surface reflectance trends for seven Landsat 8 spectral bands for the Libya 4 PICS are provided in figure 81. Drift estimate results indicate small decay in responsivity for all bands. The x-axis represents years since launch (February 11, 2013), and the y-axis represents surface reflectance. The seasonal effect has been reduced from all bands using appropriate models. Although still in the early stages of the mission, the Collection 2, L2 lifetime surface reflectance observations for seven Landsat 9 spectral bands for the Libya 4 PICS are provided in figure 82.

Overall, Landsat 8 and Landsat 9 OLI trends indicated stability for L2 surface reflectance based on the analysis completed. No substantial instability was monitored in any band, according to the lifetime drift estimate results.

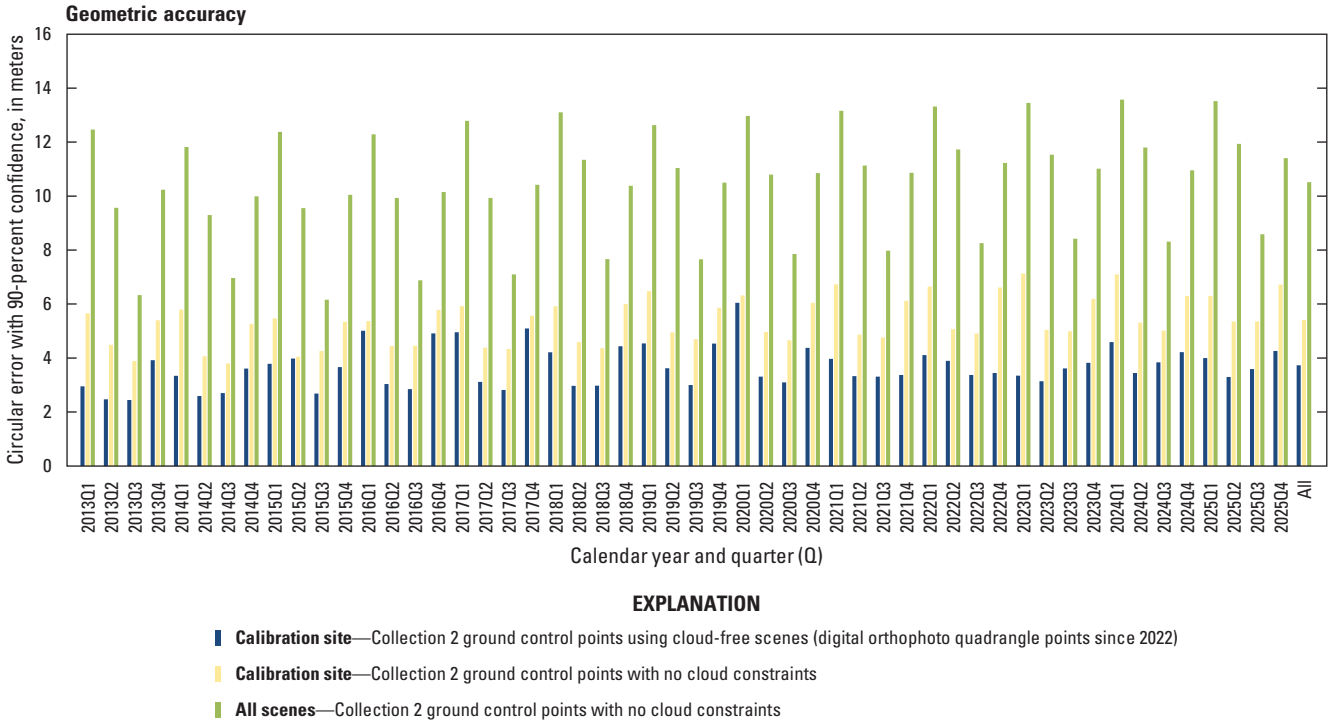

Figure 79. Graph showing Landsat 8 lifetime geometric accuracy by quarter.

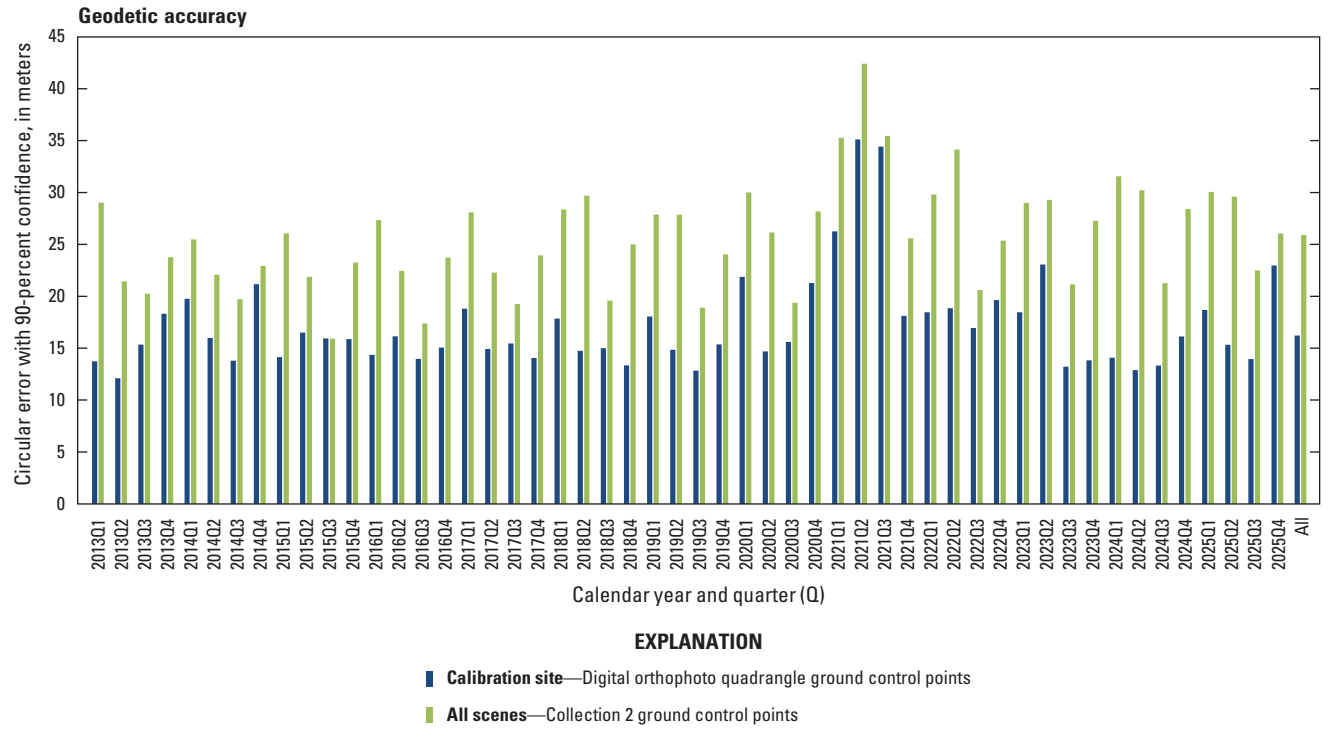

Figure 80. Graph showing Landsat 8 lifetime geodetic accuracy by quarter.

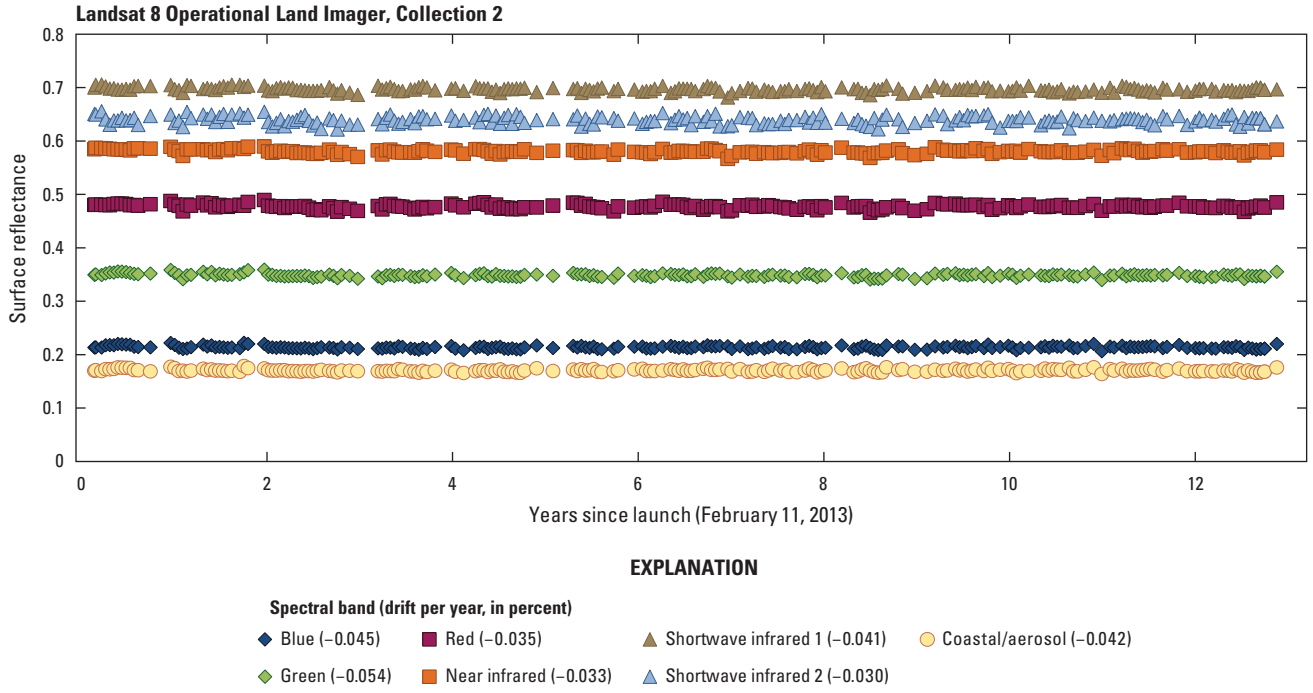

Figure 81. Graph showing Libya 4 pseudoinvariant calibration site surface reflectance trending, Landsat 8 Operational Land Imager, Collection 2.

Figure 82. Graph showing Libya 4 pseudoinvariant calibration site surface reflectance trending, Landsat 9 Operational Land Imager, Collection 2.

Summary

The Landsat 9 and Landsat 8 Operational Land Imager and Thermal Infrared Sensor on-orbit radiometric and geometric performance for quarter 4 (October–December), 2025, meets all requirements. Additionally, quarterly L2 validation results for Landsat 9 and Landsat 8 Operational Land Imager indicated stability for L2 surface reflectance.

References Cited

Barsi, J.A., Montanaro, M., Thome, K., Raqueno, N.G., Hook, S., Anderson, C.H., and Micijevic, E., 2022, Early radiometric performance of Landsat-9 Thermal Infrared Sensor, *in* Proceedings of SPIE Optical Engineering + Applications, San Diego, Calif., August 21–26, 2022: Earth Observing Systems XXVII, v. 12232, article 122320U, 31 p., accessed January 2026 at https://doi.org/10.1117/12.2634058.

Choate, M.J., Rengarajan, R., Storey, J.C., and Lubke, M., 2022, Landsat 9 geometric characteristics using underfly data: Remote Sensing (Basel), v. 14, no. 15, article 3781, accessed January 2026 at https://doi.org/10.3390/rs14153781.

Committee on Earth Observation Satellites, 2021, PICS—Pseudo-Invariant Calibration Sites: Committee on Earth Observation Satellites, Cal/Val Portal website, accessed January 2026 at https://calvalportal.ceos.org/pics_sites.

Executive Office of the President of the United States, 2007, A plan for a U.S. National Land Imaging Program—Future of Land Imaging Interagency Working Group: Washington, D.C., Executive Office of the President of the United States, National Science and Technology Council (NSTC) Office of Science and Technology Policy (OSTP) report, 110 p., accessed January 2026 at https://obamawhitehouse.archives.gov/sites/default/files/microsites/ostp/fli_iwg_report_print_ready_low_res.pdf.

Executive Office of the President of the United States, 2014, National plan for Civil Earth Observations: Washington, D.C., Executive Office of the President of the United States, Office of Science and Technology Policy (OSTP) report, 62 p., accessed January 2026 at https://obamawhitehouse.archives.gov/sites/default/files/microsites/ostp/NSTC/2014_national_plan_for_civil_earth_observations.pdf.

Executive Office of the President of the United States, 2016, The second National Civil Earth Observation Assessment—Societal benefit areas, subareas, and key objectives: Washington, D.C., Executive Office of the President of the United States, Office of Science and Technology Policy (OSTP) report, 21 p., accessed January 2026 at https://obamawhitehouse.archives.gov/sites/default/files/microsites/ostp/NSTC/the_second_national_civil_earth_observations_assessment.pdf.

Haque, M.O., Hasan, M.N., Shrestha, A., Rengarajan, R., Lubke, M., Steinwand, D., Bresnahan, P., Shaw, J.L., Ruslander, K., Micijevic, E., Choate, M.J., Anderson, C., Clauson, J., Thome, K., Kaita, E., Angal, A., Levy, R., Miller, J., Ding, L., and Pinto, C.E., 2026, ECCOE Landsat quarterly calibration and validation report—Quarter 3, 2025: U.S. Geological Survey Open-File Report 2026–1069, 55 p., accessed April 2026 at https://doi.org/10.3133/ofr20261069.

Haque, M.O., Rengarajan, R., Lubke, M., Hasan, M.N., Shrestha, A., Shaw, J.L., Denevan, A., Ruslander, K., Micijevic, E., Choate, M.J., Anderson, C., Thome, K., Barsi, J., Kaita, E., Levy, R., Miller, J., and Ding, L., 2024, ECCOE Landsat quarterly calibration and validation report—Quarter 4, 2023 (ver. 1.1): U.S. Geological Survey Open-File Report 2024–1026, 62 p., accessed January 2026 at https://doi.org/10.3133/ofr20241026.

Haque, M.O., Rengarajan, R., Lubke, M., Hasan, M.N., Shrestha, A., Tuli, F.T., Shaw, J.L., Denevan, A., Franks, S., Micijevic, E., Choate, M.J., Anderson, C., Thome, K., Kaita, E., Barsi, J., Levy, R., and Miller, J., 2023, ECCOE Landsat quarterly calibration and validation report—Quarter 3, 2022: U.S. Geological Survey Open-File Report 2023–1013, 38 p., accessed January 2026 at https://doi.org/10.3133/ofr20231013.

Haque, M.O., Rengarajan, R., Lubke, M., Tuli, F.T.Z., Shaw, J.L., Hasan, M.N., Denevan, A., Franks, S., Micijevic, E., Choate, M.J., Anderson, C., Markham, B., Thome, K., Kaita, E., Barsi, J., Levy, R., and Ong, L., 2022, ECCOE Landsat quarterly calibration and validation report—Quarter 4, 2021: U.S. Geological Survey Open-File Report 2022–1033, 38 p., accessed January 2026 at https://doi.org/10.3133/ofr20221033.

Micijevic, E., Rengarajan, R., Haque, M.O., Lubke, M., Tuli, F.T., Shaw, J.L., Hasan, N., Denevan, A., Franks, S., Choate, M.J., Anderson, C., Markham, B., Thome, K., Kaita, E., Barsi, J., Levy, R., and Ong, L., 2021, ECCOE Landsat quarterly calibration and validation report—Quarter 2, 2021: U.S. Geological Survey Open-File Report 2021–1105, 40 p., accessed January 2026 at https://doi.org/10.3133/ofr20211105.

Micijevic, E., Rengarajan, R., Haque, M.O., Lubke, M., Tuli, F.T.Z., Shaw, J.L., Hasan, N., Denevan, A., Franks, S., Choate, M.J., Anderson, C., Markham, B., Thome, K., Kaita, E., Barsi, J., Levy, R., and Ong, L., 2022, ECCOE Landsat quarterly calibration and validation report—Quarter 3, 2021: U.S. Geological Survey Open-File Report 2022–1025, 38 p., accessed January 2026 at https://doi.org/10.3133/ofr20221025.

Montanaro, M., Barsi, J.A., Lunsford, A., Rohrbach, S., and Markham, B.L., 2014, Performance of the Thermal Infrared Sensor on-board Landsat 8 over the first year on-orbit, *in* Proceedings of SPIE Optical Engineering + Applications, San Diego, Calif., August 17–21, 2014: Earth Observing Systems XIX, v. 9218, 14 p., accessed January 2026 at https://doi.org/10.1117/12.2063457.

National Geospatial Advisory Committee, 2020, Landsat data—Community standard for data calibration (October 2020): Landsat Advisory Group, 12 p., accessed January 2026 at https://www.fgdc.gov/ngac/meetings/october-2020/ngac-paper-landsat-data-community-standard-for.pdf.

Rengarajan, R., Choate, M., Hasan, M.H., and Denevan, A., 2024, Co-registration accuracy between Landsat-8 and Sentinel-2 orthorectified products: Remote Sensing of Environment, v. 301, article 113947, accessed January 2026 at https://doi.org/10.1016/j.rse.2023.113947.

Rengarajan, R., Storey, J.C., and Choate, M.J., 2020, Harmonizing the Landsat ground reference with the Sentinel-2 Global Reference Image using space-based bundle adjustment: Remote Sensing (Basel), v. 12, no. 19, article 3132, accessed January 2026 at https://doi.org/10.3390/rs12193132.

U.S. Geological Survey [USGS], 2019a, Landsat 8 (L8) data users handbook (ver. 5.0, November 2019): U.S. Geological Survey, Earth Resources Observation and Science (EROS) Center, LSDS–1574, 106 p., accessed January 2026 at https://www.usgs.gov/landsat-missions/landsat-8-data-users-handbook.

U.S. Geological Survey [USGS], 2019b, Landsat 9 (ver. 1.3, August 2022): U.S. Geological Survey Fact Sheet 2019–3008, 1 p., accessed January 2026 at https://doi.org/10.3133/fs20193008.

U.S. Geological Survey [USGS], 2020a, Landsat 8–9 Operational Land Imager (OLI)—Thermal Infrared Sensor (TIRS) Collection 2 Level 1 (L1) data format control book (DFCB) (ver. 7.0, March 2025): U.S. Geological Survey, Earth Resources Observation and Science (EROS) Center, LSDS–1822, 58 p., accessed January 2026 at https://www.usgs.gov/media/files/landsat-8-9-olitirs-collection-2-level-1-data-format-control-book.

U.S. Geological Survey [USGS], 2020b, Landsat 8–9 Operational Land Imager (OLI)—Thermal Infrared Sensor (TIRS) Collection 2 Level 2 (L2) data format control book (DFCB) (ver. 7.0, December 2022): U.S. Geological Survey, Earth Resources Observation and Science (EROS) Center, LSDS–1328, 72 p., accessed January 2026 at https://www.usgs.gov/media/files/landsat-8-9-olitirs-collection-2-level-2-data-format-control-book.

U.S. Geological Survey [USGS], 2021a, EarthExplorer: U.S. Geological Survey database, accessed January 2026 at https://earthexplorer.usgs.gov.

U.S. Geological Survey [USGS], 2021b, EROS Cal/Val Center of Excellence (ECCOE): U.S. Geological Survey website, accessed January 2026 at https://www.usgs.gov/calval.

U.S. Geological Survey [USGS], 2021c, Landsat 8–9 Calibration and Validation (Cal/Val) algorithm description document (ADD) (ver. 4.0, January 2021): U.S. Geological Survey, Earth Resources Observation and Science (EROS) Center, LSDS–1747, 807 p., accessed January 2026 at https://www.usgs.gov/media/files/landsat-8-9-calibration-validation-algorithm-description-document.

U.S. Geological Survey [USGS], 2022, Landsat 9 data users handbook (ver. 1.0, February 2022): U.S. Geological Survey, Earth Resources Observation and Science (EROS) Center, LSDS–2082, 115 p., accessed January 2026 at https://www.usgs.gov/media/files/landsat-9-data-users-handbook.

U.S. Geological Survey [USGS], 2023, Temporary pause in Landsat 8 product processing: U.S. Geological Survey website, accessed January 2026 at https://www.usgs.gov/landsat-missions/news/temporary-pause-landsat-8-product-processing.

For more information about this publication, contact:
Director, USGS Earth Resources Observation and Science Center
47914 252nd Street
Sioux Falls, SD 57198
605–594–6151

For additional information, visit: https://www.usgs.gov/centers/eros

Publishing support provided by the
USGS Science Publishing Network,
Rolla and Lafayette Publishing Service Centers

ISSN 2331-1258 (online)
https://doi.org/10.3133/ofr20261014